Simulation of Large Scale CO_2 Injection at the Aquistore Injection Site Estevan, SK

by

Ramin Safaei Jazi

A thesis submitted in partial fulfillment of the requirements for the degree of

Master of Science

Department of Earth and Atmospheric Sciences
University of Alberta

Abstract

Physical impacts of CO_2 injection into the Cambro-Ordovician Aquifer in the Williston Basin were simulated by using the TOUGH2-ECO2N simulator. A simulation domain starts from the top of the Precambrian crystalline bedrock up to the surface Glacial Till with a total vertical depth of 3345 metres including 11 aquifers and 12 aquitards. Three injection horizons were defined within the Cambro-Ordovician Aquifer and the lateral extent of the model domain was set to R=50 kilometres. A 30-year injection period followed by a 70-year post injection period at a rate of 1000 tonnes per day was simulated. Results showed that there was no CO_2 leakage from the reservoir into the overlying formations for a 100-year period and CO_2 appears to be safely trapped under the Icebox Aquitard. The maximum lateral CO_2 migration reached up to 2 kilometres at 100 years after the injection and occurred within the middle injection horizon. Carbon dioxide saturation decreased significantly within the lower and upper horizons, while it remained almost unchanged within the middle horizon. Vertical pressure profile showed that there is no built up pressure above the Ordo-Silurian Aquifer. Lateral pressure profile also showed that the maximum pressure buildup occurs at the injection well and decreases laterally toward the model boundaries. Seventy years after the injection stops, almost the entire system reached the equilibrium or hydrostatic conditions except for the area around the injection well corresponds to a footprint area of $5.3\ km^2$. Results also showed no vertical brine migration across the Prairie Formation. Therefore, brine leakage into the shallow fresh water aquifers (e.g., Belly River Formation) is very unlikely.

In order to obtain accurate results the injection cell width needs to be less than 1.5 metres and the vertical grid discretization also should be no more than 5 metres especially in the storage formation and its overlying sealing unit. Results also showed that no flow boundary conditions overestimate the excess pressure up to 1.5 Mpa compare to the hydrostatic boundary conditions. Thus, assigning the Dirichlet or hydrostatic boundary conditions is essential to obtain valid results. Results showed that MODFLOW could be used as an approach to simulate the head rise caused by the injection at the regions far away from the injector where only one phase is present.

The Aquistore injection site appears to have a good storage potential to safely store supercritical carbon dioxide and will essentially contribute toward reducing CO_2 emissions.

Keywords: CO_2 sequestration, TOUGH2-ECO2N, Aquistore injection site, Williston Basin.

یک روز رسد غمی به اندازه کوه

یک روز رسد نشاط اندازه دشت

افسانه زندگی همین است عزیز

در سایه کوه باید از دشت گذشت...

Acknowledgements

I would like to express my sincere gratitude to my advisor, Dr. Ben Rostron, for his tremendous support during my study at the University of Alberta. I would like to appreciate him for his motivation, patience, and immense knowledge. I could ask for no better mentor.

I am also grateful to my committee members, Dr. Carl Mendoza and Dr. Daniel Alessi as well as Dr. Murray Gingras for their insightful guides, and encouragements. Without the overwhelming support of my advisor and committee members, this thesis would not have been written.

I would also like to appreciate the tremendous supports from Dr. Stefan Finsterle from Lawrence Berkeley National Laboratory (LBNL) and Mrs. Alison Alcott from Rockware Inc.

Finally, I would like to express my gratitude to my parents (Mohammad Safaei Jazi and Parvin Khosravi) for always being there for me, when times get hard. Thank you for being such a great supporters and I greatly appreciate you for everything that you have done for me.

Table of Contents

List of Tables

List of Figures

1 Introduction

Carbon dioxide capture and storage (CCS) is a process consisting of the separation of CO_2 from industrial sources, the transport to a storage site through a pipeline or ground transportation, and finally isolation from the atmosphere for a long period of time (IPCC, 2005). Carbon sequestration in deep geological formations (e.g., saline aquifers, depleted oil and gas reservoirs, and coal beds) is considered to be a promising technique to mitigate the adverse impacts of climate change (Holloway, 1996; Gale, 2004; IPCC, 2005; Hepple and Benson, 2005). Carbon dioxide can be captured from stationary sources, such as large industrial facilities and power plants, compressed to a fluid or supercritical state, and injected into deep underground geologic formations (aquifers) with high porosity and permeability (Birkholzer et al. 2009). Carbon dioxide capture and storage (CCS) is one of many other options to mitigate carbon dioxide emissions such as nuclear power; renewable energy sources; reduction of non- CO_2 greenhouse gas; and enhancement of biological sinks (IPCC, 2005). However, CO_2 storage in deep geological aquifers is the most attractive option because of the enormous volume of pore space available for storing carbon dioxide as well as the extensive distribution of these aquifers on the earth (Hitchon et al., 1999; Lemieux, 2011).

Figure 1.1 schematically represents the process and potential of the large-scale CO_2 injection into a deep saline aquifer. Carbon dioxide is injected in a supercritical state down an injection well into a storage complex (consisting of one or more permeable storage formations) below a sealing layer. This creates a physical CO_2 plume around the injection well that migrates outward (Figure 1.1). The footprint area of the surface indicates the lateral extent of the physical CO_2 plume.

Even if the CO_2 plume is safely trapped under a sealing unit, the footprint area (Figure 1.1) of the pressure buildup is much larger than the footprint of the carbon dioxide plume. Depending on the properties of the reservoir formations and sealing layer (e.g., porosity, permeability, etc.) a larger area around the injection zone is impacted by the injection (Birkholzer et al., 2009). Associated with injection is an increased pressure region that extends laterally and vertically beyond the CO_2 plume. This creates a pressure footprint at the surface.

Injected carbon dioxide in the storage formation moves the brine away from the injection well, causing brine displacement in the storage formation. Thus, several potential hazards to groundwater resources associated with carbon sequestration need to be considered such as CO_2 or brine leakage into the overlying fresh water aquifers, pressure buildup, and brine displacement that might impact up dip groundwater resources (Bergman and Winter, 1995; Holloway and Savage 1993, and Lemieux, 2011).

Carbon dioxide is buoyant; therefore it has a tendency to migrate upward. If the sealing layer(s) overlying the storage formation are fractured or faulted, CO_2 or brine leakage could occur. This also might happen through poorly cemented or abandoned boreholes (IPCC, 2005). In addition, once CO_2 dissolves into the formation water, it produces carbonic acid and modifies the pH. This could impact the quality of groundwater. (Wang and Jaffe 2004; Kharaka et al. 2010, Lemieux, 2011).

1.1 Supercritical Carbon Dioxide

Supercritical fluids have special physical properties and form a key part of this work; therefore, a brief review is warranted.

Carbon dioxide is in a gaseous state at atmospheric conditions and has less density compared to water. The density variation causes CO_2 buoyancy. When CO_2 pressure and temperature exceed 73.9 bar (7.39 Mpa) and 31.1 C respectively, CO_2 changes to a gas-type phase known as a supercritical CO_2 phase with a liquid-like higher density and viscosity (Bachu, 2003). The higher the density, the less buoyant force there is available to drive vertical migration of CO_2. Hence, most CO_2 storage sites utilize supercritical CO_2.

Assuming a normal pressure gradient of 10 Kpa per metre, supercritical pressure conditions will be encountered in basins below a depth of 739 metres. Thus, storage formations must be deeper than 800 metres for CO_2 storage potential because there is lower buoyancy at this depth (Lemieux, 2011).

The density of supercritical CO_2 is strongly dependent on temperature as well (Figure 1.2). For example, the density of CO_2 at an injection depth of 2000 metres with an average surface temperature of 10 C and geothermal gradient of 20 C/km is about 700 kg/m^3.

1.2 Behavior of CO_2 during and after injection

When supercritical CO_2 is injected into a saline aquifer it forms a non-wetting phase that is partially immiscible (Bachu, 2008). The amount of CO_2 that will dissolve in the formation water depends on the time that CO_2 interacts with native brine (Bachu, 2008). The longer the interaction, the more carbon dioxide will dissolve. Estimates are that up to 30% of supercritical CO_2 can dissolve in the formation water after tens of years. Ultimately the entire plume could dissolve over few centuries (McPherson and Cole 2000; Doughty et al. 2001).

Dissolution of CO_2 in the brine also increases the brine density. Thus, this may create convection flow(s) close to the injection zone (Gasda et al., 2004). Formation water saturated with CO_2 is heavier and sinks down toward the bottom of the storage formation (Ennis-King and Paterson 2003; Audigane et al. 2007). Downward moving CO_2 stimulates the contact between formation water (not saturated with CO_2) and the injected CO_2 plume and causes faster dissolution of CO_2 in the undersaturated brine.

Saturation of formation water with CO_2 also contributes to a longer residence time of dissolved CO_2 since CO_2 flows toward the bottom of the storage formation instead of migrating upward to the surface (Lemieux, 2011).

1.3 Trapping mechanisms

It is clear from the preceding that CO_2 entrapment at any location and time at a site is controlled by a number of different mechanisms. Proposed mechanisms include structural/stratigraphic; hydrodynamic; residual; and mineral (IPCC, 2005). Figure 1.3 shows the various trapping mechanisms. The security of the CO_2 storage is a function of the combination of various trapping mechanisms for which the proportion evolves with time (Lemieux, 2011). For example, at an early stage, structural and stratigraphic mechanisms are dominant but residual and solubility mechanisms become more effective with time (Lemieux, 2011). No single and independent trapping mechanism can provide adequate sealing and trapping capacity for geological storage. Instead, the combination of physical and geochemical trapping mechanisms controls the effectiveness of a CO_2 geological storage site. Since the physical behavior of injected CO_2 changes over the time (section 1.2), so the importance of different trapping mechanisms changes over time as well (Figure 1.3). Each of these trapping mechanisms is briefly described below.

1.3.1 *Structural and stratigraphic trapping*

In the structural/stratigraphic trapping mechanism, buoyant CO_2 is physically confined beneath a low permeability sealing unit (e.g., shale, silt) that is geologically formed by folding and/or sealed fault(s). Pure structural trapping exists where there is vertical and lateral closure. In the stratigraphic trapping, there is no lateral confinement (Lemieux, 2011). At early stages of injection, structural/stratigraphic trapping mechanisms provide the majority of the CO_2 retention (Figure 1.3) (IPCC, 2005).

1.3.2 *Hydrodynamic trapping*

Hydrodynamic or solubility trapping occurs when CO_2 dissolves partially or completely into formation water below a stratigraphic trap and migrates slowly with formation water over great distances (Bachu et al. 1994). The time that dissolved CO_2 needs to reach the surface could be very long, for example, millions of years (Bachu et al. 1994) and this time is considered long enough to ensure the safety of the storage complex (Lemieux, 2011).

1.3.3 *Residual trapping*

Residual trapping occurs when non-wetting fluid (CO_2) no longer forms a continuous phase and CO_2 saturation will reach the residual saturation (Lemieux, 2011). In this way, CO_2 is retained in the pore space by capillary forces (IPCC, 2005). A significant amount of CO_2 could become immobile during this process (Obdam et al., 2003; Kumar et al., 2005).

1.3.4 *Mineral trapping*

Mineral or geochemical trapping mechanism occurs when supercritical CO_2 reacts with aquifer materials and precipitates a solid CO_2 phase (e.g., calcite, magnesite, etc.) in the pore space (IPCC, 2005). Mineral trapping is a very slow process, taking hundreds, thousands or even millions of years (IPCC, 2005), thus it is not effective at early stages. This mechanism is considered as the most permanent form of CO_2 trapping.

1.4 Numerical simulation approach

Numerical models are helpful to predict the long-term behavior of the storage formation in response to CO_2 injection. There are numerous parameters that can be predicted using numerical simulations such as changes in the reservoir pressure; CO_2 plume distribution within the storage formation; volumetric brine displacement in lateral and vertical directions; long-term dissolution of CO_2 in the formation water; and the integrity of sealing layers to prevent CO_2 and brine leakage from the reservoir formations. In addition, numerical simulations are important to design the cost-effective monitoring programs, because the results will influence the location of monitoring wells and soil gas/water measurements (IPCC, 2005).

Before reviewing the approach taken for this project, a review of some important CCS projects and their simulation work is warranted.

1.5 Previous CCS projects

A brief review of previous numerical studies conducted at CCS projects (modeling) will be presented to set the stage for the simulations conducted for this project. The impact of CO_2 injection in deep saline aquifers has been studied considerably to determine the near-field and far-field impacts of CO_2 injection in geological formations. Yet, much remains to be done. Table 1.1 represents the summary of the studies addressing the far-field impacts of CO_2 storage (Lemieux, 2011). Table 1.2 also shows the some of the most important large-scale CCS projects in the world[1].

Nicot (2008) conducted the first quantitative study on the large-scale impact of CO_2 injection in deep saline aquifers. He studied CO_2 injection into the Texas Gulf Coast Basin by using a well-calibrated 3D MODFLOW model to simulate the impact of CO_2 injection into 50 wells over 50 years. Two different injection rates were considered in this study as one and five million tonnes (Mt) CO_2 per year/well. He determined that the average water level rise in the unconfined section of the overlying aquifer was 1 and 15 metres respectively. Furthermore, base flow to surface-water bodies did not increase in the base-case scenario but it would be doubled for the higher injection rate. This study showed that

[1] https://www.globalccsinstitute.com/projects/large-scale-ccs [Last accessed: 2016.01.10]

the MODFLOW model is able to calculate the head rise beyond the injection zone where only one phase is present. However, it is not able to simulate the multiphase fluid flow at the regions near the injection zone where two phases are present.

Birkholzer et al. (2009) studied the impact of CO_2 injection in a generic stratified system particularly the interlayer communications between low permeability units and aquifers. This study explicitly modelled the spatial evolution of CO_2 plume with the TOUGH2-ECO2N multiphase flow simulator (Pruess, 2005, Pruess et al., 1999). Vertical migration of and the intra-layer movement of brine is considered in this study. Their results showed considerable pressure buildup (0.7 bar; equivalent to 7 metres of freshwater) in the storage formation is predicted but the lateral brine displacement is negligible. This study also determines the impacts of different seal permeability on the reservoir pressure and lateral and vertical brine migration comprehensively. However, these results were only simulated and not based on any field data.

A site-specific basin-scale impact of CO_2 in the Mt. Simon Aquifer in the Illinois Basin was investigated by Birkholzer et al. 2008b; Birkholzer and Zhou 2009; Zhou et al. 2010. The Illinois Basin hosts a CO_2 storage demonstration project (Illinois Basin-Decatur project) located at the Archer Daniels Midland site in Decatur (Lemieux, 2011). Birkholzer used TOUGH2-ECO2N to simulate the multiphase flow through the Mt. Simon aquifer. The CO_2 injection scenario is that 5 Mt CO_2 per year will be injected using 20 wells at the centre of the basin with a lateral distance of 30 kilometres between the injectors. Carbon dioxide will be injected into the Mt. Simon aquifer, which is 300-730 metres thick at a depth of 1200-2700 metres. Their results showed that there is no CO_2 leakage through the low-permeability caprock. They concluded that the lateral migration of CO_2 after 200 years becomes limited as the CO_2 saturation reached the residual saturation and eventually becomes immobile. Unlike the CO_2 plume, the pressure buildup moves further and faster. A pressure change of 1 bar and 0.1 bar (equivalent to 10 metres and 1 metre of freshwater) were simulated at lateral distances of 150 and 300 kilometres away from the injection area respectively. It was also predicted that there will be an upward brine migration through the Eau Claire sealing layer due to pressure buildup in the Mt. Simon aquifer. However, most of the brine migration occurs above the injection area where the overlying aquifers are not used. A smaller fraction of brine leakage into the overlying fresh water aquifers occurs in northern Illinois but the impact on the salinity would be smaller than that caused by the historic pumping of the freshwater resources in the area (Birkholzer et al. 2008b; Birkholzer and Zhou 2009; Zhou et al. 2010). However, this study does not evaluate the CO_2 injection impacts on the layers above the uppermost sealing unit within the Illinois Basin.

Far-field impacts of CO_2 injection were conducted by Yamamoto et al. (2009) in the Tokyo Bay area also using the TOUGH2-MP-ECO2N. This study also investigated the impacts of CO_2 injection on the regional groundwater flow system. Simulations were conducted for 1000 years for carbon dioxide injection at a rate of 1 Mt CO_2 per year into an array of 10 boreholes. Simulations predicted that pressure could increase up to 1.5 bar (equivalent to 15 metres of freshwater) into the overlying aquifers close to the injector. In addition, groundwater discharge to the shallow aquifers will increase up to few millilitres per year due to CO_2 injection, so brine displacement is not a major concern in the Tokyo Bay area. However, the sensitivity analysis showed that simulated results rely heavily on parameters such as hydraulic conductivity of caprock and pore compressibility that are uncertain. However, the model calibration against observed heads has not been performed in this study.

Dong et al. (2009) evaluated the potential impact of CO_2 injection in the Songliao Basin in China on the fresh shallow water aquifers. They applied the same approach as Zhou et al. (2010) and Yamamoto et al. (2009) used to model both brine displacement and CO_2 plume development. Their main conclusion showed that the pressure in upper aquifer could increase up to 2 bar and highly depends on the caprock permeability. However, the injection impacts on the layers above the sealing unit have not taken into account.

Since this study only focuses on the carbon storage in geological formations, the operated Enhanced oil recovery (EOR) projects are beyond the scope of this study. Important large-scale non-EOR geological CO_2 storage projects that contributed toward reducing CO_2 emissions are Sleipner, Snohvit, In Salah, Quest, Gorgon, and Aquistore that are shortly described as follows:

The Sleipner project is an offshore CCS project operated by Statoil located in the Norwegian North Sea, 250 kilometres from the west coast of Norway. Injection of CO_2

started in 1996 and one million tonnes of CO_2 is injected per year in the Utsira Formation–a fine to medium grained poorly consolidated sandstone aquifer−which is located 700-1000 metres below the sea floor. Cavanagh (2013) introduced a benchmark model for the CO_2 site by using a black oil model (Eclipse 100). The Sleipner Benchmark introduces a numerical grid and geological description of the upper part of the Utsira Formation, based on high-resolution 4D seismic mapping of the uppermost layers of CO_2 over the period 1999-2008. This allowed for calibrated simulations of a decade of plume dynamics, and prediction of both free phase and dissolved CO_2 distributions (Cavanagh, 2013). According to their simulations, CO_2 plume is much closer to a stable distribution and is likely to further stabilize due to significant dissolution in the decades immediately following injection. Results also showed that most of the injected carbon dioxide becomes accumulated at the top of the reservoir formation under the sealing unit, a few years after injection stops.[2]

The Snohvit project was an offshore CCS project managed by Statoil in the Barents Sea in Norway. The carbon dioxide was captured at the LNG plant onshore and transported to the subsea. Injection started in April 2008 at a rate of 700,000 tonnes per annum into the Tubaen Formation located 2600 metres below the sea floor. Estublier et al. (2009) conducted a long-term simulation of CO_2 into a deep (2700 metres) saline formation in the Snohvit field for a period of 1000 years. They considered several scenarios to analyse different possible CO_2 migration pathways by focusing on the sealing capacity of the main faults and of the saline formation caprock. According to their simulations, CO_2 plume behavior is controlled by the fault permeability. If the faults are assumed to be sealed, CO_2 remains trapped within the reservoir and pressure increases significantly while permeable faults allow CO_2 to migrate away from the injector (Stublier et al., 2009). However, the injection into the Tubaen Formation was stopped after 3 years in April 2011 due to pressure buildup that impacted the injectivity of the reservoir formation. The CO_2 injection continued in the Sto Formation and by early 2013, around 2 million tonnes of carbon dioxide was stored.

[2]http://www.statoil.com/en/TechnologyInnovation/NewEnergy/Co2CaptureStorage/Pages/SleipnerVest.aspx [Last accessed: 2015.11.02]

Geophysical investigations such as 4D seismic monitoring confirmed no leakage into the overlying sealing layers.[3]

The InSalah CCS project started in 2004 is located in Krechba, Algeria and is a joint venture between British Petroleum (BP), Statoil, and Sonatrach. The carbon dioxide was separated from the produced natural gas and re-injected at a depth of 1880 metres into the Krechba Formation which is 20 metres thick. Carbon dioxide was injected through the long-reach horizontal wells. Around 3.8 million tonnes of CO_2 was injected and stored from 2004 to 2011. The storage performance has been monitored using geological and geochemical techniques including time-lapse seismic, microseismic, wellhead sampling, InSAR satellite data and core analysis (Ringrose et al., 2013). However, the CO_2 injection was suspended in June 2011 due to concerns about the integrity of the sealing unit. Future injection strategy is under review.[4]

The Gorgon CO_2 injection project is located on the Barrow Island, off Australia's northwest coast operated by Chevron. Once underway, Gorgon will be the largest geological CO_2 storage project in the world with the rate of 3.4 to 4 million tonnes of CO_2 per year. Carbon dioxide is separated at the liquefied natural gas (LNG) power plant and transported by pipeline to the injection sites to be injected into the Dupuy Formation through nine injection wells. The reservoir formation has adequate permeability for injectivity. The storage formation is overlain by several sealing layers up to the surface. In order to reduce the pressure buildup in the reservoir, four water production wells are designed to produce formation water and manage the reservoir pressure. The produced water will be injected into the overlying Barrow Group. Simulation results indicated that the CO_2 plume movement is influenced by water off-take from the reservoir is rapid during the injection but limited following site closure. An on-going monitoring program including seismic surveys, soil gas sampling and observation wells will be applied to determine the plume migration into the reservoir.[5]

---

[3] http://www.statoil.com/en/TechnologyInnovation/NewEnergy/Co2CaptureStorage/Pages/Snohvit.aspx [Last accessed: 2016.01.20]

[4] https://www.globalccsinstitute.com/projects/salah-co2-storage [Last accessed: 2016.01.20]

[5] https://unfccc.int/files/methods/other_methodological_issues/application/pdf/gorgon_co2_injection_project_new.pdf [Last accessed: 2016.02.11]

The Quest CO_2 injection project is a joint venture between Shell Canada Energy, Chevron Canada Limited, and Marathon Oil Canada Corporation.[6] The injection site is located near Fort Saskatchewan, Alberta in Canada and is designed to capture and permanently store about 1.2 million tonnes of CO_2 each year. Carbon dioxide is injected up to three injection wells into the Basal Cambrian Sandstone that is a deep saline geological formation at a depth of 2100 metres. The reservoir formation is overlain by a low permeability shale layer. The simulation of CO_2 injection was conducted for a 25 year period, showing that the pressure will increase after 25 years and pressure front will extend beyond the area of the CO_2 plume. According to their results, the radius of influence for pressure will depend mainly on the total injected CO_2 volume, formation compressibility, and maximum allowable bottom-hole pressure. Furthermore, the pressure response in the storage formation is seen to extend 20 to 40 kilometres away from the injection wells[6].

1.6 Purpose of the study

Previous modeling studies at the CO_2 injection sites have focused on the CO_2 plume matching monitoring (i.e., seismic) or ignored overlying aquifers. Large scale physical impacts of the CO_2 injection into the saline aquifers such as pressure buildup, lateral and vertical brine displacements are relatively unstudied. The novelty of this work is that the simulated bottom-hole pressure (BHP) is calibrated against the actual BHP values obtained from the observation well.

There are few CCS projects in the world (i.e., Weyburn, Aquistore, Quest) that are equipped with such facilities to measure the bottom-hole pressure directly.

In addition, this study evaluates the impacts of the injection on the entire hydrostratigraphic profile in the Williston Basin (i.e., from the Precambrian bedrock up to the ground surface) while other studies have only focused on the storage formation and its overlying caprock.

[6] http://s05.static-shell.com/content/dam/shell-new/local/country/can/downloads/pdf/aboutshell/our-business/oil-sands/quest/01-quest-vol-1-mainreportprojectdescription.pdf [Last accessed: 2016.02.11]

This study quantifies the physical impacts of the CO_2 injection on the Cambro-Ordovician Aquifer at the Aquistore injection site with particular emphasis on the distribution of CO_2 plume along with pressure buildup and brine displacement.

1.7 Study Area

The Aquistore CO_2 injection site is located in southeastern Saskatchewan, Canada approximately 10 kilometres outside of the community of Estevan and few kilometres from the SaskPower's Boundary Dam facilities (Figure 1.4). Aquistore is designed to demonstrate the safety of storing carbon dioxide in deep saline Cambro-Ordovician aquifers within the Williston Basin and will serve as the slipstream storage for the first commercial-scale post-combustion CO_2 capture, transportation, utilization and storage in the world, based on a coal-fired power plant. The storage complex includes the Cambro-Ordovician aquifers (i.e., Deadwood formation and the Black Island Member of the Winnipeg Formation) and major sealing units including the Icebox shale as a primary sealing unit lying above the storage formation, the Prairie Formation that is the secondary sealing unit and shales of the Colorado Group. Results obtained from the Aquistore project as well as the derived technologies will then be globally applicable for other geological CO_2 storage sites.[7]

Carbon dioxide will be injected in the Cambro-Ordovician aquifers from the injection well that is designed for the rate of 1000 tonnes per day. The injection well has the total vertical depth of 3396 metres and was completed in September 2012. In order to examine the migration of CO_2 within the storage formations, the observation well with a total vertical depth of 3400 metres was also drilled located 150 metres away from the injection well and is instrumented with fluid samplers, geophones, temperature and pressure gauges.[8] The data collected from the observation well will also be used for model calibration and verification.

1.8 Thesis Questions

There are number of concerns associated with CO_2 sequestration in deep saline aquifers that this study tries to address:

---

[7] http://aquistore.ca/project [last accessed: 2016.02.11]
[8] http://aquistore.ca/project [last accessed: 2016.02.11]

- What will be the CO_2 plume distribution at the end of the injection?
- What will be the pressure plume distribution at the end of the injection?
- Will the pressure buildup caused by injection impact the overlying fresh water aquifers in the study area?
- Will there be any displaced brine that will reach the up dip fresh water resources?
- How much brine will be laterally and vertically displaced at the end of the injection?
- Is the Aquistore injection site potentially able to store CO_2 for a long period of time?
- Will the storage complex be able to safely store CO_2, or will there be any CO_2 leakage from the reservoir?

1.9 Outline

These questions will be answered in the following:

- **Chapter 2 : Methodology**

  This chapter first provides the regional geology and hydrogeology of the study area. Next, the numerical conceptual and grid model approaches, as well as the input parameters for this simulation, are explained. In addition, a background of single and multiphase flow through porous media, corresponding governing equations, and the TOUGH2-ECO2N simulator are included.
- **Chapter 3: Development of Optimal Model and Detailed Extended Numerical Approaches**

  This chapter provides approaches to developing the optimal model and evaluates the effects of different grid refinements and boundary conditions on the simulation results. Furthermore, it evaluates the capability of the MODFLOW to simulate the CO_2 injection process.
- **Chapter 4: Numerical Simulation of CO_2 Injection Results**

  This chapter presents the results of the optimal model of CO_2 injection into the Cambro-Ordovician Aquifer. It explains the physical impacts on the reservoir formations including lateral and vertical pressure buildup and brine displacement as well as CO_2 plume distribution through the injection layers during and after the injection period.

- **Chapter 5: Discussion and Conclusions**

  This chapter represents the conclusions of this study and provides the answers to the questions outlined in Chapter One. Furthermore, some suggestions are also provided for future works.

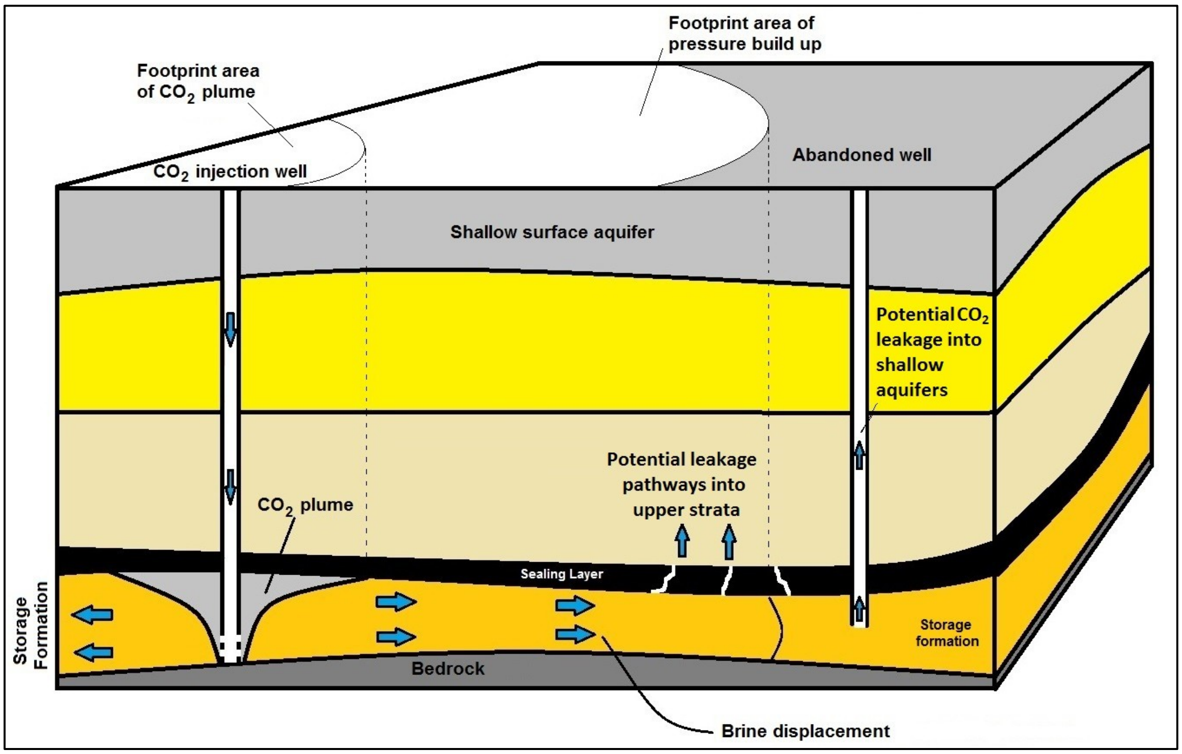

Figure 1.1 Schematic of CO_2 injection well, the extent of the CO_2 plume, pressure plume and potential impacts of large scale CO_2 injection into the geological formations.

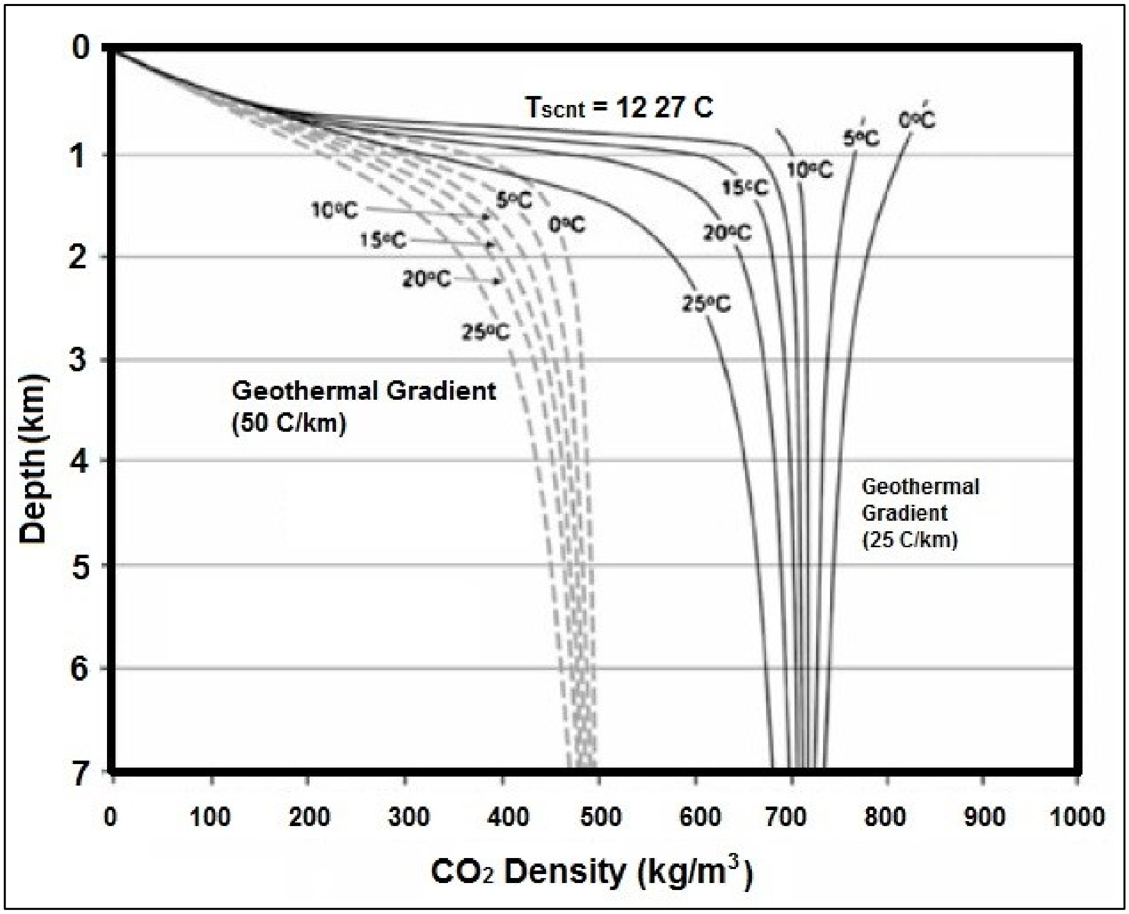

Figure 1.2 Variation of CO_2 density with depth in sedimentary basins for various surface temperatures (Modified after Bachu, 2003)

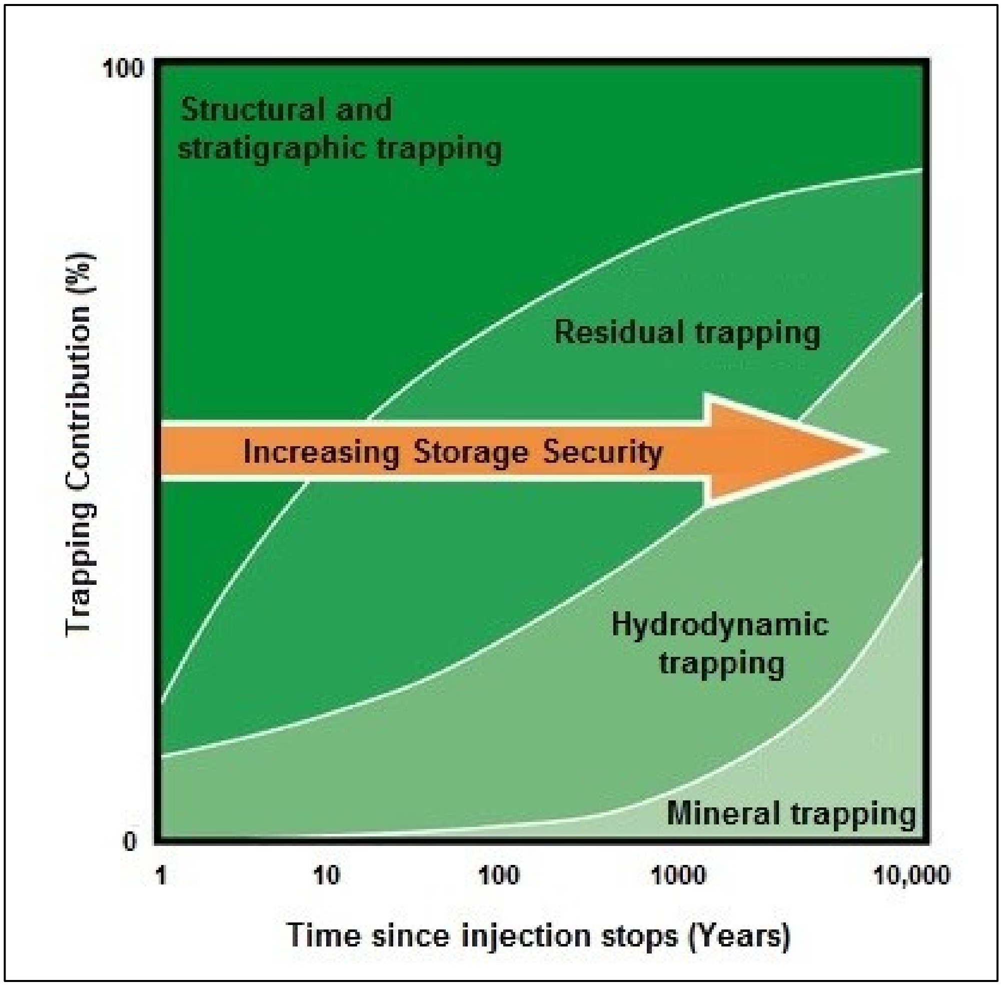

Figure 1.3 Storage of CO_2 as a function of time for different trapping mechanisms (Modified after IPCC, 2005)

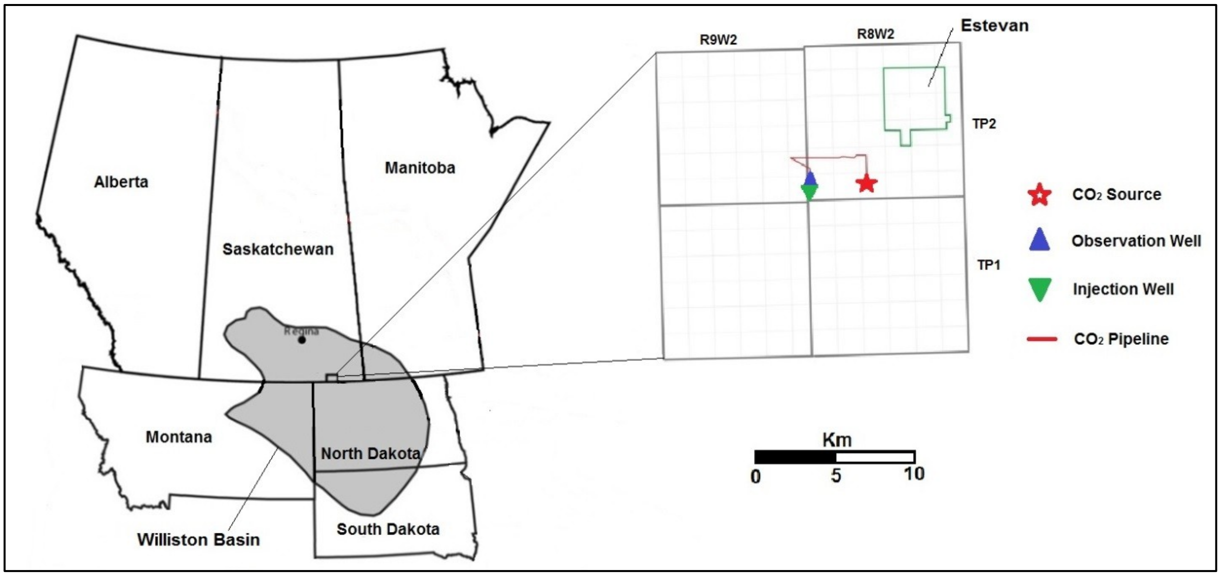

Figure 1.4 Location map of the Williston Basin and Aquistore injection site (Modified after Rostron et al. 2014)

Table 1.1 Summary of the studies addressing the large scale impacts of CO_2 storage (Modified after Lemieux, 2011)

Authors	**Simulator**	**Location**	**Injection rate**	**Duration**
Nicot (2008)	MODFLOW	Gulf Coast Basin, USA	1 and 5 Mt/year/well (50 wells)	50 years
Birkholzer et al. (2009)	TOUGH2-ECO2N	Generic	1.52 Mt/year (1 well)	30 years
Birkholzer and Zhou (2009)	TOUGH2-ECO2N	Illinois Basin, USA	5 Mt/year/well (20 wells)	50 years
Yamamoto et al. (2009)	TOUGH2MP/ECO2N	Tokyo Bay, Japan	1 Mt/year/well (10 wells)	100 years
Dong et al. (2009)	TOUGH2-ECO2N	Songliao Basin, China	1 Mt/year (1 well)	100 years

Table 1.2 The worldwide CCS projects (2016)[9]

Project name	Location	Operation date	Injection capacity (Mtpa)	Storage type
InSalah	Algeria	2004	3.8 (suspended in 2011)	Geological Storage
Quest	Canada	2015	1.0	Geological Storage
Sleipner	Norway	1996	0.9	Geological Storage
Snøhvit	Norway	2008	0.7	Geological Storage
Gorgon	Australia	2017(estimated)	3.4-4	Geological Storage
Illinois Decatur	United States	2016	1	Geological Storage
Aquistore	Canada	2014	1	Geological Storage
Weyburn	Canada	2005	2-3	CCS/EOR

[9] https://www.globalccsinstitute.com/projects/large-scale-ccs [Last accessed: 2016.01.10]

2 Methodology

This chapter provides the regional geology and stratigraphy of the study area within the Williston Basin as well as the hydrogeology of the Cambro-Ordovician Aquifer both of which were used to define and populate the model domain.

2.1 Regional geology and stratigraphy

The Williston Basin is a large sedimentary basin covering Montana, North Dakota, South Dakota, Manitoba and southern Saskatchewan (Palombi, 2008) (Figure 1.4). It lies above the Precambrian geologic basement. Figure 2.1 illustrates the stratigraphy and hydrostratigraphic units of the Williston Basin. The basin has an oval shape and covers approximately 518,000 square kilometres (Brown and Brown, 1987). The Precambrian bedrock lies about 4900 metres below the ground surface in the center of the basin (Gibson, 1995). The regional geology of the Williston Basin in the United States has been widely studied by Gerhard et al., 1982; Peterson and MacCary, 1987; Gerhard and Anderson, 1988 and many others. Mossop and Shetsen (1994) also investigated the geology of Williston Basin in Canada.

More geological characterization conducted by Whittaker et al., 2004; Christopher et al., 2006; Halabura, 2006; Kreis et al., 2006; Nicolas, 2006 have focused on the definition of a geometry and regional stratigraphic framework for selected parts of the basin (i.e. northeastern margin) in fulfillment of stratigraphy, natural gas and petroleum studies and CO_2 storage in the provinces (Palombi, 2008).

The targeted injection layers in the Aquistore project are the Deadwood and Winnipeg Formations. These are the deepest sedimentary formations above the Precambrian crystalline bedrock within the Williston Basin in the Estevan area more than 3000 metres deep. These layers are saturated with brine (i.e., TDS>100,000 mg/Litre) (Palombi, 2008). The reservoir formations are overlain by multiple sequences of aquifer-aquitard systems up to the surface (Palombi, 2008).

Here an overview of the storage complex stratigraphy including the Deadwood and Winnipeg aquifers, the Icebox and the Prairie Formation as well as the Colorado Group is presented.

The Deadwood Formation consists of fine- to coarse-grained Cambrian sandstones with some interbedded shale and siltstone layers representing near-shore sandstone from a Precambrian shield source in the east (Kent, 1994; Potter, 2006). It has the maximum thickness of 270 metres in the center of the basin including siliciclastic rocks of quartz arenites, siltstones, quartz wackes and lesser carbonate rocks (LeFever et al., 1987 and Paterson, 1988) but it is 145 metres thick at the Aquistore injection site. Porosity and permeability values of the Deadwood Aquifer typically range from 10-15% and 300 millidarcy respectively (Houseworth et al., 2011).

The Winnipeg Formation consists of two units: the lower (Black Island Member) which is continuous, well-sorted quartz-rich sandstone; and the upper (Icebox Member) that consists mostly of shale with some interbedded sandstone (Nicolas and Barchyn, 2008). The Black Island and Icebox Members are 44 and 25 metres thick respectively at the injection well.

The Icebox Member of the Winnipeg Formation is considered to be the primary sealing unit lying above the storage formations. It is composed of marine shale and siltstone and ranges from 43 metres thick in the centre of the basin and becomes thinner outward to 29 metres in southeast Saskatchewan (Paterson, 1988). This layer serves as an effective hydraulic barrier separating the overlying Red River Formation from the Black Island Sandstone (Ferguson et al., 2007).

The Prairie Formation is the most significant evaporite in the basin (lying above the Winnipegosis Formation) and is mined for potash (Palombi, 2008). The Prairie Formation is 153 metres thick and is composed of halite, carnallite, and sylvite with dolomitic and anhydrite seams (Kendall, 1975; Reinson and Wardlaw, 1972; Gerhard and Anderson, 1988; Kreis et al., 2003).

The Colorado Group is a stratigraphic unit of Cretaceous age in the Western Canadian Sedimentary Basin and is 187 metres thick at the injection well. The Colorado Group mostly consists of shale (Palombi, 2008) and lies below the Belly River Aquifer that is the main fresh water aquifer in the Aquistore site.

2.2 Hydrogeology

Previous regional groundwater mapping in the Williston Basin proposed that all formation waters flow from SSW to NNE across the basin (Downey, 1984a, b; Hannon, 1987; DeMis, 1995; Bachu and Hitchon, 1996). The source of water is meteoric waters which enter the basin in the uplifted recharge zones (e.g., the Black Hills, the Bighorn and the Beartooth Mountains) in the south-west. The groundwater then discharges to the northeast of the Manitoba Escarpment (Palombi, 2008).

The Deadwood-Winnipeg interval contains total dissolved solids (TDS) of 330 g/L in the Aquistore site (Palombi, 2008). The amount of TDS increases toward the deeper portions of the Cambro-Ordovician aquifer in the Williston Basin (Brunskill, 2006). Therefore, the regional groundwater flux within the basin may be relatively low and negligible due to the high density of brine (Houseworth et al. 2011). Figure 2.2 and 2.3 illustrate the structural cross section of the Williston Basin and total dissolved solids (TDS) map in the Cambro-Ordovician aquifer respectively.

2.3 Single phase fluid flow through porous media

Single phase fluid flow through porous media is expressed by combining Darcy's law (Eq. 2-1) and the continuity equation (Eq. 2-2) (Scheidegger, 1957).

$$q = -\frac{k}{\mu}(\nabla P - \rho g) \tag{2-1}$$

$$-\emptyset \frac{\partial \rho}{\partial t} = \nabla(\rho q) \tag{2-2}$$

Where q is specific discharge, k is permeability, μ is fluid viscosity, ∇P is the pressure gradient, ρ is fluid density, g is acceleration gravity, $\emptyset$ is porosity, and t is time.

Fluid flow through the pore spaces is controlled by the rock properties such as porosity ($\emptyset$) and permeability (k). The porosity represents the ratio of voids to the total volume and determines the space available for storing fluid within the pores. Permeability is the ease with which fluid can transport through the porous media (Schwartz and Zhang, 2003). Poorly-sorted rocks with smaller grain sizes and high clay/cement content typically have a lower permeability (k_h) (Byrnes et al., 2009).

2.4 Multiphase fluid flow through porous media

When two or more phases are present, part of the pore space is occupied by one fluid and the rest of pore space will be filled with other phases. Fluids with higher saturation are more continuous, so they flow across the porous medium easier and faster (Scheidegger, 1957). Thus, this leads to the concept of relative permeability which is the ratio of the effective permeability of a fluid at a given saturation to intrinsic permeability. The effective permeability is a measure of the conductance of a porous medium for one fluid phase when the medium is saturated with more than one fluid (Amyx et al., 1960). For supercritical CO_2 -water system, Darcy's law, and continuity equations are modified and defined as follows:

$$q_{CO2} = -K\frac{k_{rCO2}}{\mu_{CO2}}(\nabla P_{CO2} - \rho_{CO2}.g) \tag{2-3}$$

$$q_l = -K\frac{k_{rl}}{\mu_l}(\nabla P_l - \rho_l.g) \tag{2-4}$$

$$-\emptyset\frac{\partial(\rho_{CO2}.S_{CO2})}{\partial t} = \nabla(\rho_{CO2}.q_{CO2}) \tag{2-5}$$

$$-\emptyset\frac{\partial(\rho_l.S_l)}{\partial t} = \nabla(\rho_l.q_l) \tag{2-6}$$

Where k_{rCO2} and k_{rl} are relative permeability of CO_2 and water respectively, S_{CO2} and are S_l are the saturation of CO_2 and water respectively ($S_{CO2} + S_l = 1$) and P_{CO2} and P_l are CO_2 and water pressures in the system.

For carbon dioxide sequestration and prior to injection (Figure 2.4a), the host aquifer is fully saturated with formation water (i.e., brine). When CO_2 is injected, two fluids will compete to occupy and flow through the pore spaces (Figure 2.4b). After the injection, CO_2 no longer forms a continuous phase and reaches the residual saturation and becomes immobile (Figures 2.4c and 2.4d).

When supercritical CO_2 dissolves in water, two miscible fluid phases are generated: 1) the formation water which is not saturated with CO_2 and 2) formation water saturated with dissolved CO_2. The mixing and mass transport of the dissolved species are described by advective-dispersion equation (Scheidegger, 1957; Aggelopoulos et al., 2012).

$$\frac{\partial C_{CO2}}{\partial t} = D\nabla C_{CO2} - \frac{q}{\emptyset}.\nabla C_{CO2} \pm (\frac{\partial C_{CO2}}{\partial t})_{rxn} \quad (2\text{-}7)$$

Where; C_{CO2} is the concentration of dissolved carbon dioxide in the formation water, $(\frac{\partial C_{CO2}}{\partial t})_{rxn}$ is the change in CO_2 concentration during the reaction and D is the hydrodynamic dispersion.

Equations 2-3 to 2-7 are governing equations that are used to the simulation of the multiphase of fluid flow and transport through the porous media. The reservoir and its overlying formations are discretized into cells or grids (Representative Elementary Volume or REV) and values of permeability, porosity, capillary pressure, relative permeability, and saturation are assigned into each grid block. This represents an average over a collection of pore spaces within the scale of the grid block (Doughty et al., 2008).

2.5 Factors influencing CO_2 distribution in porous media

2.5.1 *Permeability (k_h and k_v)*

Rocks with smaller grain size, high cement content and poorer sorting have a lower permeability (Byrnes et al., 2013). In the CO_2 sequestration process, vertical permeability (k_v) has a significant impact on the mobility of CO_2 (Hermanson, 2014) because carbon dioxide flow occurs mainly in the vertical direction. Flow is either upward due to buoyancy, or downward by convective flow process (i.e., Chapter 1.2).

2.5.2 *Porosity ($\emptyset$)*

Porosity determines the space available for storing carbon dioxide in a reservoir formation. Lateral migration of CO_2 plume will decrease in high porosity formations because more pore volumes are available to be occupied by injected CO_2. In addition, pressure buildup caused by injection is lower in high porosity formations since excess pressure can be released easier through the aquifer (see sensitivity analysis in chapter 3).

2.5.3 *Capillary Pressure and Relative Permeability*

Capillary pressure is controlled by grain size, pore throat and connectivity of the pore spaces. Rocks with large and connected pores have smaller grain surface areas and represent lower irreducible water content (S_{ir}) while rocks with smaller and poorly connected pore spaces have higher S_{ir}. Having higher irreducible water content decreases the mobility of CO_2 through the pore spaces due to the smaller spaces available for CO_2 migration (Hermanson, 2014).

The relative permeability for liquid phase is calculated by van Genuchten's equation (1980). Gas capillary pressure is calculated by Corey's equation (1954). The relative permeability and capillary pressure depend on the saturation of each fluid in the system as well as drainage and imbibition process due to hysteresis (Hillel, 1980; Osman, 2013).

Liquid relative permeability (van Genuchten, 1980):

$$k_{rl} = \sqrt{S}\left(1 - \left(1 - (S)^{1/m}\right)^{m}\right)^{2} \tag{2-8}$$

Where;

$$S = (S_l - S_{ir}) / (S_{ls} - S_{ir}) \tag{2-9}$$

k_{rl} is relative permeability values for liquid phase (water), S_l is the liquid saturation, S_{ir} is the irreducible liquid saturation and S_{ls} is the liquid saturation when the pore space is fully saturated by the wetting phase (normally is set to 1).

The exponent m controls the slope (shape) of the liquid relative permeability and capillary pressure curves (van Genuchten, 1980) and will be explained in following sections, P_e is capillary entry pressure and P_c is capillary pressure at a given saturation.

Capillary pressure (van Genuchten, 1980):

$$P_c = -P_e\left[(S)^{-1/m} - 1\right]^{1-m} \tag{2-10}$$

Gas relative permeability (Corey, 1954; Pruess et al., 1999):

$$k_{gr} = \left(1 - \hat{S}\right)^{2}(1 - \hat{S})^{2} \tag{2-11}$$

Where;

$$\hat{S} = (S_l - S_{ir}) / (1 - S_{ir} - S_{gr}) \tag{2-12}$$

Where k_{rg} is relative permeability for gas phase (CO_2) and S_{gr} is the residual gas saturation.

When CO_2 is injected into a fully saturated Representative Elemental Volume (REV), it displaces the water in the pore space (Figure 2.4b). This process is called drainage because a non-wetting phase (i.e., CO_2) invades the pore space and moves the wetting phase (i.e., brine) away from the pore. Capillary pressure increases during the drainage process. Drainage continues until the maximum gas saturation and minimum water saturation is reached. However, some of the water remains in the pore space and is held by capillary forces that are defined as irreducible water saturation (S_{ir}).

After injection, saturation of the wetting phase increases and capillary pressure decreases. This process is called imbibition. During the imbibition, CO_2 saturation decreases until the minimum gas saturation and maximum water saturation is reached. The amount of CO_2 which is left behind is termed maximum residual gas saturation (S_{grM}). Figure 2.5a shows the capillary pressure curves for drainage and imbibition processes.

Relative permeability curves for water and CO_2 are also illustrated (Figure 2.5b). During the drainage process, when the CO_2 saturation increases, the relative permeability to CO_2 increases, showing that the non-wetting phase can flow easier and faster through the pore space, while during the imbibition process the relative permeability to CO_2 decreases and the relative permeability to water increases. The difference between the curves is called hysteresis (causing by the irreducible water and residual gas saturations).

Using hysteretic capillary pressure and relative permeability curves requires additional parameters and is difficult, so for more simplicity, the equations of the non-hysteretic Corey (1954) and van Genuchten (1980) functions were used in this study. Figure 2.6 illustrates the non-hysteretic curves for the capillary pressure and relative permeability used in this study.

2.5.4 *van Genuchten factor (m)*

The shape or slope of the capillary pressure and liquid relative permeability curves in van Genuchten function (1980) is controlled by the *m* factor and generally reflects how poorly or well-sorted a material is (Morgan and Gordon, 1970; Krevor et al., 2012). In poorly-sorted materials with more clay/cement content and a wide range of pore sizes, the capillary pressure curve tends to have greater change with respect to the saturation. Therefore, smaller *m* value is considered for low porosity and permeability materials. In well-sorted materials such as coarse-grained sandstone higher *m* value is considered indicating larger pore spaces and higher liquid permeability and smaller capillary pressure at any given saturation. Figure 2.7 represents the difference between the capillary pressure curves in two different materials.

In numerical simulation of CO_2, the value of *m* is commonly set to 0.457 (Pruess et al., 2001; Xu et al., 2003; Xu et al., 2005; Zhang et al., 2009; Yamamoto and Doughty, 2011; Kihm et al., 2012).

2.5.5 *Capillary entry pressure (P_e)*

In order to have the CO_2 flow through the saturated pore spaces, the displacement or threshold value of capillary pressure is required which is called capillary entry pressure (P_e) (Leverett, 1941). The capillary entry pressure is the required pressure for a non-wetting fluid to enter the pores. Rocks with smaller pore throats have higher P_e values, while well-sorted materials with larger pore throats have lower P_e. This parameter has a significant role in the CO_2 trapping mechanism. Low permeability formations such as shale or siltstone with high capillary entry pressure act as sealing units and are able to stop CO_2 from upward migration.

2.5.6 *Residual gas saturation (S_{gr})*

Residual gas saturation represents the volume of CO_2 trapped during the imbibition process (Figure 2.4d). When injection is stopped and CO_2 is not being replenished by further injection, the saturation of CO_2 plume will decrease. When residual saturation of CO_2 is reached, CO_2 no longer forms a continuous phase and becomes immobile.

2.5.7 *Irreducible water saturation (S_{ir})*

Irreducible water saturation is the immobile trapped water within the pore space (Figure 2.4c). Materials with heterogeneities and higher mineral surface area that water can adhere to represent higher irreducible water content (Morgan and Gordon, 1970; Perrin and Benson, 2010). In CO_2 sequestration, higher irreducible water saturation decreases the mobility of CO_2 to flow through the pore space because the higher volume of pore space is occupied by water (Hermanson, 2014).

2.6 TOUGH2 Simulator

In this study, the TOUGH2-ECO2N simulator was used to simulate the multiphase flow and transport of carbon dioxide. The spatial CO_2 plume distribution, vertical and lateral brine flux, as well as the pressure buildup in the reservoir, were simulated for both injection (30 years) and post-injection (70 years) periods. In order to visualize the simulation results, Petrasim (Thunderhead Engineering) was used as a pre- and post-processing for the TOUGH2 simulator.

TOUGH2 simulates the flow of multicomponent, multiphase fluids in porous and fractured media in one, two, and three dimensions. TOUGH2 was designed mainly to be applied in nuclear waste disposal, geothermal reservoir engineering, environmental assessment, and remediation as well as unsaturated and saturated zone hydrology (Pruess et al., 1999). TOUGH2 is designed by Lawrence Berkeley National Lab (LBNL) and was first released to the public in 1991, updated in 1994 to include conjugate gradient solvers were added for more efficiency and larger problems (Pruess et al., 2005). This code is written in FORTRAN 77, includes a comprehensive description of the thermodynamics and thermophysical properties of CO_2-brine mixtures. The ECO2N module can describe all possible phase conditions for CO_2-brine mixtures and introduces the transition between the sub and supercritical conditions as well as phase change between liquid and aqueous CO_2 (Pruess, 2005). The experimental range for temperature, pressure, and salinity conditions in TOUGH2 are within the range of 10°C ≤ T ≤ 110 °C, P ≤ 600 bar, and salinity from zero up to full halite saturation (Pruess, 2005).

2.7 Conceptual model setup

A two-dimensional radially symmetric model was designed to represent the carbon dioxide injection in the Cambro-Ordovician Aquifer at the Aquistore site (Figure 2.8). Implementing boundary conditions at the model boundaries (i.e., top and bottom) are convenient in two-dimensional models. Furthermore, since the model domain is radially symmetric and layers are assumed to be horizontal, a two-dimensional model is a better choice rather than a three-dimensional model because implementing a 3D model will only increase the simulation time.

In a 2D model (i.e., XZ grid model in this study), an injection well is typically placed in the centre of a model domain and reservoir parameters are calculated in steady state and transient state conditions for the area that is highlighted.

The simulation domain (Figure 2.9) starts from the top of the Precambrian crystalline bedrock up to the surface Glacial Till with a total vertical depth of 3345m. The final domain has 23 layers including 11 aquifers and 12 aquitards. Low permeability formations such as shale, siltstone, and salt were considered as sealing units or aquitards and high permeability formations (e.g., sandstone, limestone) were assigned as aquifers or reservoirs. The targeted reservoir formations include the Deadwood and Black Island Member of the Winnipeg Formation, capped by the Icebox Shale and sequences of sealing units up to the surface. The well log data of the injection and observation wells were used to define the thickness of each layer in the conceptual model. The model layers are assumed to be homogeneous, uniform and horizontal. Two injection horizons were considered within the Deadwood Formation (i.e., Lower and middle) with high permeability values. These horizons are separated by a low permeability sealing layer while the entire thickness of the Black Island was defined as the upper injection horizon. The total thickness of the Cambro-Ordovician Aquifer is 187 metres.

The reservoir pressure and temperature at the depth of 3345 metres are 343 bar and 120 C respectively. The geothermal temperature gradient of 2 C per 100 metres depth was assumed in this study which varies linearly from 25 C at the surface to 120 C at the bottom of the model. However, the simulations in this study are isothermal. The bottom of the reservoir formation is formed by the low permeability and porosity Precambrian crystalline bedrock, so it is assumed as no-flow boundary conditions, meaning no flow can cross the bottom of the model boundary. The lateral extent of the model domain was also set to R=50 kilometres, representing an area of $7850\,\text{km}^2$. The upper boundary was also set to the atmospheric pressure where the atmospheric conditions are present (e.g., pressure=1 bar, T=25 C). The long-term CO_2 injection is scheduled for a period of 30 years at the rate of 1000 tonnes per day followed by a 70 year post-injection period. So, the simulation totally covers a time period of 100 years.

Injecting carbon dioxide into a saline aquifer causes localized pressure buildup which expands the pore volumes for further injection. Furthermore, phase volume reduction resulting from dissolution of supercritical CO_2 into the aqueous phase also helps to accommodate carbon dioxide into the aquifer (Birkholzer et al., 2009). After injection stops, the system will return to the equilibrium state, where the system is under the initial hydrostatic pressure or steady-state conditions prior to the injection. There is no lateral variation in the model parameters, representing that the system is stagnant before the injection, so the regional groundwater flow is neglected. Top three layers of the model were assumed to be saturated with fresh water by setting the salt mass fraction to zero. Figure 2.9 illustrates the conceptual model of the study area.

2.8 Grid Design

A finer grid model allows more accurate simulations of flow and transport through the porous media but as long as the simulation time is concerned, this could be impractical especially in the case of large-scale simulations such as reservoir scale models. Therefore, the grid design needs to be a trade-off between accuracy and efficiency (Hermanson, 2014). A uniform radial spacing is a better choice for the greater distances from the injection well. However, they are not able to solve short injection periods. Longer injection and post injection scenarios are more applied when the chemical reactions between the injected supercritical CO_2 and rock materials are concerned (e.g., up to 10,000 years) (Hermanson, 2014).

The injection cell width representing the injection well was set to 0.3 metres (30 cm) and the increasing factor of 1.05 was used to radially increase the grid spacing away from the injection zone. This approach increases the computational efficiency by creating higher grid resolution at the regions in which pressure gradient and CO_2 saturation are higher (i.e., injection well). In order to have better and more accurate results the area around the observation well located 150 m from the injector was also refined (Figure 2.10).

The appropriate vertical grid spacing also needs to be applied in CO_2 injection models. Coarser vertical grid refinement tends to underestimate the extent of buoyancy driven flow, causing a reduction in the flux of upward supercritical CO_2 and eventually decreases the extent of lateral migration of carbon dioxide in the storage formation (Doughty and Pruess, 2004; Yamamoto and Doughty, 2011). In addition, carbon dioxide dissolution seems to be overestimated in coarser grid models during the short injection times because all of the liquid in the grid needs to become saturated with CO_2 before any supercritical CO_2

forms. This, in turn, leads to numerical errors that increase with increasing cell size (Audigane et al., 2007; Frykman, 2012; Green and Ennis-King, 2012, Hermanson, 2014).

2.9 Time discretization and solution control

The maximum number of time steps is controlled by the user (Zhang, 2013). However, an infinite time step scheme was used in this study. TOUGH2 allows eight iterations for each time step. As soon as the maximum number of iteration is reached, TOUGH2 automatically decreases the time steps by the factor of four (Pruess, 1999).

The stabilized bi-conjugate solver was applied in this study. This solver is a linear equation solver and reportedly converges while other solvers fail (Xu et al., 2004). The default convergence criterion in TOUGH2 is 10^{-5} and was used in this simulation. If the model is not able to achieve the convergence within eight iterations, the time step size becomes smaller and new iteration starts to reach the convergence. Other options such as upstream weighting and boundary condition interpolation were set as default. The upstream weighting is a default interface that calculates the density interfaces between the elements, average mobility as well as the relative and absolute permeability values (Pruess, 1999).

The boundary condition interpolation controls the interpolation of the CO_2 injection rate into the aquifer. The step function method was used in this study which considers the rates as the average of the table values corresponding to the beginning and end of the time step (Pruess, 1999). Table 2.1 represents the solution control for this simulation.

2.10 Boundary conditions

Two basic types of boundary conditions can be applied in TOUGH2 simulations: The Dirichlet conditions which prescribe thermodynamic conditions (e.g., pressure, temperature) at the model boundary, and Neumann conditions that prescribe fluxes of mass or heat across the surface boundaries. There is a special case in Neumann conditions in which no flow is specified across the model boundary (Pruess et al., 1999). This case is the default boundary conditions in the TOUGH2-ECO2N simulator which represents a closed system that does not allow the fluid to escape the model domain. To minimize the effect of the model boundaries on the simulations, Dirichlet conditions can be implemented. This approach assigns very large volumes (e.g., $V=10^{50}\ m^3$) to the elements at the model boundaries, so the thermodynamic properties of the boundary elements will not change during the simulation (Pruess et al., 1999). In this study, the Dirichlet conditions were assigned to the surface and lateral boundaries of the model (located 50 kilometres away from the injection well) to make sure that the model boundaries have minimum impact on the simulations. The bottom of the model was also set to the Neumann conditions to represent no flow conditions at the base of the model.

The injection cells (i.e., sources and sinks) were specified at the bottom of each injection horizon. This can be introduced either through data block GENER in the output file or by selecting the cells and specifying them as sinks and sources in PertaSim. The injection rates can also be at a constant rate or time-dependent tabular rates. Figure 2.10 illustrates the specified injection cells and rates in this simulation. Due to lower permeability and porosity of the Black Island Sandstone compare to the Deadwood Formation, lower injection rate (i.e., 2.5 kg/sec) was assigned to the upper injection horizon. Note that only the storage formations and primary sealing unit are illustrated in figure 2.10 (depth from 3345 to 3133 metres below the ground surface).

2.11 Input parameters and initial conditions

The input parameters in this study such as reservoir lithology and thickness, intrinsic permeability, porosity, residual gas and water saturations for the model layers as well as the bottom-hole pressure (BHP) and temperature were obtained from PTRC injection and observation well log data along with previous studies in the Williston Basin such as leakage risk assessment report for carbon dioxide disposal in Saskatchewan, Canada by Housworth et al., 2011. In order to calculate the capillary pressure and relative permeability, van Genuchten function was applied (van Genuchten, 1980). This function contains two fitting parameters including m and α; van Genuchten m is pore size distribution and van Genuchten α roughly represents the inverse of capillary entry pressure for the non-wetting phase (i.e., supercritical CO_2) (Birkholzer et al., 2009).

For simplification, all formations in this study were classified into four divisions: 1) RES1 represents two horizons within the Deadwood Formation, 2) RES2 represents the Black Island Member of the Winnipeg Formation, 3) SALT represents the Prairie Evaporite

Formation and is considered as the secondary sealing unit in this study, and 4) SEAL which represents all low permeability sealing units (e.g., shale, silt) within the model domain. Table 2.2 shows the input parameters assigned to the model layers.

After assigning the parameters in the model, the first task is to obtain the hydrostatic profile, including temperature, pressure, CO_2 and salt mass fractions for each element within the model domain. This can be achieved by running the simulation in the steady-state mode (e.g., no injection or production) for a very long period of time (e.g., 10,000 years). TOUGH2 generates the initial conditions as file INCON. By loading this file and re-running the model for the same time period, the simulation progresses rapidly by increasing time steps and eventually terminates after few time steps resulting in the steady state conditions which represent the hydrostatic profile prior to the transient state mode.

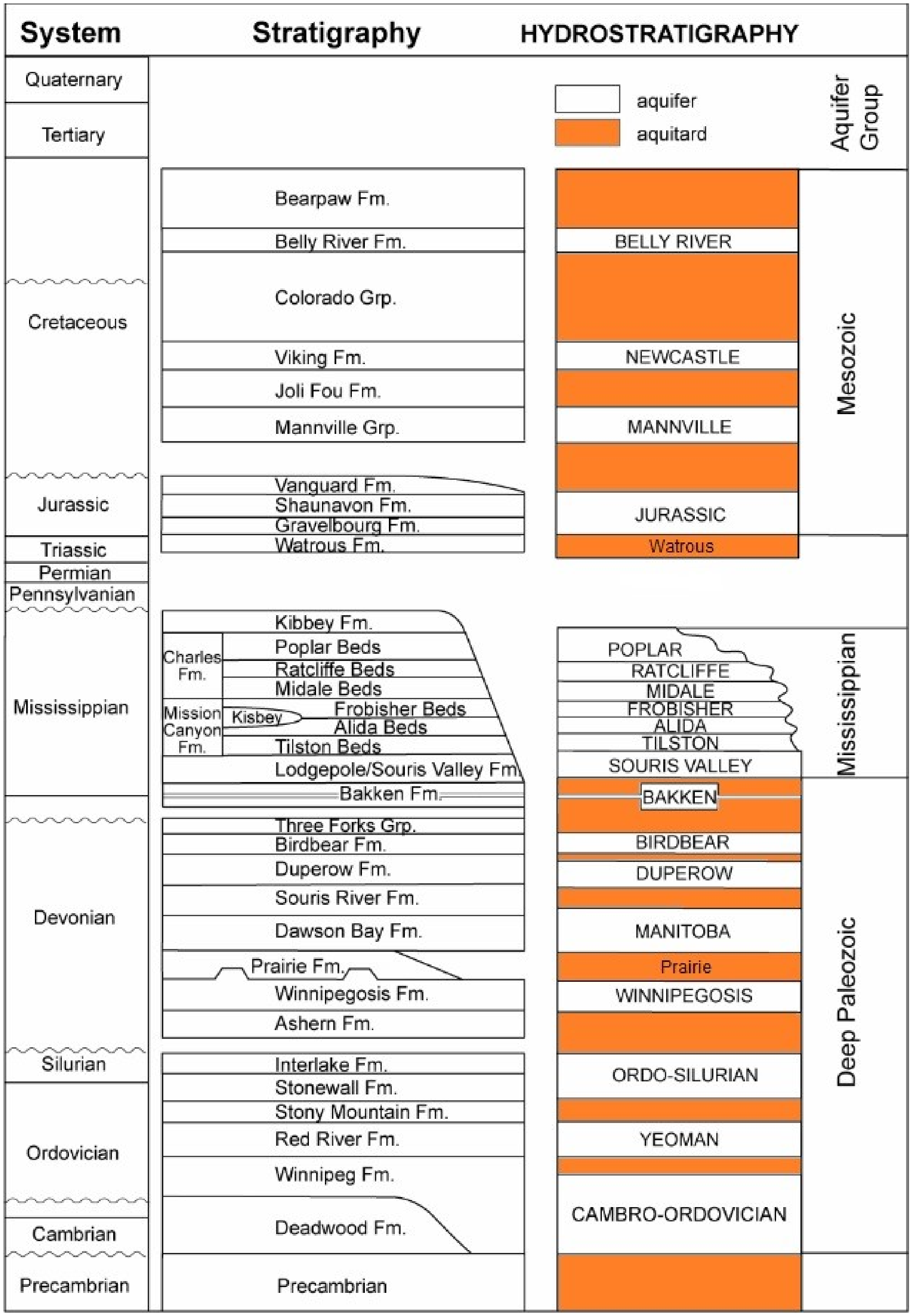

Figure 2.1 Stratigraphy and hydrostratigraphic units of the Williston Basin (Modified after Khan and Rostron, 2004)

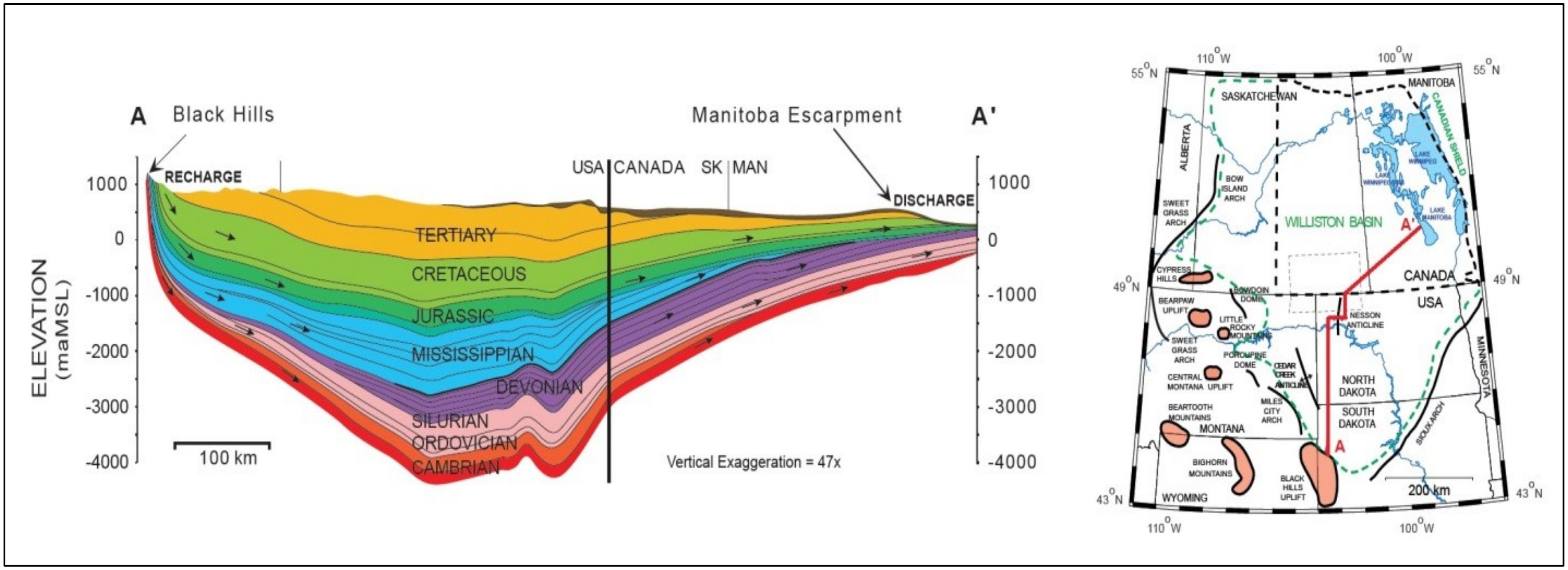

Figure 2.2 Structural cross-section A to A' through the line of section shown in the plan view of the Williston Basin (Modified after Benn and Rostron, 1998)

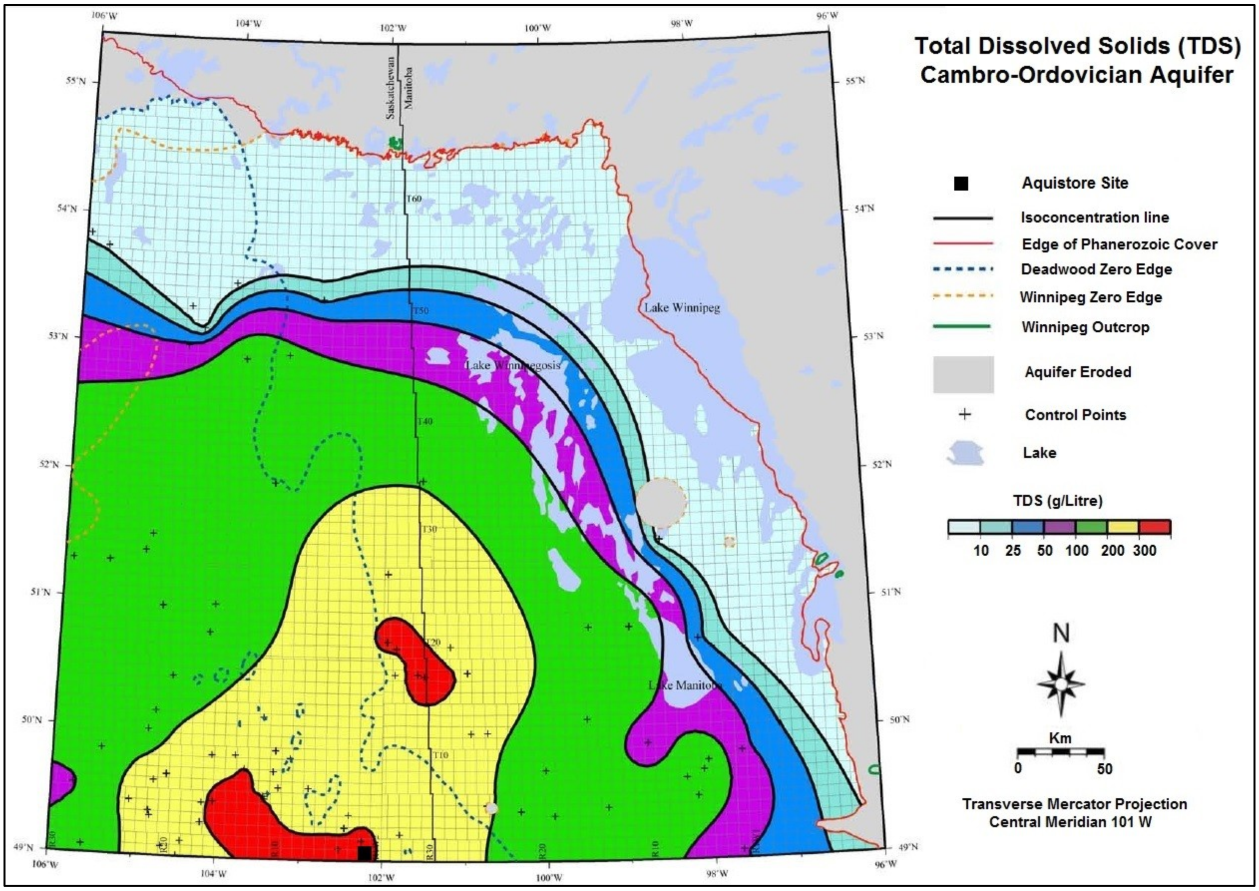

Figure 2.3 Total Dissolved Solids (TDS) in the Cambro-Ordovician aquifer (Modified after Palombi, 2008)

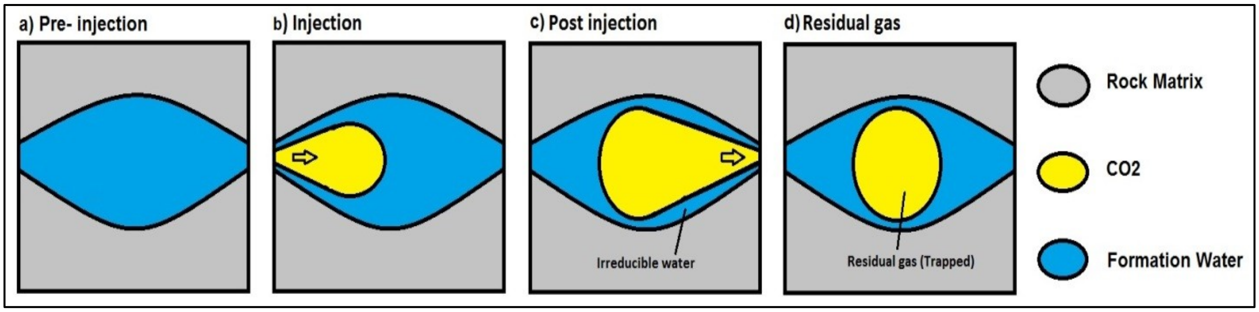

Figure 2.4 Schematic multiphase flow through a pore space during CO_2 injection process: a) The pore space is fully saturated with formation water prior to injection. b) After the injection, supercritical CO_2 invades into the pore space. Some part of the formation water is attached to the edge of the pores and is immobile (Irreducible water saturation). c) Once the injection is stopped, water starts imbibing into the pore space. d) Some of the injected CO_2 is trapped between pores and left behind as a residual gas (Modified after Hermanson, 2014).

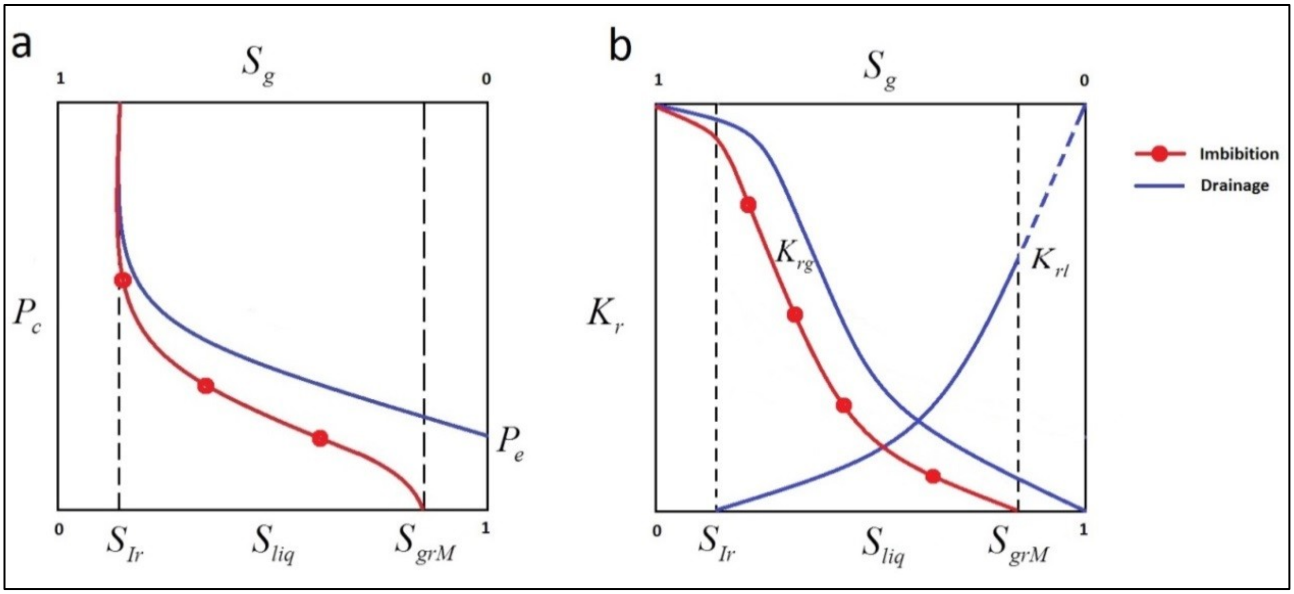

Figure 2.5 a) Hysteretic capillary pressure and b) relative permeability curves in a gas-water system.

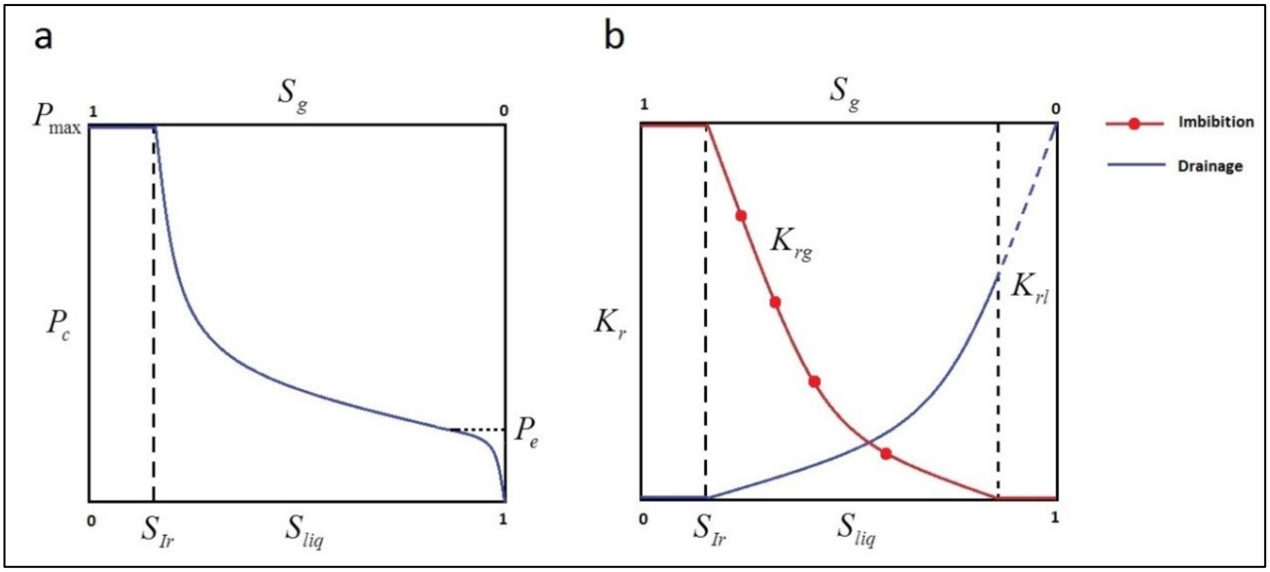

Figure 2.6 Non-hysteretic curves for capillary pressure and relative permeability used in the TOUGH2 simulator: a) capillary pressure (van Genuchten, 1980), and b) liquid relative permeability (vanGenuchten, 1980) and gas relative permeability (Corey, 1954).

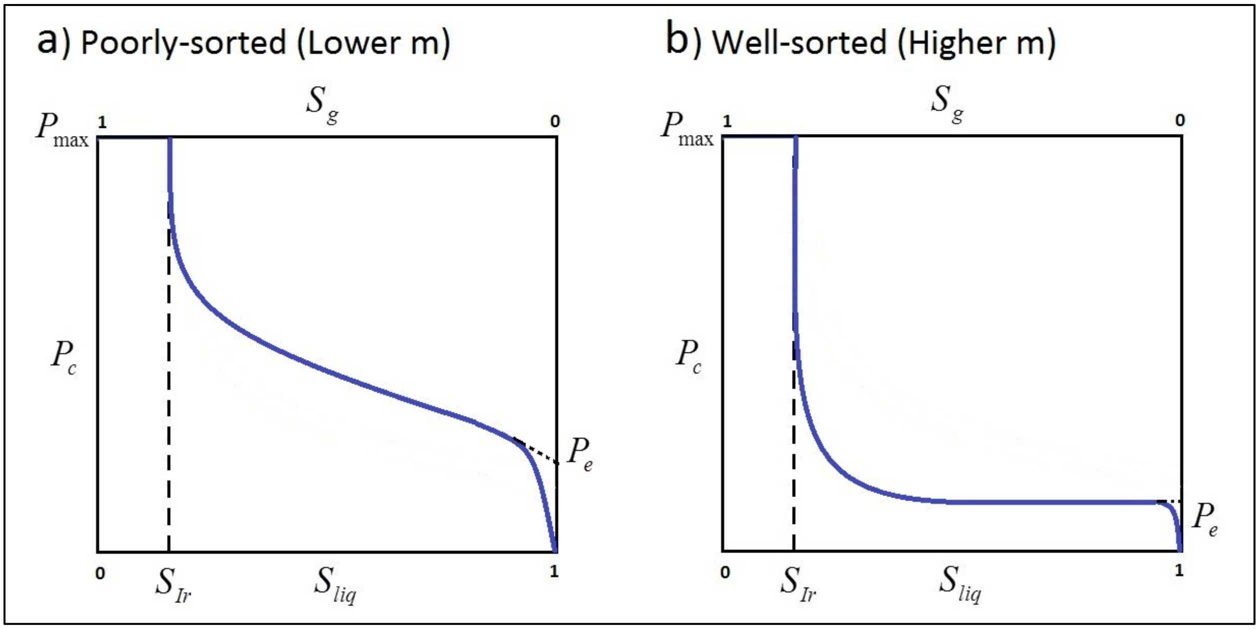

Figure 2.7 Capillary pressure in different rock materials: a) poorly-sorted, and b) well-sorted.

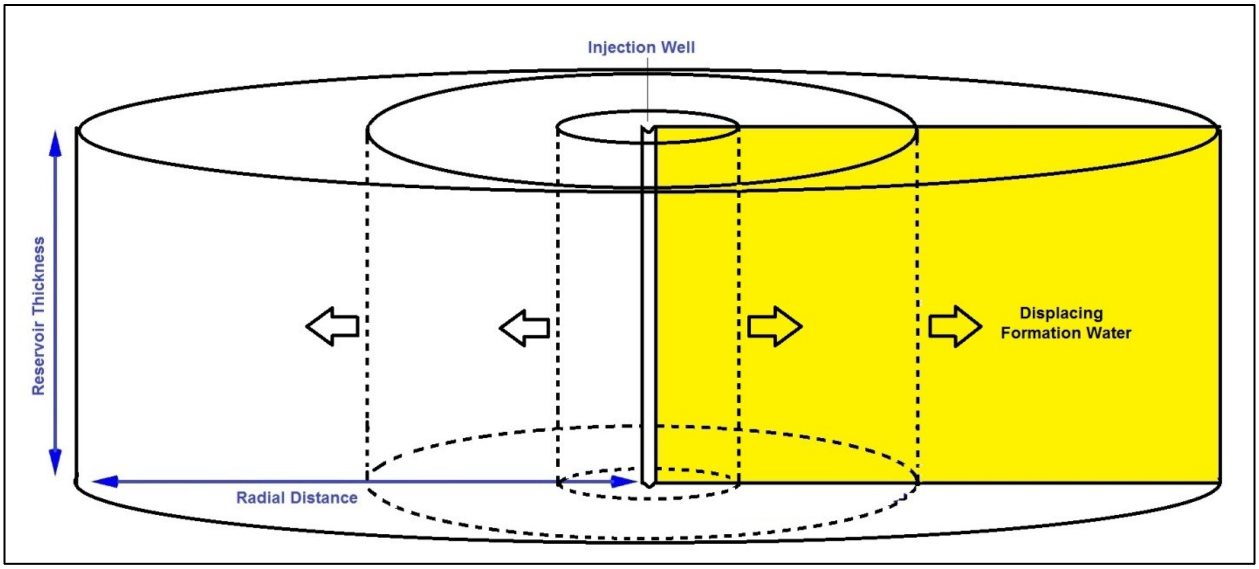

Figure 2.8 Schematic 2D radial model in the TOUGH2 simulator.

.

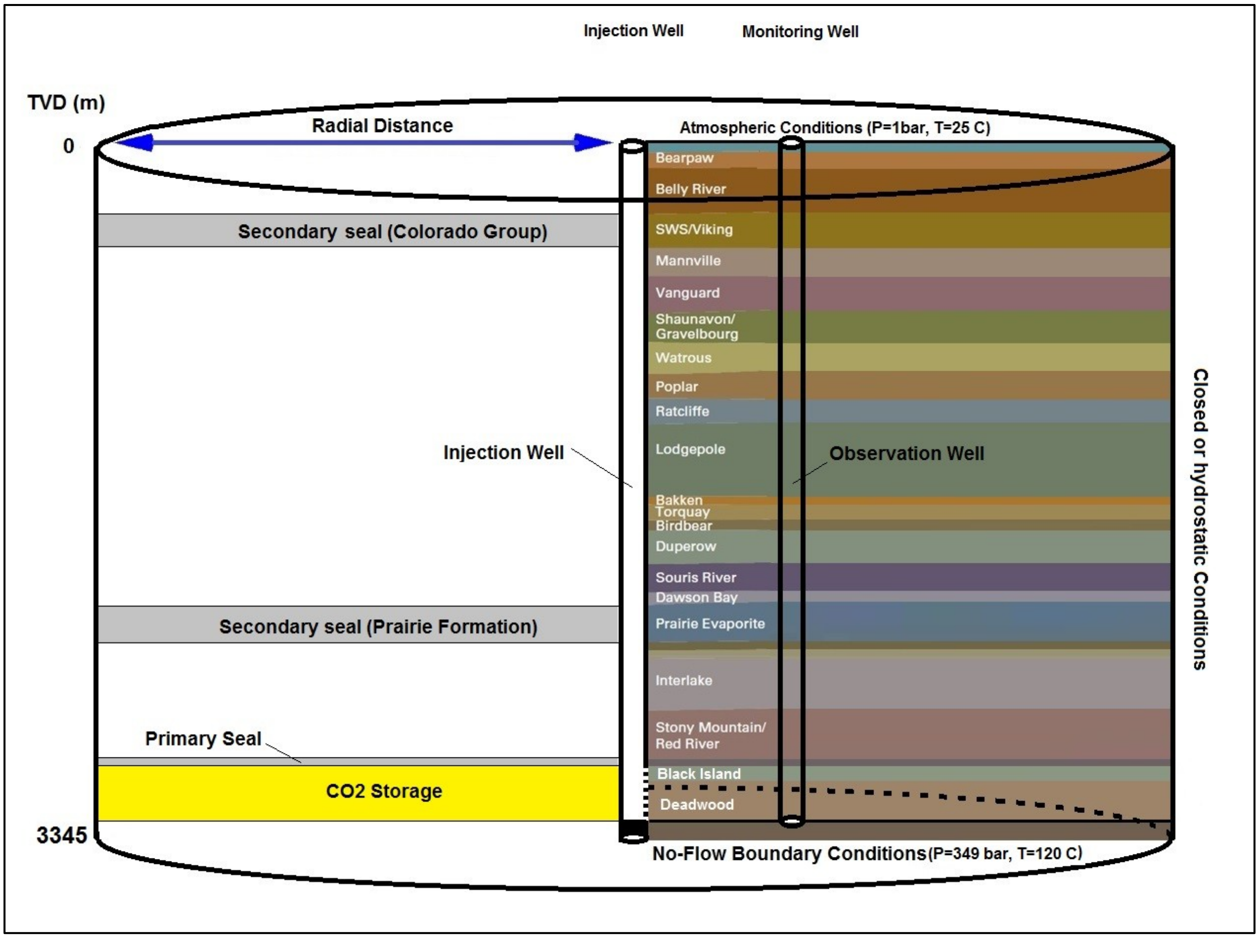

Figure 2.9 Conceptual model of the study area.

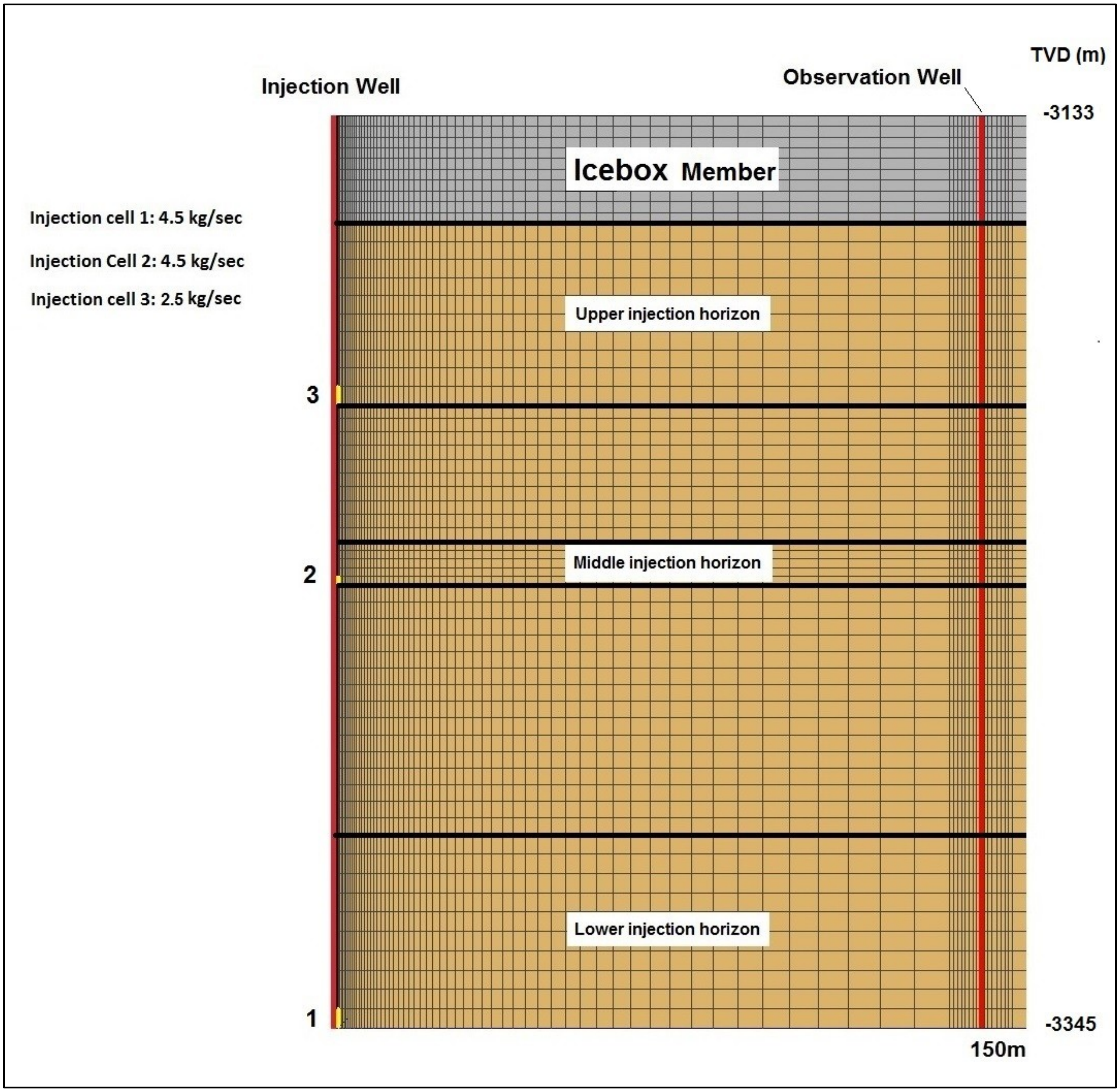

Figure 2.10 Injection cells and rates specified in the simulation (Cells are highlighted with yellow color).

Table 2.1 Solution control and convergence criteria assigned in the simulation

<table>
<tr><th colspan="2">Time</th></tr>
<tr><td>Start Time - TSTART</td><td>0 sec</td></tr>
<tr><td>End Time - TIMAX</td><td>3.1536E+09 sec</td></tr>
<tr><td>Time Step - DELTEN</td><td>1 sec</td></tr>
<tr><td>Max. Number of Time Steps - MCYC</td><td>Infinite</td></tr>
<tr><td>Max. CPU Time - MSEC</td><td>Infinite</td></tr>
<tr><td>Max. Iteration Per Step - NOITE</td><td>8</td></tr>
<tr><td>Reduction Factor - REDLT</td><td>4</td></tr>
<tr><th colspan="2">Solver</th></tr>
<tr><td>Conjugate Gradient Solvers</td><td>Stabilized Bi-Conjugate – DSLUCS</td></tr>
<tr><td>Z-Preconditioning - ZPROCS</td><td>Small Constant –Z1</td></tr>
<tr><td>O-Preconditioning - OPROCS</td><td>None</td></tr>
<tr><td>CG Convergence Criterion - CLOSUR</td><td>1.0E-7</td></tr>
<tr><th colspan="2">Weighting</th></tr>
<tr><td>Mobility at Interface - MOP(11)</td><td rowspan="3">Upstream Weighted</td></tr>
<tr><td>Density at Interface - MOP(18)</td></tr>
<tr><td>Permeability at Interface</td></tr>
<tr><td>Diffusive Flux at Interface - MOP(24)</td><td>Coupled Harmonic Weighting</td></tr>
<tr><th colspan="2">Convergence</th></tr>
<tr><td>Relative Error Criterion (RE1)</td><td>1.0E-5</td></tr>
<tr><th colspan="2">Options</th></tr>
<tr><td>Composition of Produced Fluids - MOP(9)</td><td>Relative Mobilities</td></tr>
<tr><td>Boundary Condition Interpolation - MOP(12)</td><td>Step Function</td></tr>
</table>

Table 2.2 Input parameters assigned for the simulation.

Properties	RES1	RES2	SALT	SEAL
Porosity ($\emptyset$)	0.15	0.1	0.04	0.05
Permeability (k) - m^2	3.4E-13	1.0E-13	1.0E-19	1.0E-18
Residual water saturation	0.3	0.3	0.3	0.3
Residual CO_2 saturation	0.15	0.15	0.35	0.35
Pore compressibility (Pa^{-1})	4.5E-10	4.5E-10	9.0E-10	9.0E-10
van Genuchten (α) (Pa^{-1})	5.0E-05	5.0E-05	5.0E-07	5.0E-07
van Genuchten (m)	0.457	0.457	0.457	0.457

3 Development of Optimal Model and Detailed Extended Numerical Approaches

This chapter provides the approaches to developing the optimal or calibrated injection model and also addresses the effects of different grid refinement and boundary conditions on the simulation results. The model sensitivity with respect to some key input parameters as well as capability of MODFLOW as a single-phase flow simulator to simulate the CO_2 injection process is also evaluated in this chapter.

3.1 Optimal model

The optimal CO_2 injection model in this work represents the model that is calibrated and validated based on the real field bottom-home pressure measurements. There are few large-scale CO_2 injection projects in the world (e.g., Aquistore, Weyburn) that are taking advantage of direct measurement of the bottom-hole pressures. So, the novelty of this study is the possibility of calibrating the simulated reservoir pressure with respect to the actual bottom-hole pressure obtained from the observation well located 150 metres from the injector that is drilled completely down to the base of the reservoir.

The 5-day CO_2 injection into the Cambro-Ordovician reservoir was started on April 16th, 2015 at a rate of 2000 tonnes per day and the bottom-hole pressure at the observation well was measured. The injection rate was later reduced down to 1000 tonnes per day to avoid excess buildup pressure into the reservoir (Figure 3.1).

The conceptual and grid model approaches were explained in chapter two and were used to develop the optimal model. This includes the maximum grid refinement around the injection and the observation well and the hydrostatic boundary conditions to the model boundaries (see section 3.5).

3.2 Model calibration

A model calibration demonstrates that the model is capable of producing field-measured parameters (e.g., pressure, saturation, head, and flow) which are the calibration values (Anderson and Woessner, 1992). Calibration is the adjustment of input parameters in order to match with measured or observed values. After running the simulation for a 5-day period, the bottom-hole pressure at the observation well was calculated. The key input parameters such as intrinsic permeability, porosity, and residual gas saturation, as well as the injection rates at the injection horizons, were changed systematically to obtain the best fit between the simulated and measured BHP values. The best matching simulated BHP values were plotted and compared with the measured BHP (Figure 3.2). The results represent a good match between the simulated and observed pressures showing the root mean square error (RMSE) of 6.28 percent. Figure 3.3 also illustrates the carbon dioxide saturation after five days of injection.

3.3 Lateral (horizontal) grid spacing effects

Refining the elements in the areas with the highest gradient such as the injection well and beneath of the sealing units will minimise the effects of numerical dispersion and allows more accurate predictions (Green and Ennis-King; 2012, Anderson and Woessner; 1992). Small radial cell sizes close to the injection zone and large cells at further distances will resolve the gradients close to the injection zone. However, these changes can increase the simulated lateral migration of CO_2 due to an increase in the numerical dispersion at greater distances from the injection well (Hermanson, 2014). Therefore, an evaluation of lateral and vertical grid spacing is warranted while only the hydrostatic boundary conditions are considered for all cases.

In order to evaluate the effects of lateral grid spacing on the simulation results, five cases were defined and the increasing factor or multiplier of 1.05 was used to increase the cell widths gradually to the model boundary for all cases. The first case (base case) used the finest possible grid spacing with the width of 0.3 metres at the injection cell and the increasing factor of 1.05 was used to increases the cell widths gradually to the model boundary. The choice of the increasing factor was based on the rule of thumb that is applied to expand the grid spacing from the injector to the model boundary. However, in order to obtain more accurate results, the nodal spacing should not be more than 1.5 times the previous nodal spacing (Anderson and Woessner, 1992). In the other cases, the injection cell widths were increased but the vertical discretization, as well as the lateral increasing factor for all cases, remained unchanged (i.e., 1.05). Table 3.1 represents the injection cell size and number of elements for all scenarios.

A five day injection period was then set as the simulation time for all cases, allowing for comparison of with the calibrated model (base case scenario). Carbon dioxide saturations and CO_2 plume distributions for all five cases are shown in figure 3.4. Figure 3.5 also shows the CO_2

mass fractions (i.e., dissolved carbon dioxide) for the defined cases. As the grid size increases, the plume expands horizontally and thin vertically.

Coarse-scale grids overestimate the lateral extent of the plume as well as the mass of dissolved carbon dioxide in the aquifer. This leads to an increase in the amount of dissolved CO_2 (mass fraction of CO_2) in coarse-scale grids compare with the fine-scale grids, as dissolution scales linearly with the amount of fluid present in the grid blocks (Green and Ennis-King, 2012).

Maximum lateral plume sizes within the lower injection horizon after five days are between 30 and 150 metres for the base case scenario and case 5 respectively. Case 5 is clearly unrealistic given that no CO_2 was detected in the injection well. From inspection, cases 3 and 4 are clearly overwhelmed with numerical dispersion as well.

With grid sizes below 10 metres (figure 3.4), visual inspection of the plume shape looks similar, yet with some overshoot. Thus, with grids < 1.5 metres (i.e., case one) there is little difference compared to the base case scenario, indicating that the grid spacing is still small enough to obtain acceptable results.

3.4 Vertical grid spacing effects

An appropriate vertical grid refinement also needs to be applied in the simulation of CO_2 injection along with the lateral grid spacing. A model with larger grid blocks (i.e., coarser vertical discretization) impedes the gravity override (i.e., less dense CO_2 flows over denser groundwater) of a CO_2 plume and underestimates its size (Yamamoto and Doughty, 2011). The effects of vertical grid refinement were evaluated by designing two models with different vertical grid spacing keeping the lateral discretization unchanged for both models (Figure 3.6). Figure 3.6A shows the model with finer vertical grid spacing as used in the base case scenario with vertical grid block size of 5 metres (dz=5 metres) and the vertical grid spacing in the coarse grid model (Figure 3.6B) was reduced by a factor of two (dz=10 metres). A constant injection rate of 1000 tonnes per day was set for a period of thirty years for both models.

CO_2 saturations after 30 years for two different grids are shown in figure 3.7. It is clear that there are considerable differences between two defined models due to different vertical discretization. The lateral plume extent in the coarse-grid model (Figure 3.7B) are underestimated as expected and are about 946, 1800, and 1196 metres for the lower, middle and upper injection layers respectively that are 72, 110, and 57 metres less than the corresponding plume extent in the fine grid model (Figure 3.7A).

Vertical discretization in the base grid model was further decreased by a factor of 2 but the simulation did not show any differences compare to the fine grid model and gave identical CO_2 saturation results. This shows an appropriate vertical spacing in the fine base case grid. A finer vertical spacing would serve only to lengthen the simulation time.

3.5 Effects of boundary conditions on the calibrated model

Assigning appropriate boundary conditions to a model is challenging and significantly controls the model output (Anderson and Woessner, 1992). In the previous chapter, two possible boundary conditions implemented in TOUGH2 simulator were reviewed, including the Dirichlet or fixed state conditions in which the thermodynamic parameters at the model boundaries such as pressure, temperature, carbon dioxide and salt mass fractions are set to the hydrostatic conditions and, the Neumann conditions which no flow is specified across the model boundary.

In order to obtain an appropriate boundary conditions, two conceptual models were created for testing; 1) a model with fixed state or hydrostatic conditions on the lateral and the upper boundaries while the lower boundary (i.e., base of the mode) was set as no flow, and 2) a model in which all boundaries were set to no flow conditions, so the entire model acted as a closed system. The choice of either of these scenarios controls the model output.

In the first model, a very thin layer (i.e., 10 cm) was defined as the upper boundary of the model and atmospheric conditions (i.e., P=1bar, T=25 C, zero salt and CO_2 mass fractions) were assigned and fixed to that layer. After running the model in the steady state mode and obtaining the initial conditions for all elements, the cells adjacent to the lateral boundary of the model were also set to the hydrostatic conditions. This procedure assigns a very large volume to the model boundaries, so their thermodynamic properties such as temperature, pressure, etc. will not change during the simulation.

In the second model, the no-flow conditions were assigned to all model boundaries, so the injected fluid could not escape the model domain

The effects of different boundary conditions on the pressure results were evaluated spatially (up to 50 kilometres from the injector). Figure 3.8 shows the pressure change at the lower injection zone with respect to the distance from the injector.

Assigning the no-flow conditions to the model boundaries overestimates the reservoir pressure and creates a pressure buildup of approximately 1.5 Mpa compared to the Dirichlet (fixed state) conditions.

3.6 Sensitivity analysis

The purpose of a sensitivity analysis is to quantify the uncertainty of the calibrated model caused by uncertainty in the estimates of reservoir parameters, boundary conditions, and stresses. During this process, calibrated values for reservoir parameters are systematically changed within the previously established plausible range (Anderson and Woessner, 1992).

The overall performance of a simulation project can be better analysed by sensitivity analysis of the input parameters. The sensitivity analysis helps to better understand the system's response to changing parameters. If a model is sensitive to an input parameter, additional data on that variable can improve the model calibration (Tesfaye, 2009). Sensitivity analyses were applied in this study to determine which input parameters had the largest effect on the simulated bottom-hole pressure (BHP) values at the observation well.

In order to determine the sensitivity of the model with respect to the main input parameters, three components among the input parameters were investigated: intrinsic permeability, porosity, and residual gas saturation of the lower and middle injection horizons within the Deadwood Formation. Percent changes of 25 and 50 percent were then applied to the selected parameters and resulting bottom-hole pressure values at the observation well were obtained and compared with the calibrated pressure results.

A thirty-day injection scenario was used for the sensitivity analysis. Figure 3.9 shows the sensitivity analysis chart after the model was changed in three key input parameters. The horizontal axis represents the change in input parameters and the vertical axis represents the bottom-hole pressure change at the observation well.

The highest sensitivity is with respect to the intrinsic permeability variations. For example, by decreasing the permeability down to 25 and 50 percent, the bottom-hole pressure will increase about 66 and 123 Kpa respectively. Increasing the permeability up to 25 and 50 percent will decrease the bottom-hole pressure up to 27 and 46 Kpa. This indicates that the BHP variations are a nonlinear function of permeability. Thus, the lower permeability values determine the effective behavior of the model, whereas the higher permeability values are less effective.

Porosity value also shows the moderate effect on the pressure results. For example, by decreasing the porosity down to 25 and 50 percent, the bottom-hole pressure will increase about 7 and 15 Kpa respectively while increasing the porosity up to 25 and 50 percent will decrease the bottom-hole pressure about 5 and 10 percent respectively.

On the other hand, the model represents the lowest sensitivity with respect to the residual gas saturation (S_{gr}), so increasing or decreasing the S_{gr} value will not have large impacts on the bottom-hole pressure.

Carbon dioxide Saturation is also expected to be different when the input parameters are changed. For example, with higher permeability value, CO_2 moves faster through the aquifer, so its saturation is expected to be higher at certain distances from the injector compared to the low permeability aquifer.

3.7 MODFLOW approach

This section evaluates the capability of the MODFLOW to simulate the CO_2 injection process, assuming that only one phase is present in the reservoir. MODFLOW is developed by the U.S. Geological Survey and solves the groundwater flow equation and is used to simulate the single phase fluid flow (i.e., water) through the porous media.

First, a 2-layer model was created by the TOUGH2-ECO2N simulator. The model includes a high permeability reservoir with 45-metre thick capped by a 20-metre low permeability caprock. The lateral boundary of the models was set to 50 kilometres from the injector and a 10-year injection period at a rate of 20 kg/sec was set to the model. Figure 3.10 shows the conceptual model. The injection cell width representing the injection well was set to 0.3 metres (30 cm) and the increasing factor of 1.05 was used to radially increase the grid spacing away from the injection well. The upper and lateral model boundaries were set to the hydrostatic boundary conditions while the bottom boundary was assumed as the no-flow boundary conditions. The simulated pressure buildup was then converted into the head rise values by assuming the hydrostatic pressure gradient of 10 kpa per metre.

Second, the same approaches were used to create a model by the MODFLOW simulator, including same grid refinements, boundary conditions, injection rate, and hydrodynamic properties. The calculated head rise from both simulators was plotted and compared (Figure 3.11). Results show that the difference between two approaches becomes smaller as the distance from the injector increases. This indicates that the MODFLOW could be used as an approach to calculate the head buildup beyond the CO_2 plume, far away from the injector where only one phase is present. However, it is not able to simulate the multiphase flow conditions adjacent to the injection zone.

Another key factor in the simulation process is the simulation time to calculate the parameters which highly depends on the number of model elements and the output parameters that the simulator needs to calculate. Results showed that the MODFLOW works way faster than the TOUGH2. The total simulation time in the MODFLOW approach was less than 2 minutes while the TOUGH2 simulation time was about 30 minutes. Thus, when only the head rise at large distances from the injection zone are concerned, the MODFLOW would be the fast and time efficient alternative.

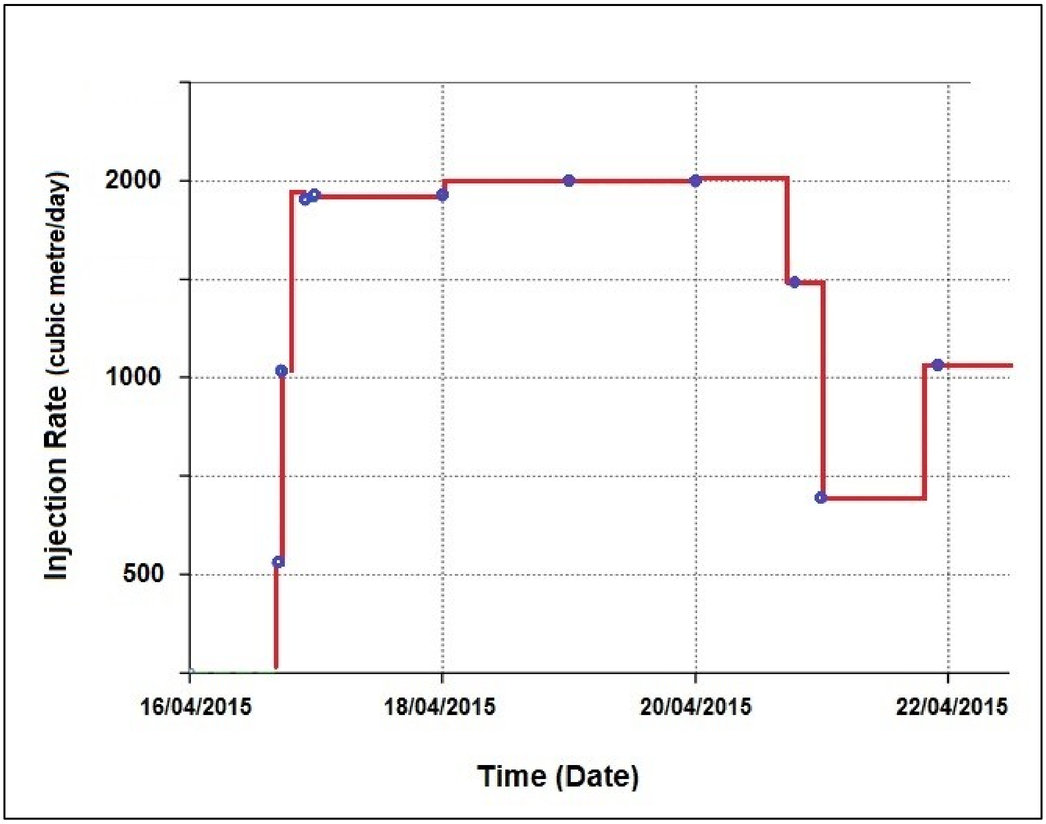

Figure 3.1 Short-term variable injection rates into the reservoir (EERC, personal communication, June 9, 2015)

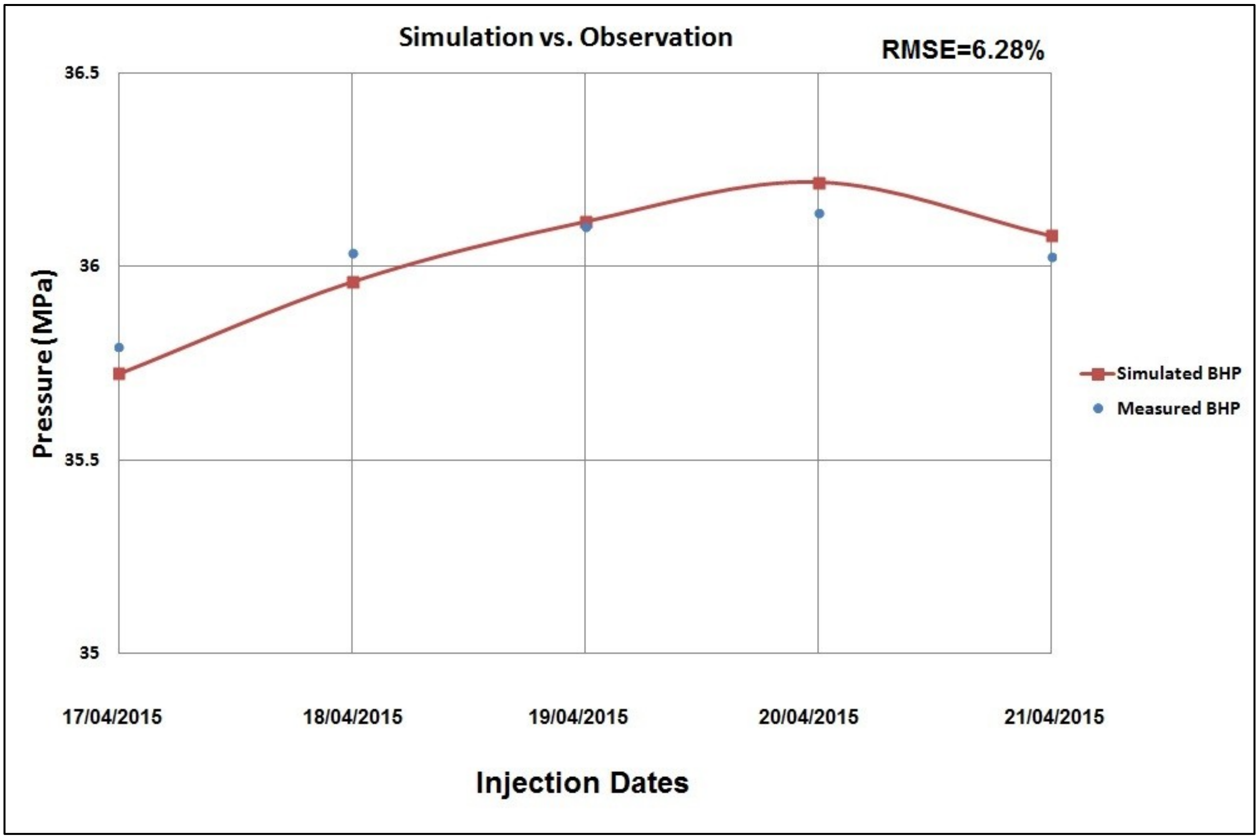

Figure 3.2 Simulated and observed BHP at the observation well (Model calibration)

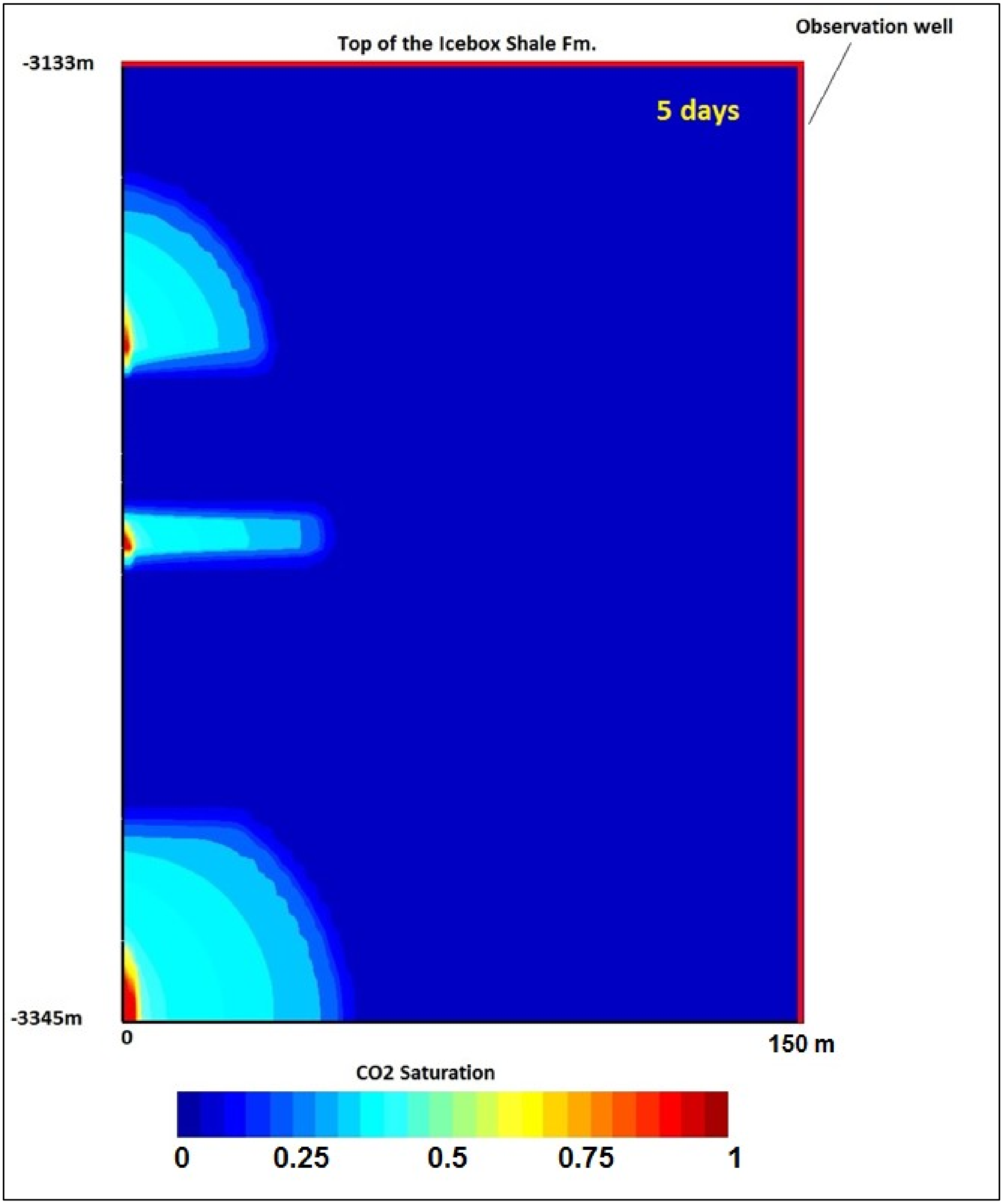

Figure 3.3 Carbon dioxide saturation within the injection horizons (five days after injection starts)

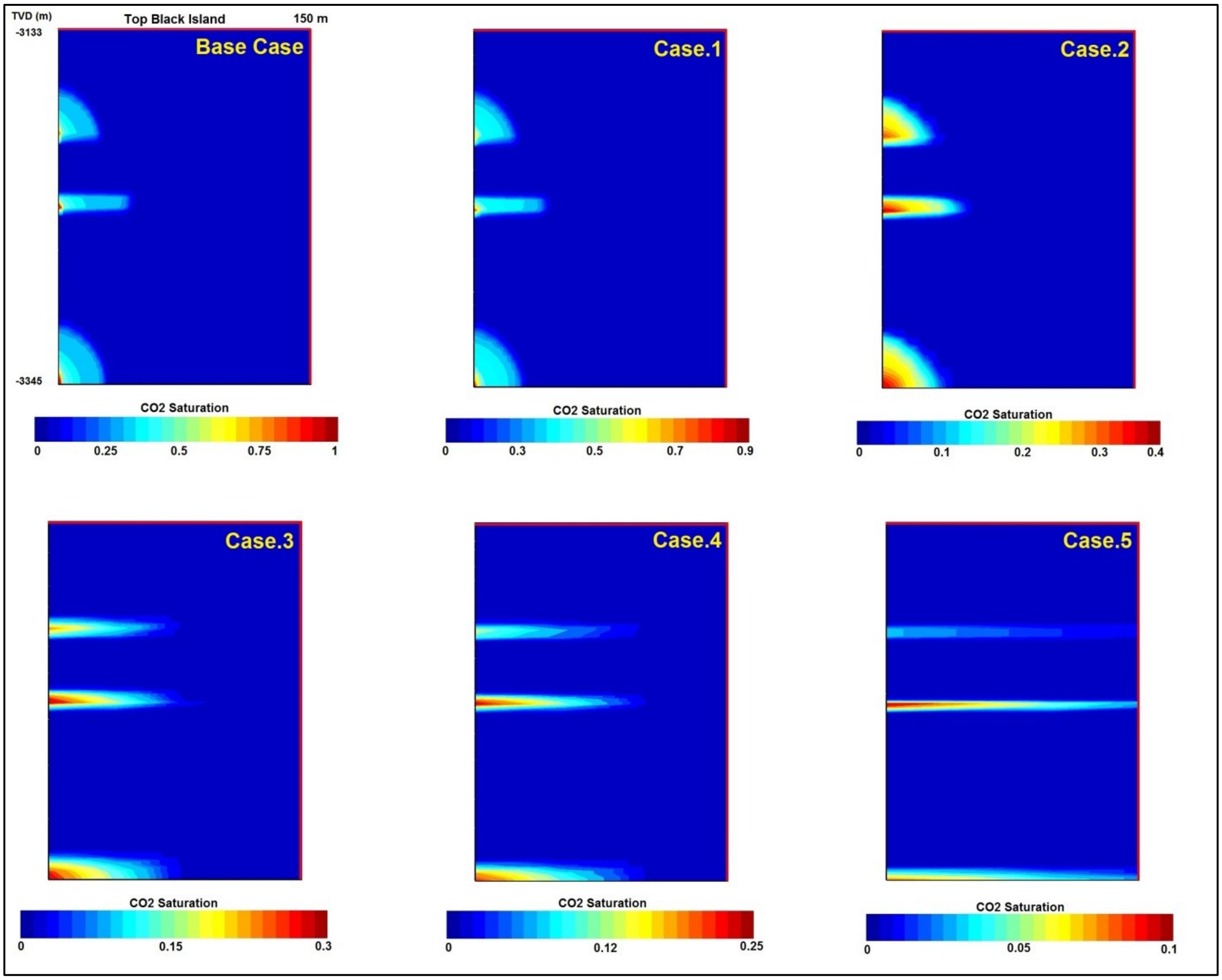

Figure 3.4 Lateral grid spacing effects on the CO_2 saturation and plume distribution.

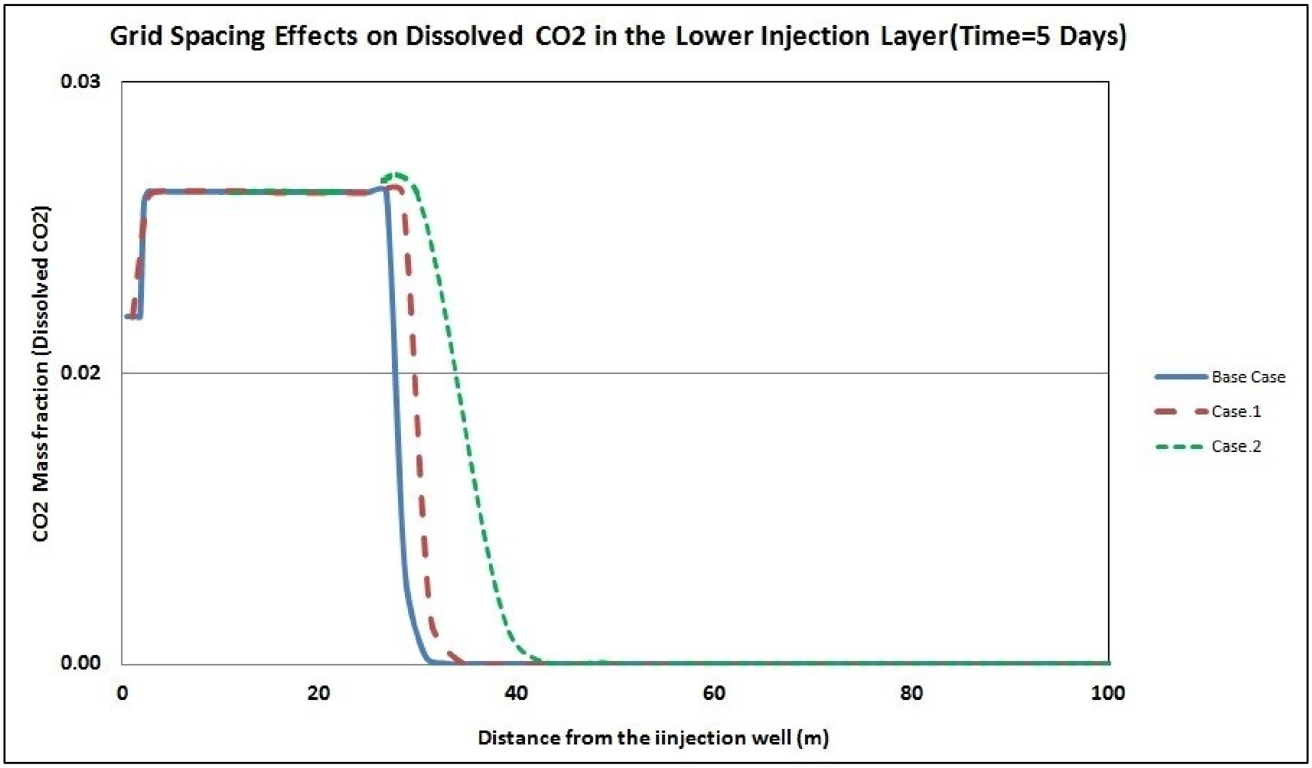

Figure 3.5 Dissolved CO_2 in the lower injection layer for different lateral grid spacing scenarios.

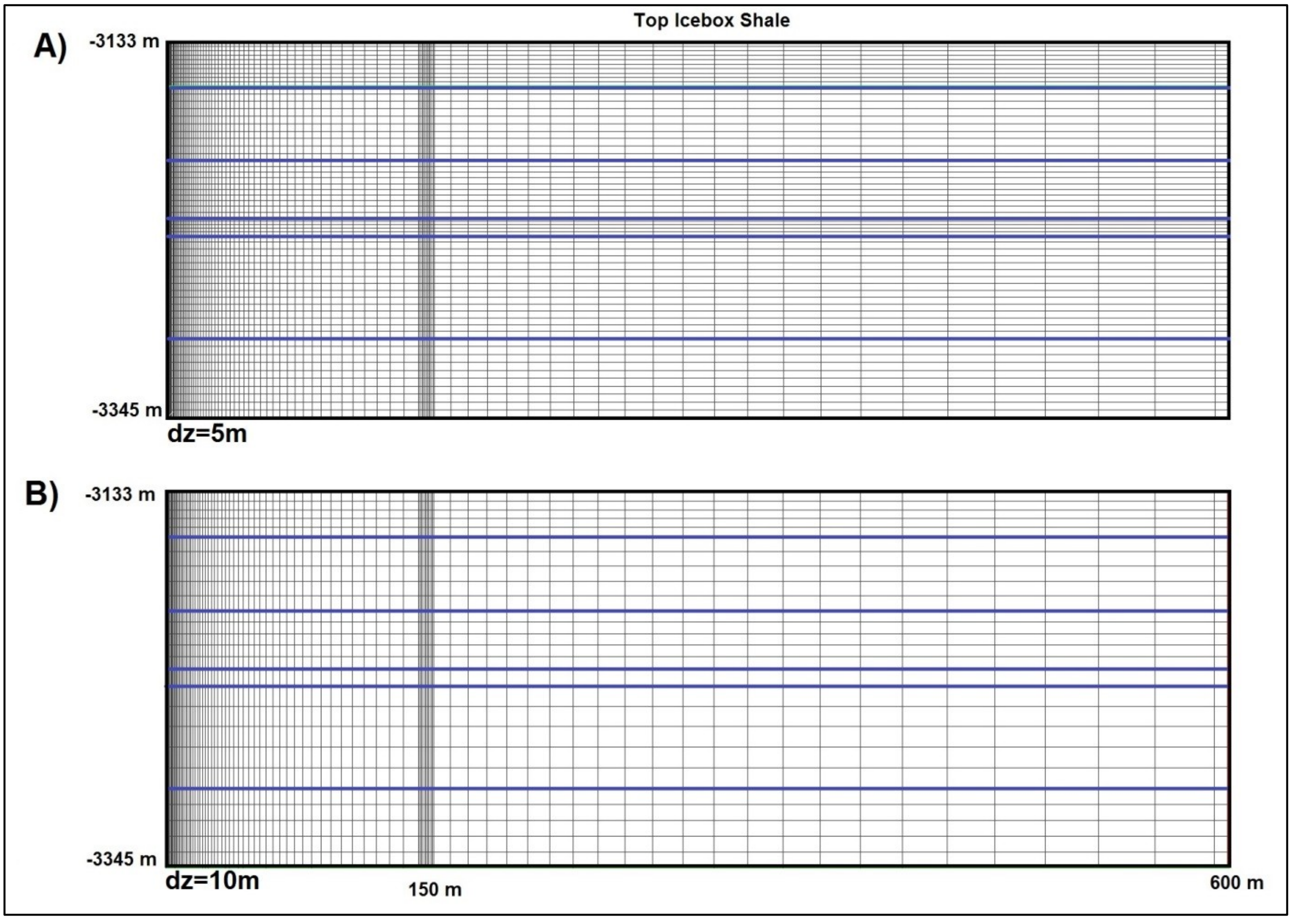

Figure 3.6 Grid models with different vertical grid spacing: A) Fine-grid and B) Coarse-grid.

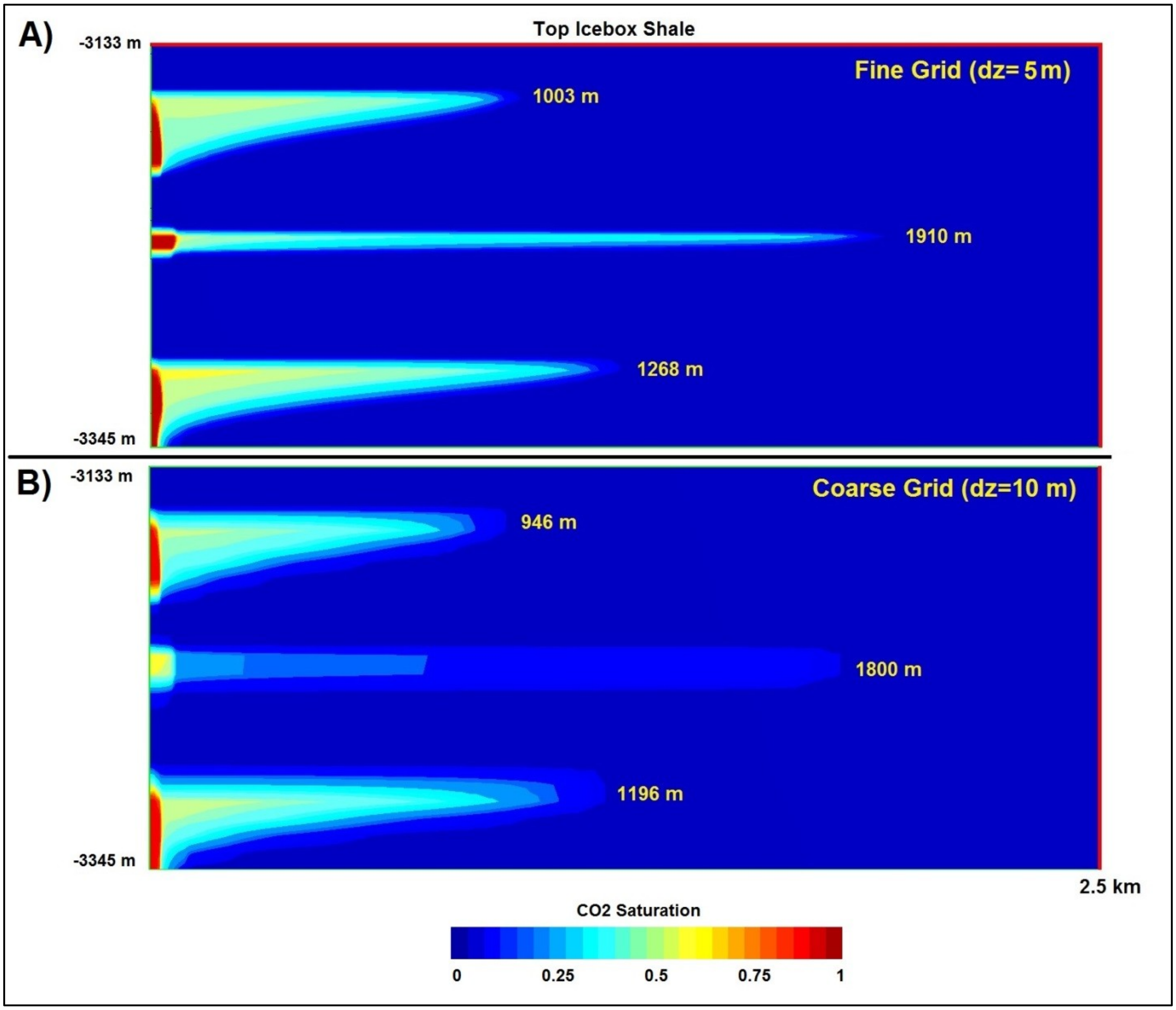

Figure 3.7 Effects of different vertical discretization on the lateral CO_2 plume after 30 years of injection: A) Fine vertical spacing (dz=5 m), B) Coarse vertical spacing (dz=10 m). Numbers represent the lateral migration distances from the injection well.

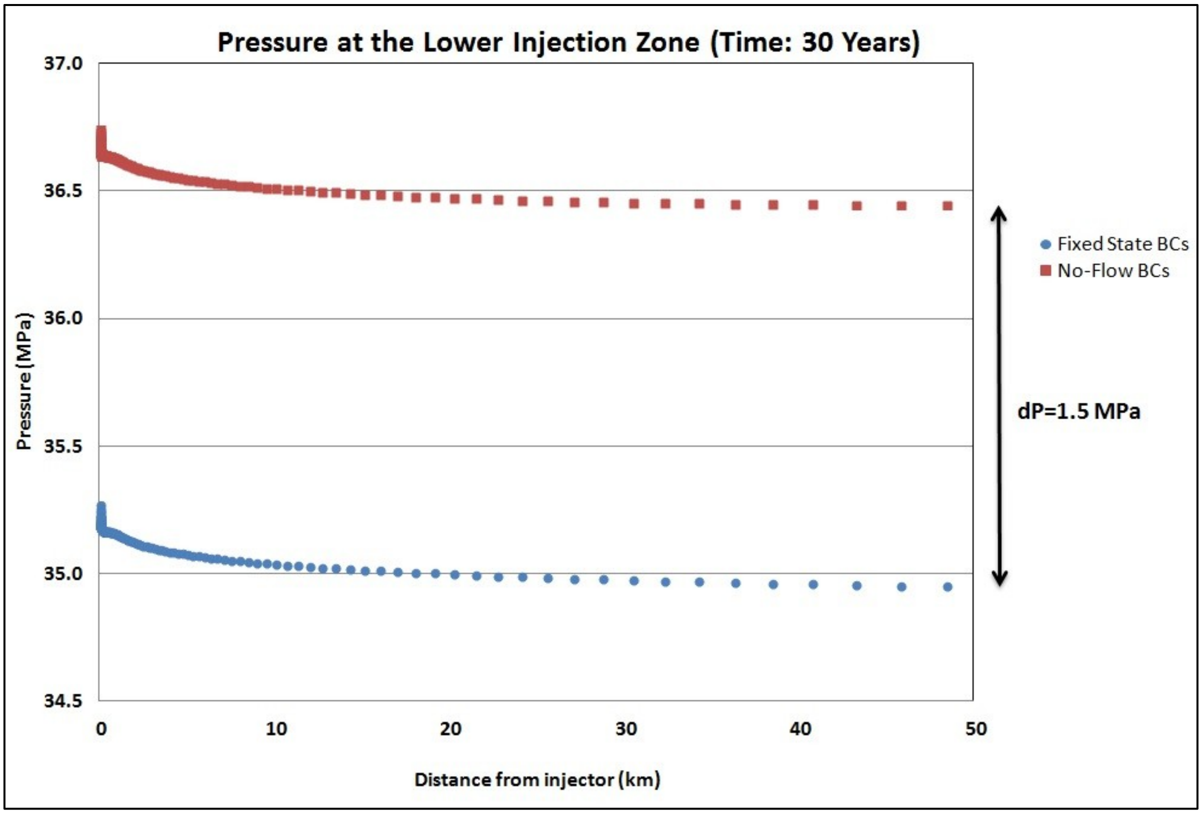

Figure 3.8 Spatial pressure change at the bottom of the reservoir for different boundary conditions.

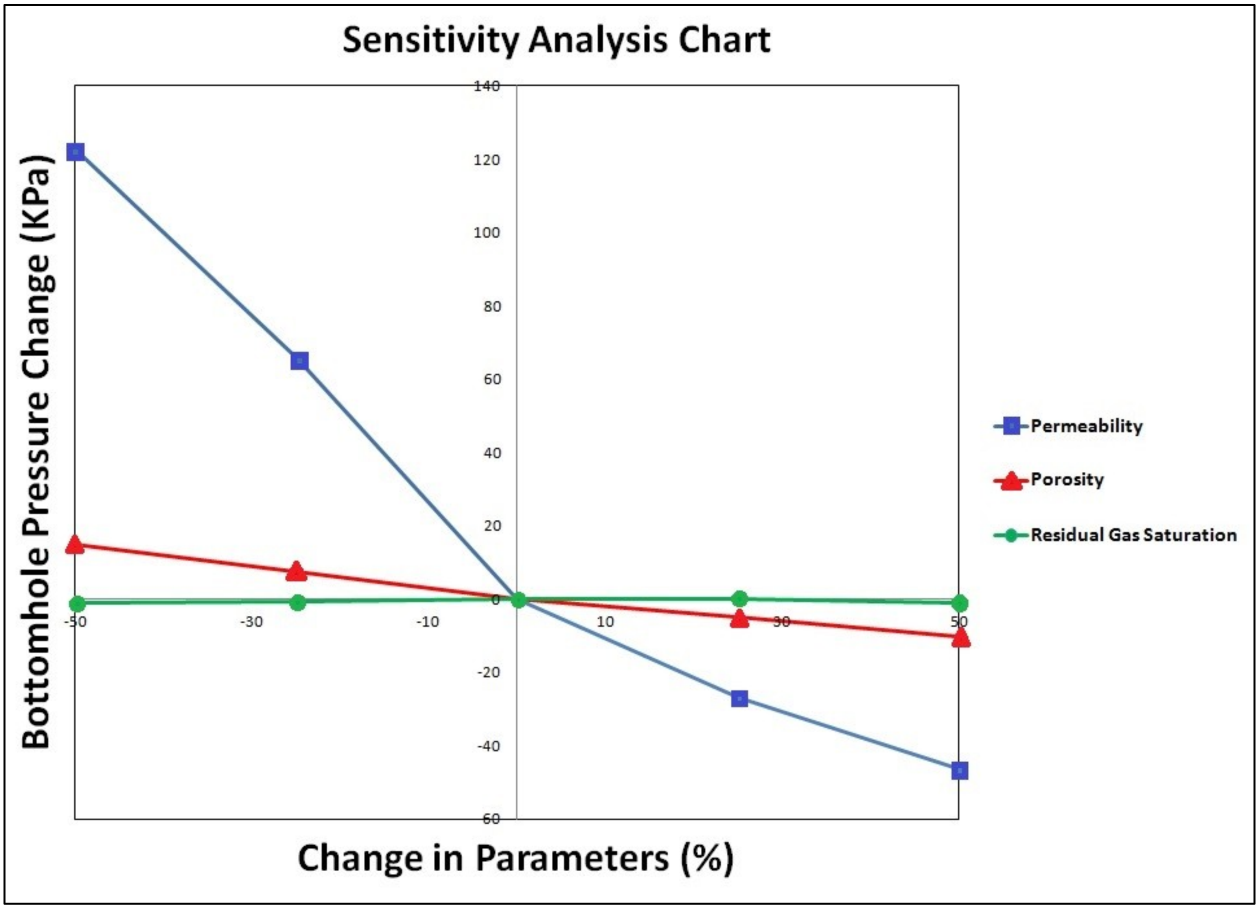

Figure 3.9 Sensitivity analysis of the key input parameters for a 30-day injection period on the base case grid (1000 tonnes per day)

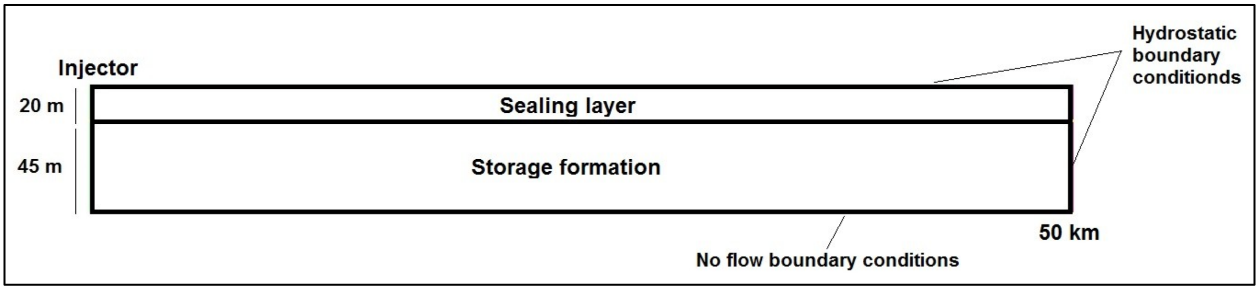

Figure 3.10 The conceptual model to compare the TOUGH2 and MODFLOW simulators.

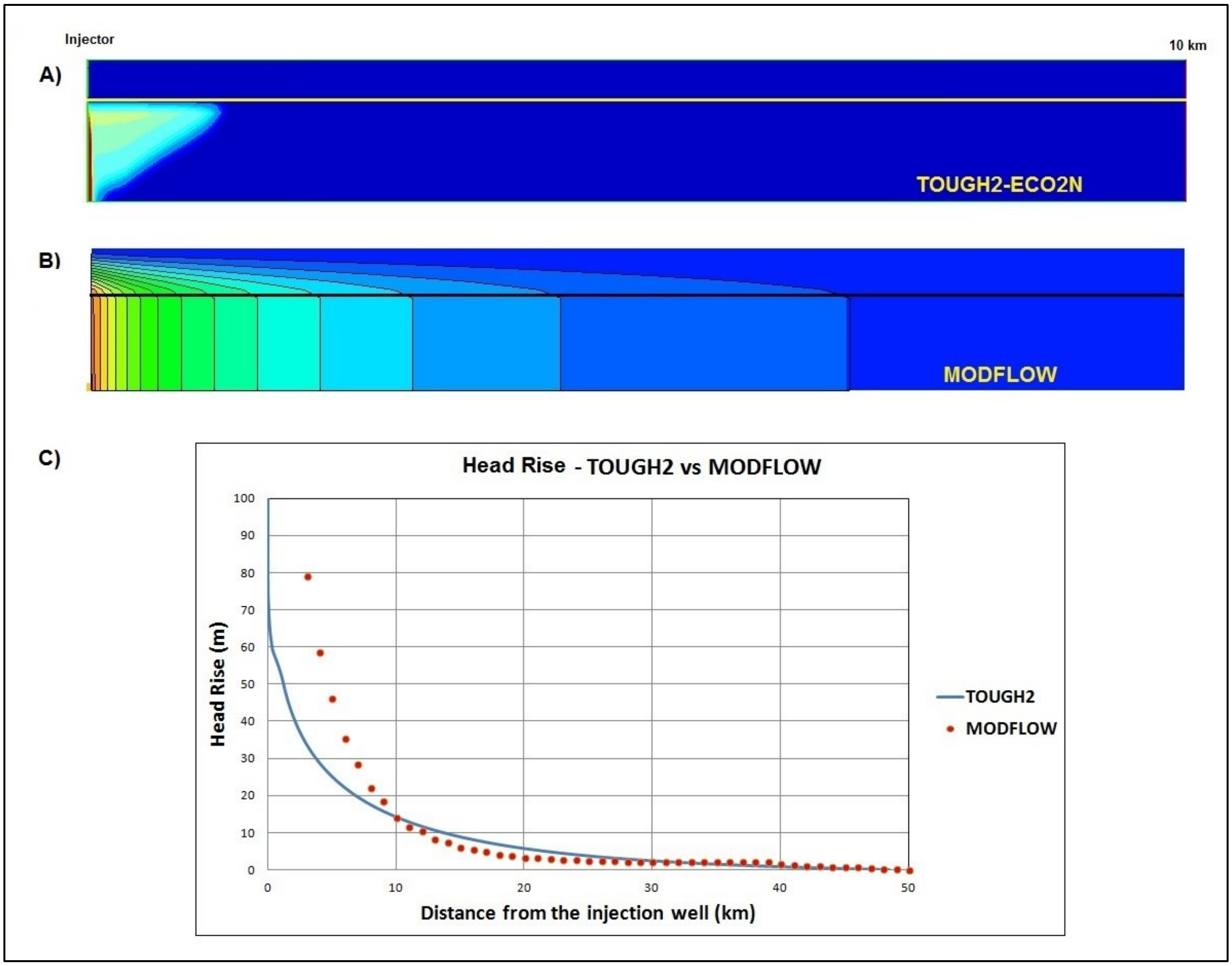

Figure 3.11 TOUGH2 vs. MODFLOW: A) Carbon dioxide saturation model created by the TOUGH2-ECO2N simulator, B) Head rise model created by the MODFLOW, C) Head buildup values in the storage formation with respect to the distance from the injector calculated by TOUGH2 and MODFLOW simulators.

Table 3.1 Scenarios defined to evaluate the lateral grid spacing impact on the simulation.

Case Scenario	Base Case	Case 1	Case 2	Case 3	Case 4	Case 5
Injection Cell Size (m)	0.3	1.5	8	40	50	100
Number of Elements	30,000	27,500	21,700	16,000	15,000	13,000

4 Numerical Simulation of CO_2 Injection Results

The input parameters for the model were calibrated based on the measured bottom-hole pressure (BHP) after a five-day injection period (Chapter 3). Long-term simulation of CO_2 injection in the Cambro-Ordovician Aquifer was undertaken using the previously described calibration model and input parameters (Chapter 3). The objective was to understand the transient CO_2 saturation and pressure distribution within and above the storage formations. The injection scenario was modelled after the proposed Aquistore injection profile: 1000 tonnes CO_2 per day for 30 years followed by a 70-year post injection monitoring period.

The physical impacts of the industrial CO_2 injection on saline aquifers include pressure buildup and brine displacement (either lateral or vertical) during the injection and post injection periods. Furthermore, the CO_2 plume distribution was also evaluated to determine the integrity of the sealing units to store injected carbon dioxide.

4.1 Plume size and distribution-injection period

After 30 years of CO_2 injection, the CO_2 distribution in the subsurface (Figure 4.1) is confined to the injection horizons vertically and within 2 kilometres of the injection well. To better display the transient nature of the CO_2 plume evolution, a series of saturation profiles for the reservoir horizons at key times was extracted for discussion (Figure 4.2).

One month after injection starts, the CO_2 accumulates within 120 metres of the injection well in the injection horizons (Figure 4.2a). Upward plume migration within the lower and upper injection layers is dominant due to the buoyancy of CO_2 and higher thickness of these layers while CO_2 migration is dominantly lateral within the middle injection layer as it has lower thickness.

One year after injection starts, CO_2 saturation increases further and injected CO_2 plume in the lower and upper injection layers will reach the bottom of their overlying sealing units (Figure 4.2b). This prevents the upward migration of CO_2 and causes the lateral distribution of CO_2 under the low permeability sealing units. The maximum lateral migration of CO_2 after one year will be about 194, 357, and 162 metres within the lower, middle, and upper injection layers respectively.

Once CO_2 has filled the reservoirs vertically, continued injection drives CO_2 laterally until the end of injection at 30 years (Figures 4.2c-e). The CO_2 saturation and lateral plume migration will increase until injection stops. The lateral distances that CO_2 will migrate after 30 years are 1268, 1910, and 1003 metres within the lower, middle, and upper injection layers respectively.

4.2 Plume size and distribution-Post injection period

Once injection stops, CO_2 saturation starts to decrease mainly in the lower and upper injection layers (Figure 4.3). This is due to the higher thickness of these layers that provides more contact with the formation water for CO_2 dissolution. However, it remains almost unchanged within the middle injection layer which represents the lowest thickness among all three injection horizons. The simulation also shows that CO_2 plumes keep spreading during the post injection period and will reach the lateral distances of 1625, 2089, and 1266 metres (within the lower, middle, and upper injection layers respectively) 70 years after injection stops (Figure 4.4a-e). However, CO_2 saturation at the plume fronts will decrease significantly. In addition injected plumes will not connect to each other during and after the injection.

4.3 Pressure Buildups

CO_2 injection into a reservoir formation increases the reservoir pressure. This could potentially cause CO_2 leakage from the storage formation if the yield strength of the sealing units is exceeded (Lemieux, 2011). There is also a concern that the increased pressure alters groundwater elevations (e.g., 1 m equivalent for each 0.1 bar). This increased pressure could also cause brine migration in both lateral and vertical directions. Thus, pressure changes by CO_2 injection were examined in more details.

4.3.1 *Lateral Pressure Buildup*

Lateral pressure changes through time were determined using the base case model for two periods as previously explained. Two horizontal sections within the storage formations including the bottom of the reservoir (lower injection layer, 3345 metres below the ground surface) and the top of the Black Island Member (upper injection layer, 3158 metres below the ground surface). Lateral pressure changes in the lower and upper injection layers 30 and 100 years after the injection stops are shown in Figures 4.5 and 4.6

After thirty years of injection, the pressure buildup at the base of the lower injection zone will be about 3.1 bar (0.31 Mpa) at the injection well. The increased pressure will decrease to the initial hydrostatic pressure at the model boundary.

Once injection stops at t=30 years, subsurface pressure starts returning to the original equilibrium conditions (i.e., hydrostatic pressure and temperature). Simulations show that 70 years after injection stops, almost the entire system beyond 500 metres from the injection well will reach the hydrostatic conditions. Within five hundred metres of the injector (correspond to the area around 0.8 km^2) will still retain a very small amount of excess pressure (i.e., 0.01 Mpa).

At the top of the upper injection layer, pressure change was also evaluated. Pressures were expected to increase even more due to the buoyancy of carbon dioxide. Simulation results show that there will be about 4.3 bar (0.43 Mpa) excess pressures at the top of the upper injection layer after 30 years of injection. This illustrates the impact of the buoyant migrating CO_2 plume at the contact between the upper injection layer and the Icebox Shale. In addition, even 70 years after injection stops, the area correspond to a footprint area of 5.3 km^2 will still be influenced by the pressure buildup that corresponds to the area of the CO_2 plume at 100 years.

4.3.2 *Vertical Pressure Buildup*

The vertical pressure change in the subsurface during the CO_2 injection was examined using three vertical profiles at different locations (i.e., 150 metres, 10 and 50 kilometres). These profiles were obtained by subtracting the hydrostatic pressure for each element from the simulated pressure values (Figure 4.7).

Pressure disturbance is very local to the injection zone. Simulation showed no buildup pressure above the Ordo-Silurian Aquifer anywhere in the domain. This indicates that the pressure plume will cease to reach the secondary sealing unit (i.e., the Prairie Aquitard). Thus, there will be no brine displacement above this unit as well.

4.3.3 *Pressure Evolution*

The magnitude of pressure buildup depends on upon hydraulic properties of the aquifers and sealing layers. During the injection, pressures are expected to increase. The rate of pressure increase is a function of distance from the injector as well as the time since injection starts. The maximum buildup pressure occurs close to the injection zone as showed in section 4.3.1 for the lateral pressure buildup.

Three different aquifers including the upper injection layer (Black Island Member), Yeoman, and Interlake (Ordo-Silurian) aquifers were selected and vertical pressure profiles at the injection well, 150 metres, 10 and 50 kilometres away from the injector (Figure 4.8). The bottom row shows the pressure change within the top of the Black Island Aquifer. The maximum pressure buildup occurs at the injection well (i.e., 0.6 Mpa or 6 bar) six months after injection starts. Then pressure declines as the time proceeds and at the end of the injection period (i.e., 30 years), the pressure will be about 33.3 Mpa. Once the injection stops, the pressure declines faster and eventually reaches the 32.95 Mpa which is 0.05 Mpa (0.5 bar) higher than the initial hydrostatic pressure. As the distance from the injection well increases, the pressure response gets weaker and occurs later.

The change in pressure buildup and the response is even more obvious in the overlying aquifers that are separated from the injection horizons by sealing units. In the second row in figure 4.8, the pressure buildup at the injection well in the Yeoman Aquifer is about 0.01 Mpa (0.1 bar) thirty years after injection starts. This shows more than 90% reduction in pressure buildup compare to the corresponding buildup within the Black Island Aquifer (i.e., 0.43 Mpa) and signifies the role of Icebox Aquitard to minimise the pressure plume distribution to reach the overlying aquifers. The third row eventually illustrates the pressure evolution within the Ordo-Silurian Aquifer and represents a very small amount of buildup pressure (less than 0.0001 Mpa) which is negligible. There is also no pressure buildup at 50 kilometres away from the injector for all selected aquifers.

The pressure evolution plots can also be applied to estimate the water table rise in each aquifer which is expressed as one-metre rise for each 0.01 Mpa (0.1 bar). The potentiometric surface in the Black Island and Yeoman Aquifers are expected to rise up to 43 and 1 metre respectively at the injection well, thirty years after the injection starts and there will be almost no potentiometric surface rise in the Ordo-Silurian Aquifer, indicating zero volume of brine flux to the overlying formations.

4.4 Brine Displacement

The conceptual model for brine displacement is shown in Figure 4.9. Injected CO_2 creates a pressure plume that in turn creates a hydraulic gradient that drives fluids away from the wellbore. Potentially, injected CO_2 can displace brine into other areas (e.g., updip shallow aquifers) that contained fresh water (Nicot, 2008). However, it was previously shown (section 4.2 and 4.3) that no pressure disturbance would be felt above the Ordo-Silurian Aquifer during the 30 years of injection.

4.4.1 *Lateral Brine Displacement*

If the entire system is assumed as to have impermeable (e.g., zero permeability) sealing units and no compressibility, the volumetric brine displacement at any radial direction would be approximately equal to the volumetric rate of injected carbon dioxide. However, in real field conditions, brine leakage into the sealing layers and compressibility makes the displaced brine much less than the injected CO_2 into the system (Birkholzer et al., 2009). The total volumetric brine flux within the Cambro-Ordovician Aquifer was calculated at different lateral directions (i.e., observation well, 10 and 50 kilometres) (Figure 4.8).

The maximum lateral volumetric brine flow rate within the reservoir at the observation well (150 metres) is about 232 m^3/day occurring one month after injection starts and is 23% of the total volume of injected carbon dioxide. As the lateral distance increases, the volumetric brine flow rate decreases and response occur lately. For example, 10 and 50 kilometres away from the injection well, the maximum lateral brine flow rates are about 208 and 141 m^3/day respectively at the end of injection period (i.e., 30 years). This corresponds to 79% and 86% brine flow reduction compare to the volumetric injected carbon dioxide.

If we assume that the entire system is a piston, the maximum possible transport velocity can also be calculated using following equation:

$$v = \frac{Q}{2\pi R b \emptyset} \qquad (4\text{-}1)$$

Where Q is the volumetric CO_2 injection rate (i.e., 1000 tonnes/day), R is the radial distance at which the flow velocity is calculated (i.e., 150 metres, 10 and 50 kilometres), b and $\emptyset$ are the aquifer thickness and porosity respectively.

Transport velocity of 57.4 metres per year at 150 metres, 0.86 metres per year at 10 kilometres, and 0.17 metre per year at 50 kilometres were calculated for the lower injection layer that is 45 metres thick and has 15% porosity. This also corresponds to the transport velocity of 0.1 to 1 metre per year in the Alberta Basin, assuming an effective porosity of 0.1 (Bachu et al., 1994, Birkholzer et al., 2009).

4.4.2 *Vertical Brine Displacement*

To evaluate the volumetric vertical brine displacement, two aquitards were selected above the storage formations; 1) the Icebox Aquitard (the primary sealing unit), and 2) the

Prairie Aquitard (the secondary sealing unit). Figure 4.11 shows the volumetric brine that will be displaced across the selected aquitards due to the injection.

The volumetric vertical brine flux represents the total volume of native brine that will migrate upward across the sealing units and is calculated for the entire area of the model domain (i.e., $7850\mathrm{km}^2$). For example, the maximum volume of brine that will migrate across the Icebox Aquitard occurs 30 years after injection starts and is about 86.75 $\mathrm{m}^3/\mathrm{day}$ which is translated to $1.1 \times 10^{-8}\ \mathrm{m}^3/\mathrm{day}$ per each m^2 of the Icebox Aquitard and is about 90% less than the volumetric injected CO_2 into the reservoir. The vertical flux across the secondary sealing unit (e.g., Prairie Aquitard) is zero, indicating no brine leakage will occur from the storage complex during and after the injection periods.

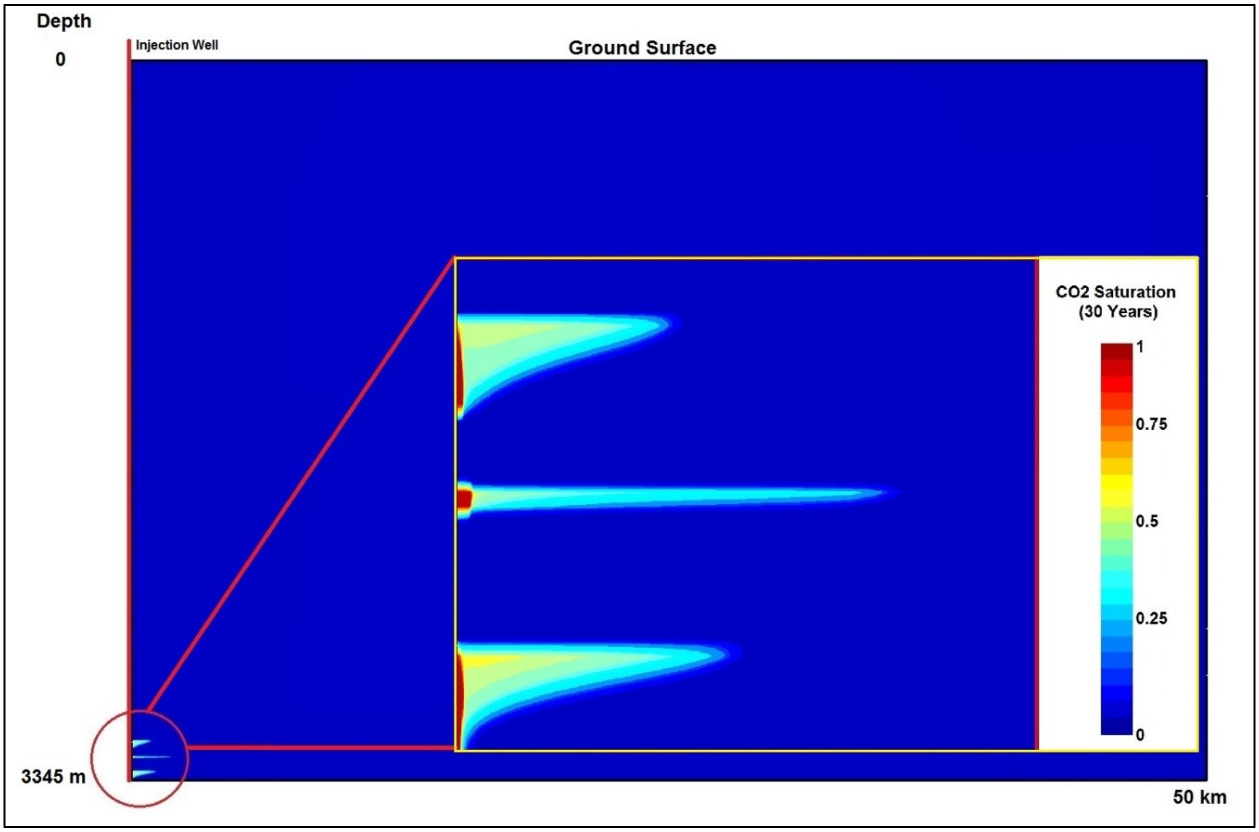

Figure 4.1 CO_2 plume migration within the storage formations at 30 years (Vertical exaggeration:10X)

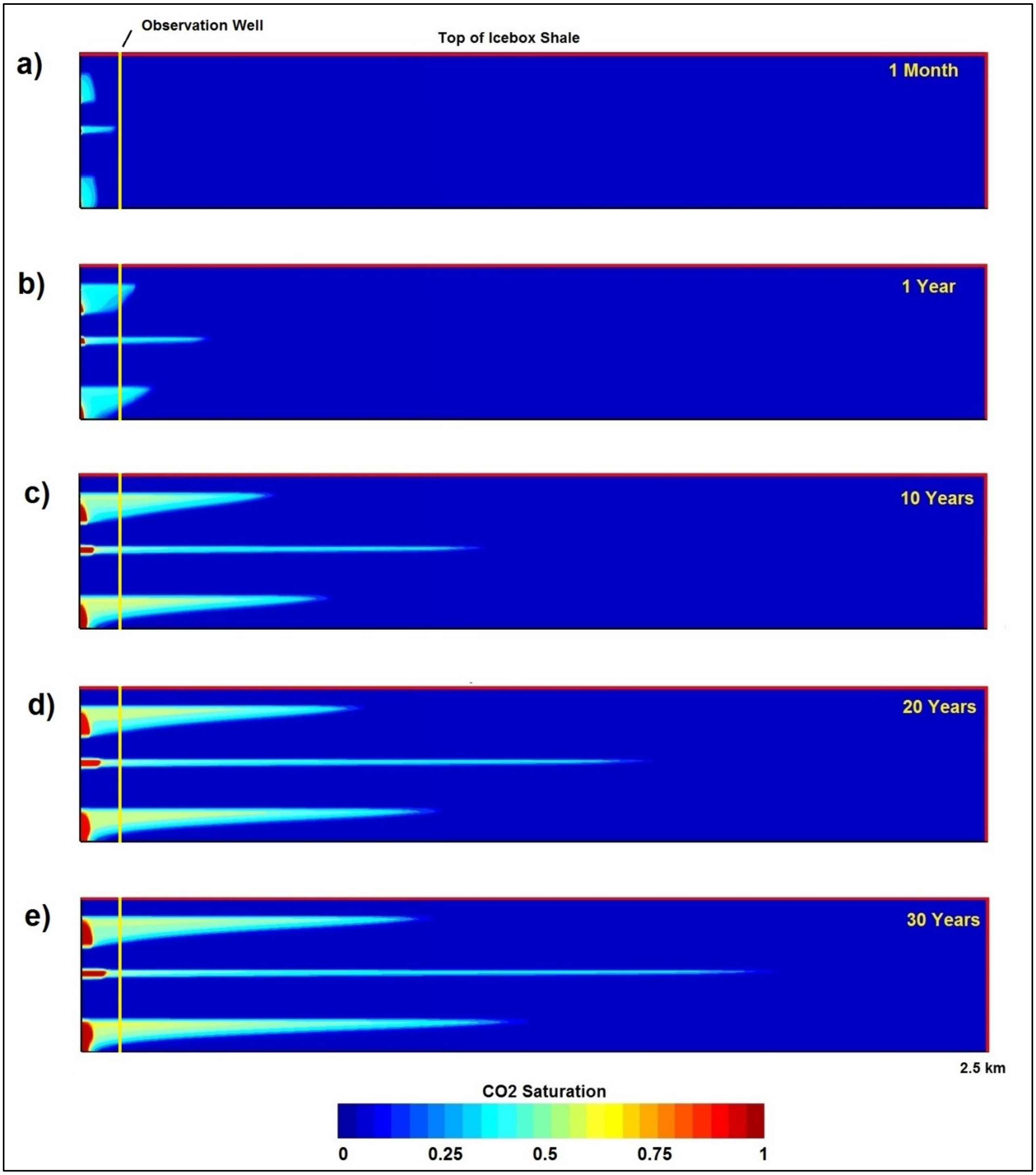

Figure 4.2 CO_2 plume evolution during the injection period (30 years). Vertical exaggeration: 2X

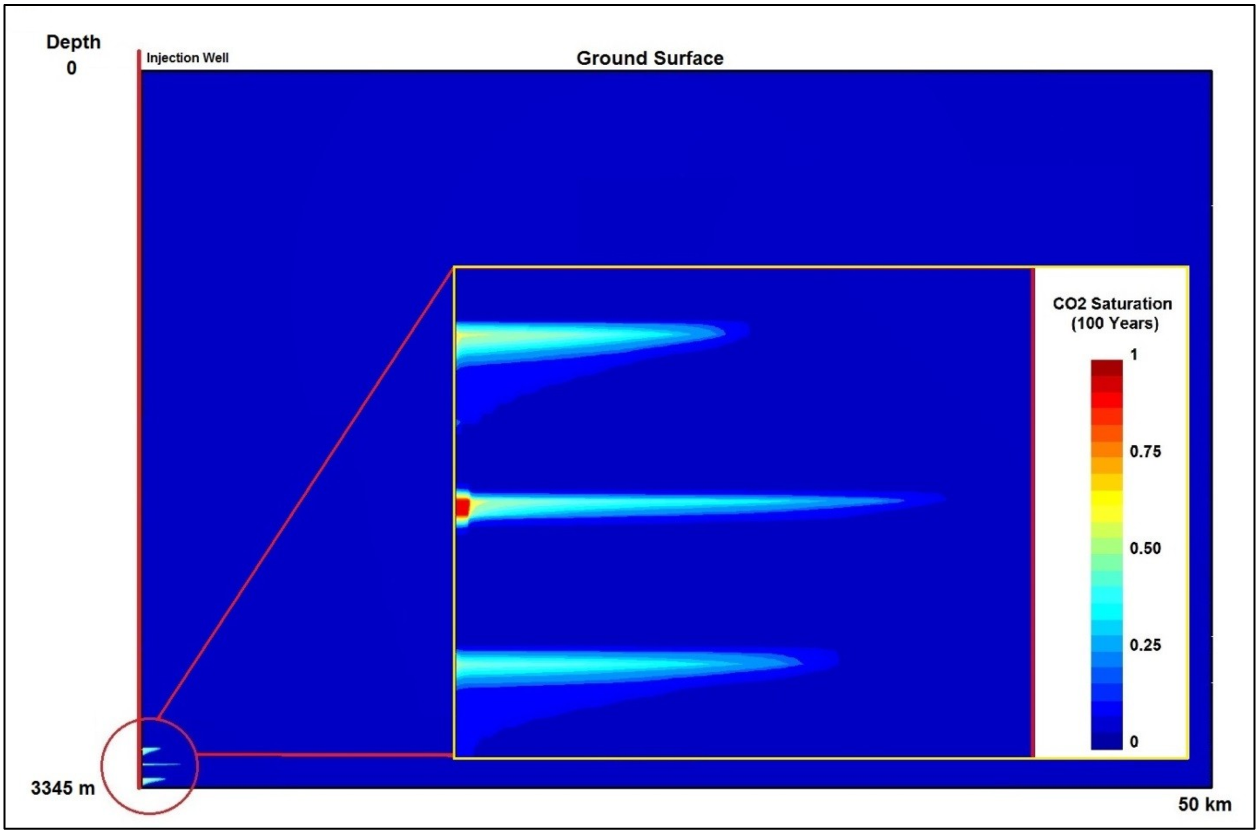

Figure 4.3 CO_2 plume migration within the storage formations at 100 years. (Vertical exaggeration: 10X)

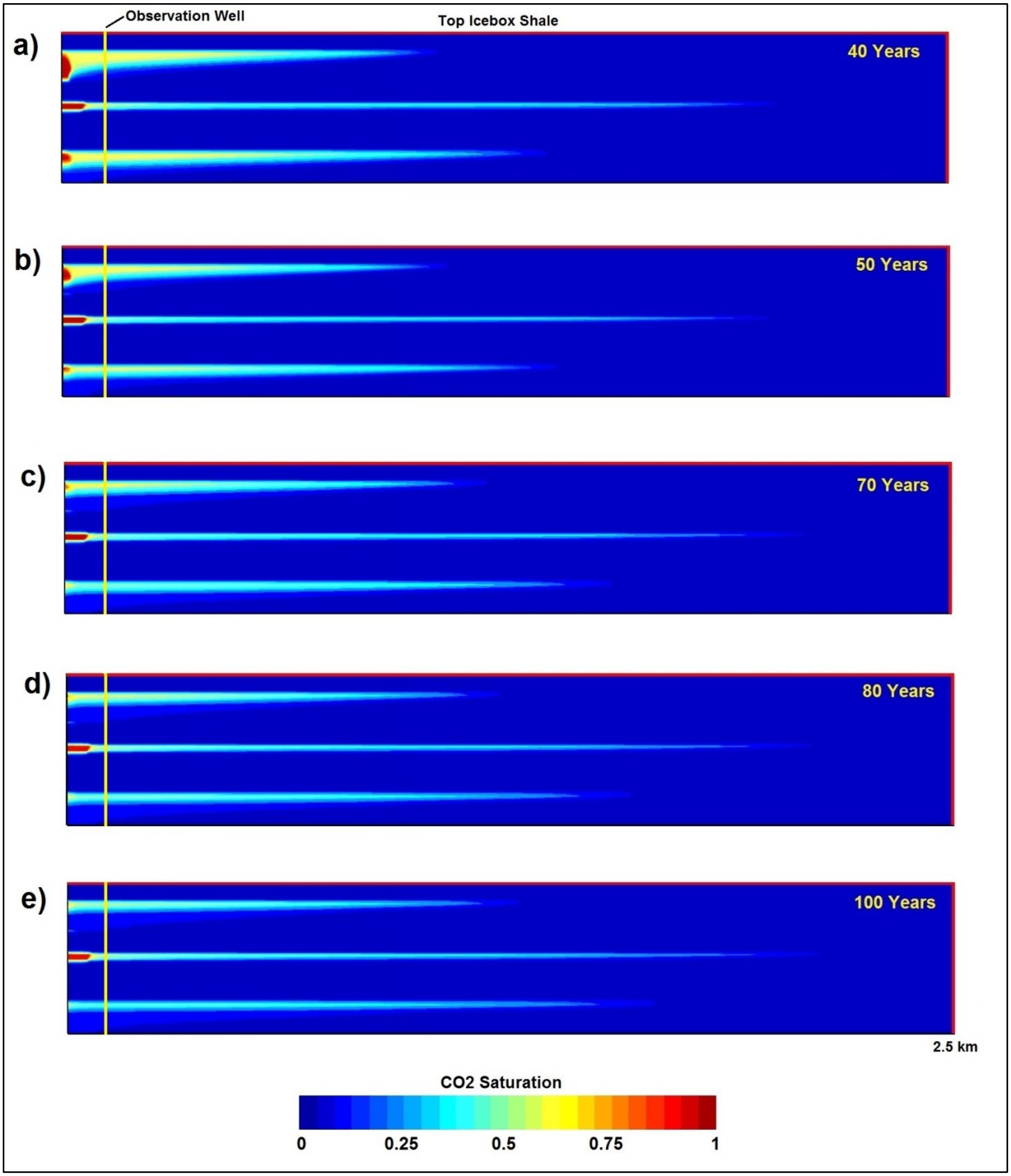

Figure 4.4 CO_2 plume evolution during the post injection period (70 years), Vertical exaggeration: 2X

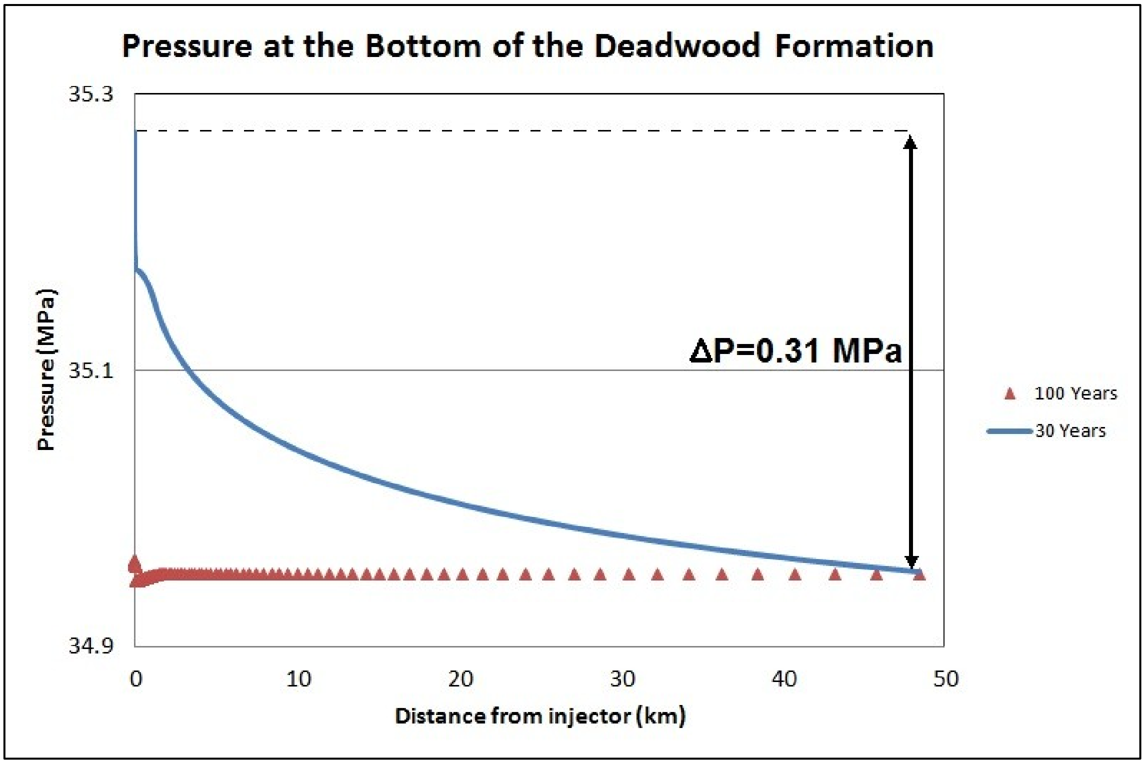

Figure 4.5 Lateral pressure buildup at the bottom of the reservoir (Lower injection layer)

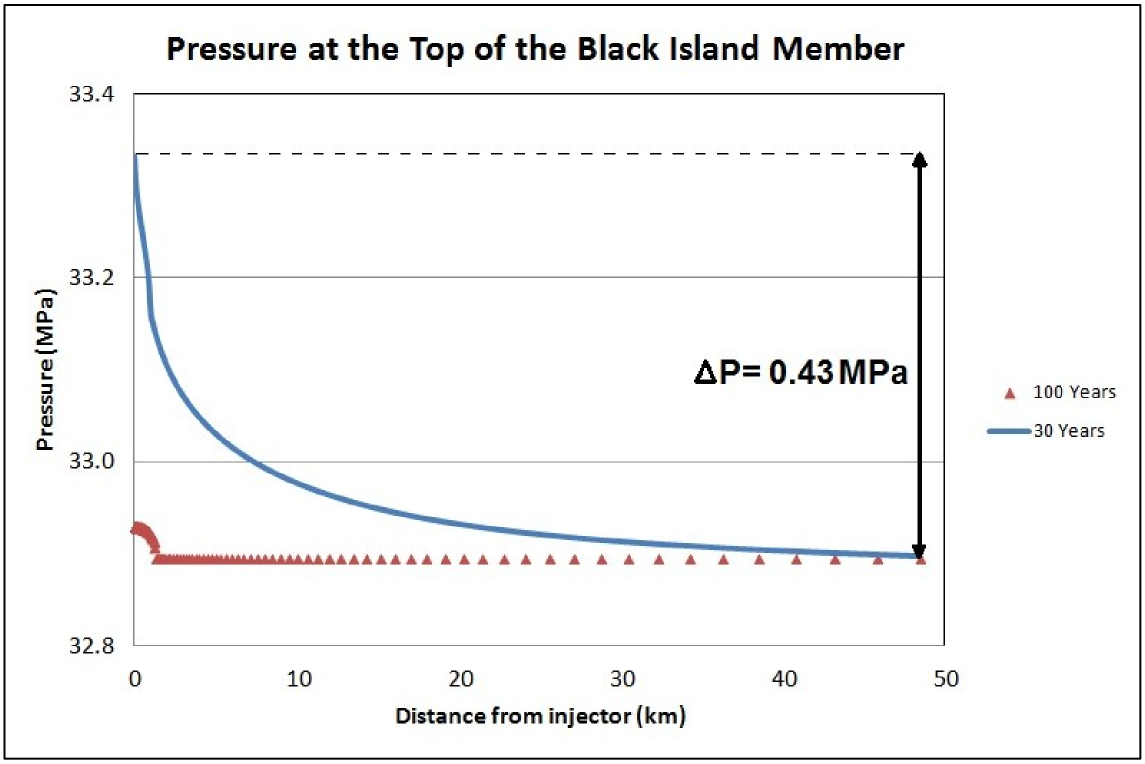

Figure 4.6 Lateral pressure distributions at the top of the storage formation (Upper injection layer)

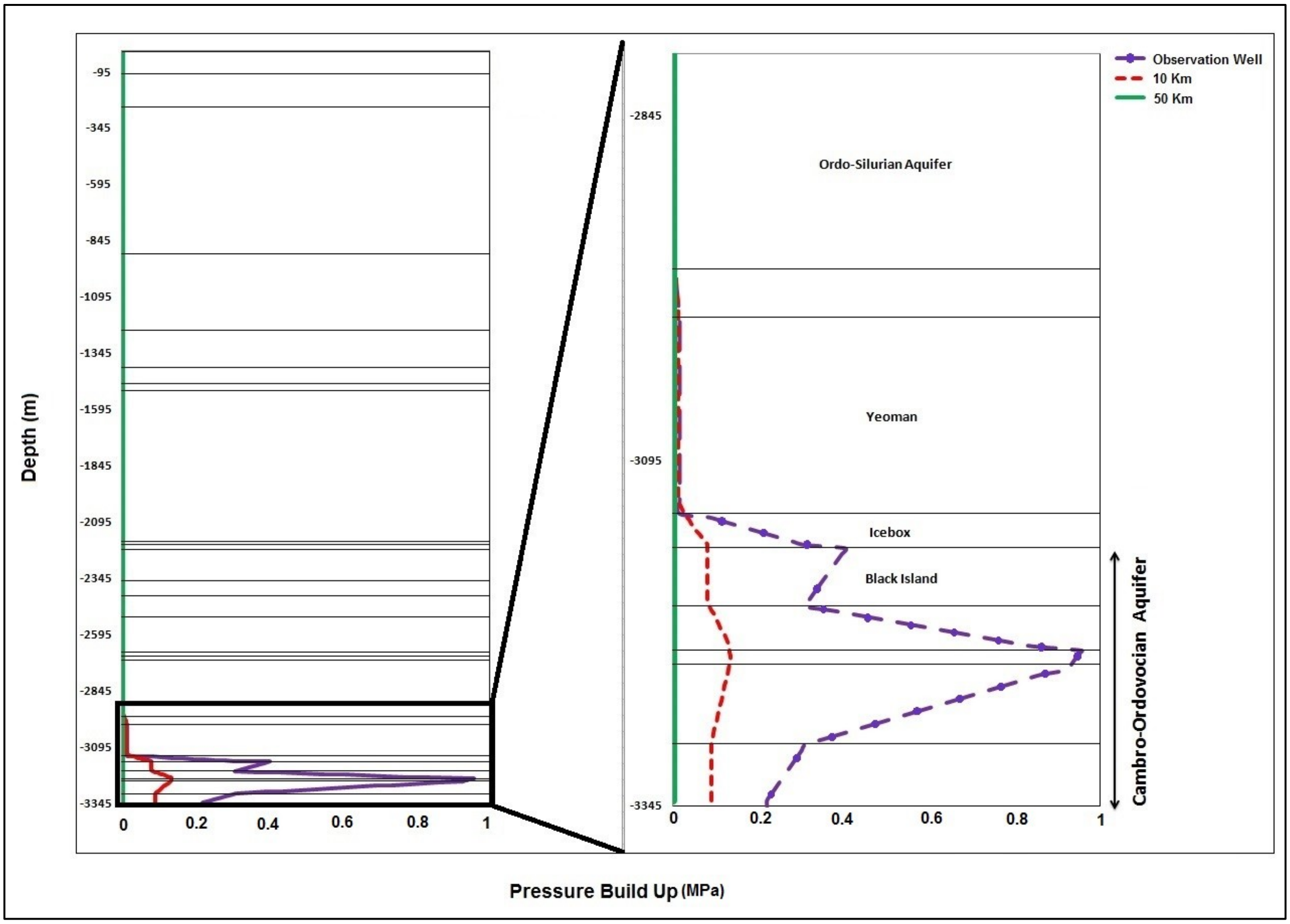

Figure 4.7 Vertical pressure buildup profiles after 30 years at different radial locations.

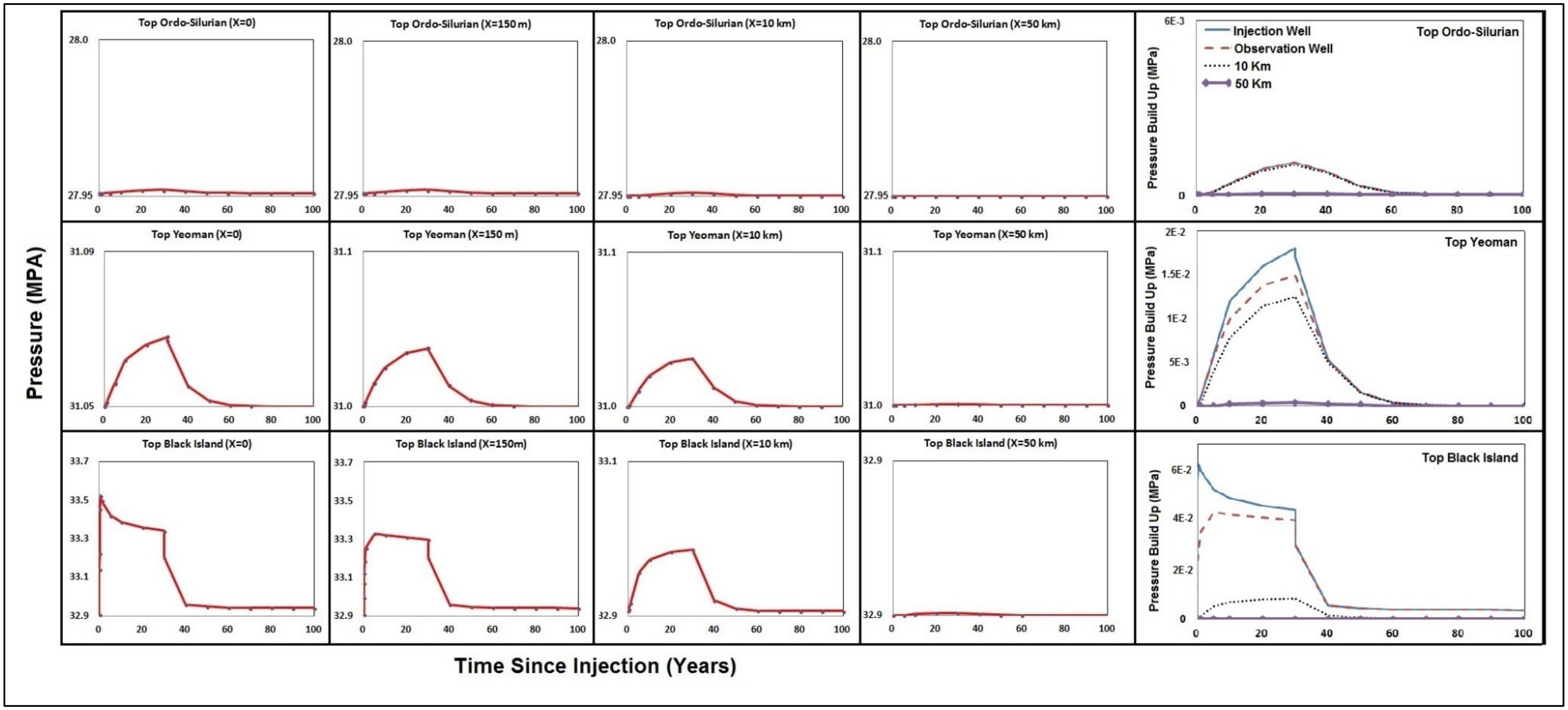

Figure 4.8 Pressure evolution and buildups at different radial distances within three aquifers, starting with the Cambro-Ordovician, Yeoman, and Ordo-Silurian (Interlake) Aquifers. (Note that the Y-axis scales are different)

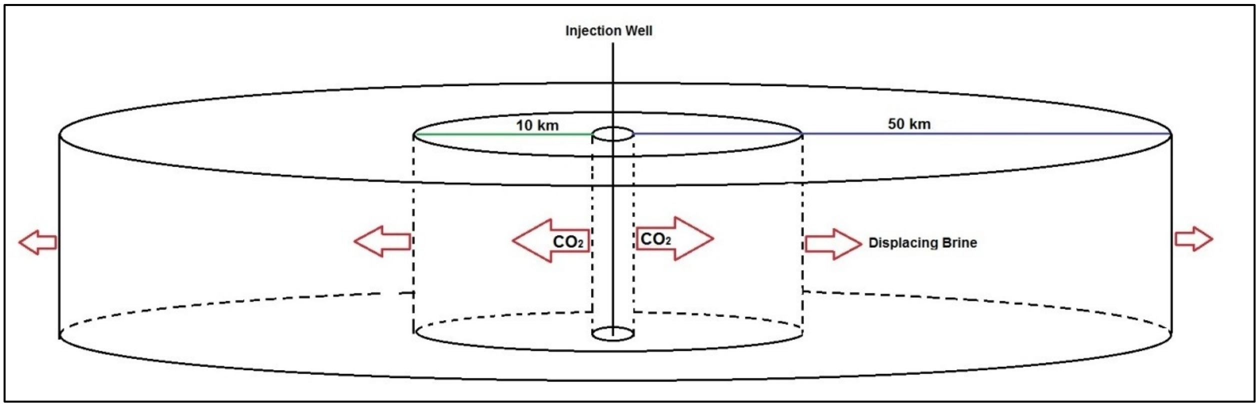

Figure 4.9 Schematic radially symmetric model of the lateral brine displacement.

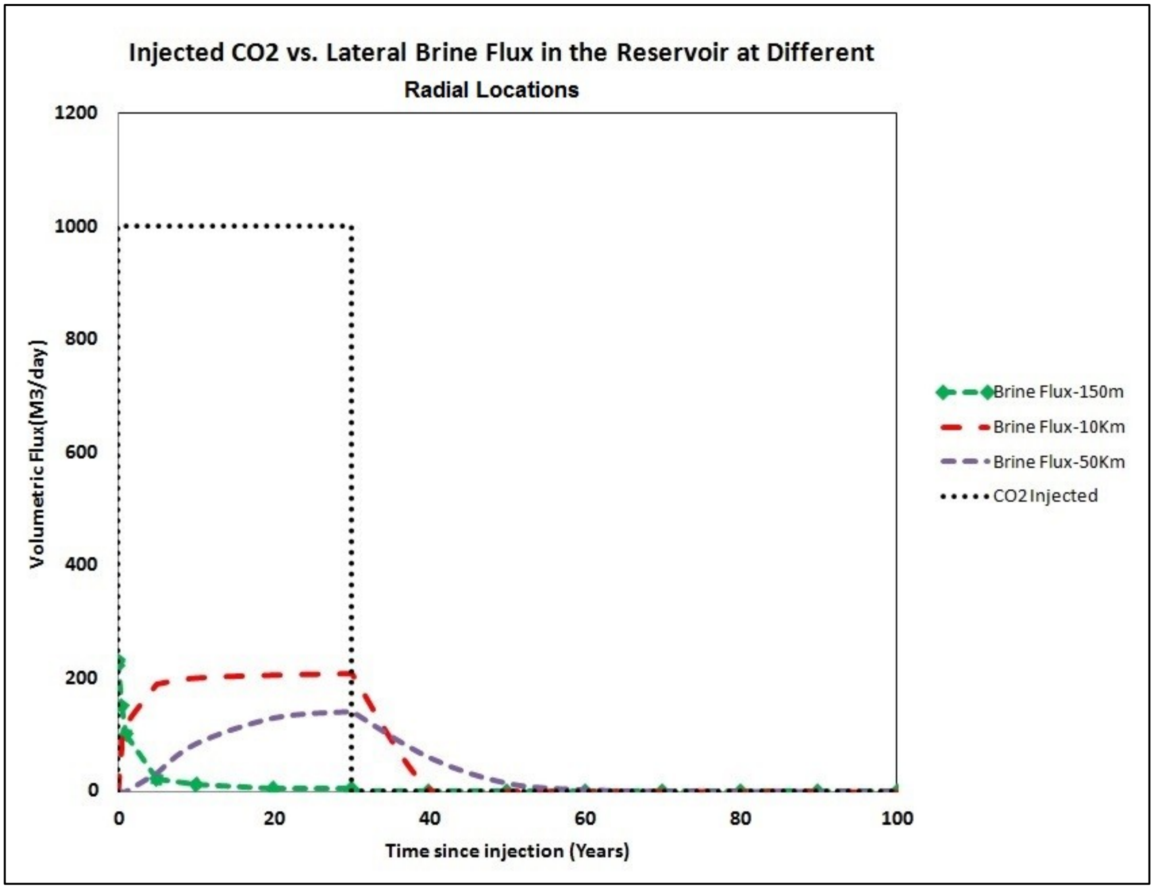

Figure 4.10 Volumetric lateral brine displacements within the reservoir at different radial locations.

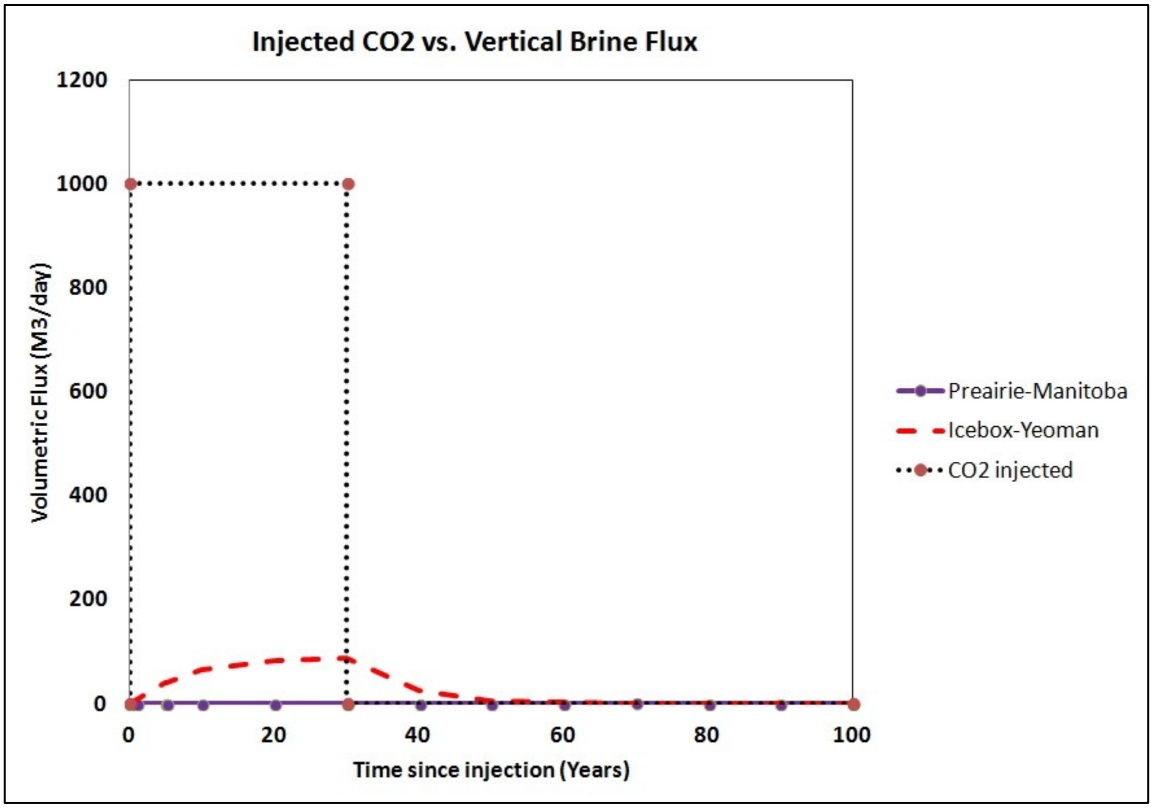

Figure 4.11 Volumetric vertical brine displacement across the primary and secondary sealing units.

5 Discussion and Conclusions

Injection of CO_2 into the Cambro-Ordovician Aquifer is expected to cause several impacts including pressure buildup and brine displacement in both lateral and vertical directions. The region of influence in a CO_2 injection project can be extremely large compared to the plume extent.

Each of these impacts was evaluated using a numerical model. Results showed that the extent of the pressure plume did not exceed more than 50 kilometres during the injection period. The system reached equilibrium conditions (i.e., hydrostatic pressure) 70 years after injection stopped. Furthermore, sealing units above the storage formations were able to stop the pressure plume from reaching the overlying freshwater aquifers and the ground surface. The vertical pressure buildup profile at the observation well also showed that the base of the Ordo-Silurian Aquifer, corresponding to the depth of 2850 metres below the ground surface was the uppermost level of the storage complex that pressure plume could reach. Therefore, no pressure change was predicted by the model in the rest of the sedimentary layers up to the ground surface.

Although the lateral pressure evolution travels fast and far within the reservoir, the lateral brine migration is considerably small and is close to the regional groundwater flow velocity (Bachu et al., 1994). The maximum possible transport velocity of the brine was calculated analytically in this study assuming a symmetric piston-type brine flow rate within the lower and middle injection horizons. The maximum brine migration distance over a 30-year injection period at 10 and 50 kilometres would be about 26 and 5.1 metres respectively. Calculated transport velocity at the distance of 200 kilometres showed that there will be almost no lateral brine migration at the end of the injection.

The vertical brine displacement was also simulated at the interfaces between the Icebox Aquitard and the Yeoman Aquifer as well as the Prairie Aquitard and the Manitoba Aquifer. The total brine that would be displaced across the first interface is about 86.75 $\mathrm{m^3/day}$ (i.e., $1.1 \times 10^{-8}\ \mathrm{m^3/day}$ per each $\mathrm{m^2}$ of the interface) and no brine leakage was calculated across the secondary sealing unit.

With respect to the results obtained from the simulation, pressure buildup and brine displacement in either lateral or vertical direction are unlikely to impact the shallow groundwater aquifers.

The storage efficiency factor was also quite small, indicating the high capacity of the reservoir formations with respect to the injected carbon dioxide. This factor is calculated as the total volume of CO_2 divided by the total available pore space of the storage formations and was calculated about 1.1×10^{-4}. To achieve higher efficiency factors, the total volume of CO_2 can be increased by designing more injection wells within the aquifer. However, interference between individual injection sites would be likely and needs to be considered to avoid building up pressure in the reservoir (Birkholzer et al., 2009).

The effects of different types of lateral grid spacing were tested in this study by designing five different cases. Coarse-scale grids overestimate the lateral extent of the plume as well as the dissolved CO_2 in the aquifer because dissolution scales linearly with the amount of liquid present in the grid blocks (Green and Ennis-King, 2012). Thus, grid blocks smaller than 1.5 metres would be appropriate to obtain acceptable results.

Different vertical grid spacing was applied to obtain appropriate vertical discretization required to obtain accurate results. A model with coarser vertical spacing impedes the gravity override of CO_2 plume and underestimates the lateral plume size (Yamamoto and Doughty, 2011). Results showed that the model with coarser vertical spacing (dz=10 metres) compared to the base model (dz=5 metres) represents lower lateral plume distribution for all injection horizons. Therefore, to obtain acceptable results, the vertical grid spacing needs to be less than 5 metres.

Assigning appropriate boundary conditions is very important in numerical simulations. Two types of boundary conditions implemented in TOUGH2 simulator were applied and tested in this study including the Dirichlet or hydrostatic conditions at the boundary elements, and Neumann conditions that are considered as no flow across the model boundaries. The lateral and upper boundaries of the model domain were set to the Dirichlet (i.e., hydrostatic) conditions while the lower boundary, corresponding to the Precambrian bedrock was set to the Neuman or no flow conditions. Results obtained from the hydrostatic boundary model were reasonable and showed a good compatibility with respect to the measured bottom-hole pressure data while assigning no flow conditions for all model boundaries created excessive pressure buildup into the system.

With respect to the objectives and concerns mentioned in the first chapter, the following results were concluded in this study:

1. Simulations showed that there is no CO_2 leakage from the reservoir into the overlying formations for a 100 year period and CO_2 appears to be safely trapped under the Icebox Aquitard.
2. Carbon dioxide plume distributions within the aquifers are different due to the thickness of the injection layers as well as the injection rates assigned for each aquifer. The maximum lateral CO_2 migration reaches up to 2 kilometres at 100 years after the injection and occurs within the middle aquifer.
3. Simulations showed that the CO_2 saturation decreases significantly within the lower and upper aquifers 70 years after the injection stops. However, it remains almost unchanged within the middle aquifer which represents the lowest thickness among all three injection horizons.
4. Vertical pressure profile showed that there is no built up pressure above the Ordo-Silurian Aquifer. This indicates that the pressure plume is stopped before reaching the secondary sealing unit (i.e., the Prairie Aquitard).
5. Simulations showed that the maximum pressure buildup occurs at the injection well. The pressure decreases laterally toward the model boundaries and reaches the hydrostatic conditions at 50 kilometres away from the injection well. Seventy years after the injection stops, almost the entire system reaches the equilibrium or hydrostatic conditions except for the area around the injection well correspond to a footprint area of 5.3km^2.
6. The lateral brine migration within the reservoir decreases as the distance from the injection well increases. At the end of the injection period (30 years), the lateral brine migration within the reservoir is 208 and 141 $\mathrm{m}^3/\mathrm{day}$ at 10 and 50 kilometres away from the injector respectively that are translated to 6.8×10^{-6} and 4.6×10^{-6} $\mathrm{m}^3/\mathrm{day}$ per each m^2 of the storage formations. So, the potential environmental impacts resulting from the lateral brine displacement and leaking into the up dip fresh water aquifers is unlikely.

7. The brine displacement in the vertical direction was also estimated across the primary and secondary sealing units (i.e., Icebox and Prairie Aquitards). Results show that there is no vertical brine migration through the Prairie Formation. Therefore, brine leakage into the shallow fresh water aquifers (e.g., Belly River Formation) is very unlikely.

8. Simulations showed that assigning appropriate boundary conditions significantly determines the accuracy of the calculated parameters (e.g., pressure buildup, CO_2 saturation, etc.). Results show that no flow boundary conditions overestimate the excess pressure up to 1.5 Mpa compare to the hydrostatic boundary conditions. Thus, assigning the Dirichlet or hydrostatic boundary conditions for upper and lateral boundaries is essential to obtain valid results.

9. A finer-grid model allows simulating more accurate pressure buildup and CO_2 saturation. The local grid refinement around the injection and the observation wells increases the computational efficiency. Results show that in order to obtain accurate bottom-hole pressure and CO_2 saturation, the injection cell width needs to be less than 1.5 metres. Furthermore, the vertical grid discretization also should not be more than 5 metres especially in the storage formation and its overlying sealing unit.

10. The MODFLOW is not able to simulate the multiphase flow conditions but it can be used to simulate the head rise at long distances from the injector where only one phase (i.e., water) is present. Furthermore, MODFLOW runs faster than the TOUGH2 and requires less simulation time. So, it would be a fast and time efficient alternative to large basin-scale models.

11. The Aquistore injection site appears to have good a storage potential to safely store supercritical carbon dioxide.

Suggestions for future work

1. The geochemical impacts of the CO_2 saturation on the Cambro-Ordovician Aquifers were not considered in this study. Simulating the possible mineralisation and chemical interactions between supercritical CO_2 and formation water in longer time periods (e.g., 10,000 years) would be useful to determine the geochemical aspect of this study. So, using the reactive geochemical transport simulators (e.g., TOUGHREACT) is suggested.

3. Along with the accuracy, the efficiency is very important especially in basin-scale simulations that contain a lot of grid elements and need more time to simulate the parameters. So, applying other multiphase flow simulators such as ECLIPSE.300, STAR, GEM, CMG, etc. is suggested to come up with the code(s) that are accurate and efficient.

4. The reservoir formations and sealing layers were assumed to be homogeneous and horizontal. So it would be useful to evaluate the impacts of reservoir heterogeneities and sloping on the CO_2 distribution and injectivity of the reservoir.

5. The geomechanical effects of the CO_2 injection on the reservoir formations and sealing layers is required to obtain the maximum injection pressure that is allowed to prevent well integrity failure.

6. The model calibration in this study was performed by comparing the simulated pressures with the actual bottom-hole pressure (BHP) data obtained from the observation well after a five-day injection period. There was a good compatibility between simulated BHP and field pressure measurements (RMSE=6.24%). However, calibrating the model with a longer injection period (e.g., 30 days or more) would lead to getting more comprehensive results, since the reservoir's behavior during a longer injection period would better reveal.

References

Aggelopoulos, C. A., and Tsakiroglou, C. D., 2012. Effects of micro-heterogeneity and hydrodynamic dispersion on the dissolution rate of carbon dioxide in water-saturated porous media. International Journal of Greenhouse Gas Control, v.10, p. 341-350.

Amyx, J. W., Bass, D. M. and Whiting, R. L., 1960. Petroleum Reservoir Engineering: Physical Properties . McGraw-Hill, 610 p.

Anderson, M. P., and Woessner, W. M., 1992. Applied groundwater modeling, Simulation of flow and advective transport. Academic Press Inc., San Diego, 381 p.

Audigane, P., Gaus, I., Czernichowski-Lauriol, I., Pruess, K., and Xu, T., 2007. Two-dimensional reactive transport modeling of CO_2 injection in a saline aquifer at the Sleipner site, North Sea. American Journal of Science, v. 307, p. 974-1008.

Bachu, S., 2003. Screening and ranking of sedimentary basins for sequestration of CO_2 in geological media in response to climate change. Environmental Geology, v. 44, p. 277-289.

Bachu, S., 2008. CO_2 storage in geological media: Role, means, status and barriers to deployment. Progress in Energy and Combustion Science, v. 34, p. 254-273.

Bachu, S., and Bennion, B., 2008. Effects of in-situ conditions on relative permeability characteristics of CO_2-brine systems. Environmental Geology, v. 54, p. 1707-1722.

Bachu, S., and Hitchon, B., 1996. Regional-scale flow of formation waters in the Williston Basin. American Association of Petroleum Geologists Bulletin, v. 80, p. 248-264.

Bachu, S., Gunter, W. D., and Perkins, E. H., 1994. Aquifer disposal of CO_2: hydrodynamic and mineral trapping. Energy Conversation and Management Journal, v. 34, p. 269-279.

Benn, A. A., and Rostron, B. J., 1998. Regional hydrochemistry of Cambrian to Devonian aquifers in the Williston Basin, Canada-U.S.A. *in*: J. E. Christopher, C. F. Gilboy, D. F. Paterson, and S. L. Bend, eds., Eighth International

Williston Basin Symposium, Saskatchewan Geological Society Special Publication no. 13, p. 238-245.

Bergman, M., and Winter, E. M., 1995. Disposal of carbon dioxide in aquifers in the U.S. Energy Conversation and Management, v. 36, p. 523-526.

Birkholzer, J. T., Zhou, Q., Zhang, K., Jordan, P., Rutqvist, J., and Tsang, C. F., 2008. Research project on CO_2 geological storage and groundwater resources: large-scale hydrogeological evaluation and impact on groundwater systems, Annual Report October 1, 2007, to September 30, 2008, Lawrence Berkeley National Laboratory, Berkeley, CA, p. 73-84.

Birkholzer, J. T., Zhou, Q., and Tsang, C. F., 2009. Large-scale impact of CO_2 storage in deep saline aquifers: a sensitivity study on pressure response in stratified systems. International Journal of Greenhouse Gas Control, v. 3, p. 181-194.

Brown, D. L., and Brown, D. L., 1987. Wrench-style deformation and paleostructural influence on sedimentation in and around a cratonic basin, *in* Peterson, J. A., Kent, D. M., Anderson, S. B., Pilatzke, R. H., and Longman, M.W., eds., Williston Basin: Anatomy of a cratonic oil province: Rocky Mountain Association of Geologists, p. 57-70.

Brunskill, B., 2006. Discussion of an Option for Geological Storage of Used Nuclear Fuel Beneath the Williston Basin of Southern Saskatchewan, *in*: Summary of Investigations 2006, Volume 1, Saskatchewan Geological Survey, Sask. Industry Resources, Misc. Rep. 2006-4.1, CD-ROM, Paper A-4, 8 p.

Byrnes, A. P., Cluff, R. M., and Webb, J. C., 2009. Analysis of critical permeability, capillary pressure and electrical properties for Mesaverde tight gas sandstones from western U.S. basins. Technical Report Submitted to U. S. Department of Energy, p. 174-180.

Carsel, R. F., and Parrish, R. S., 1988. Developing joint probability distributions of soil water retention characteristics. Water Resources Research, v. 24, p. 755-769.

Cavanagh, A., 2013. Benchmark calibration and prediction of the Sleipner CO_2 plume from 2006 to 2012. Energy Procedia (GHGT-11), v. 37, p. 3529-3545.

Christopher, J. E., Yurkowski, M., Nicolas, M., and Bamburak, J., 2006. The Cenomanian-Santonian Colorado Formation of eastern southern Saskatchewan and southwestern Manitoba. In: C. F. Gilboy and S. G. Whittaker, eds., Saskatchewan and Northern Plains Oil and Gas Symposium 2006, Saskatchewan Geological Society Special Publication, v. 19, p. 299-318.

Corey, A. T., 1954. The interrelation between gas and oil relative permeabilities. Producer Monthly, p. 38-41.

DeMis, W. D., 1995. Effect of cross-basinal hydrodynamics flow on oil accumulations and oil migration history of the Bakken-Madison Petroleum System; Williston Basin, North America. In: L. D. V. Hunter and R. A. Schalla, eds., Seventh International Williston Basin Symposium, Billings, Montana Geological Society, p. 291-301

Dong, Y., Li, G., Li, and Wu, M., 2009. The impact of large-scale CO_2 geologic storage in deep saline aquifers: an example from the Songliao Basin, China, Proceeding of the TOUGH Symposium 2009, Lawrence Berkeley National Laboratory, Berkeley, CA, 18 p.

Doughty, C., 2010. Investigation of CO_2 plume behavior for a large-scale pilot test of geologic carbon storage in a saline formation. Transport in Porous Media, v. 82, p. 49-76.

Doughty, C., Pruess, K., Benson, S. M., Hovorka, S, D., Knox, P. R., and Green, C. T., 2001. Capacity investigation of brine-bearing sands of the Frio Formation for geologic sequestration of CO_2. Proceedings of First National Conference on Carbon Sequestration, 14–17 May 2001, Washington DC, USDOE/NETL-2001/1144 Paper, National Energy Technology Laboratory, US DOE, Washington DC, p. 32-48.

Doughty, C., Freifeld, B. M., and Trautz, R. C., 2008. Site characterization for CO_2 geologic storage and vice versa: the Frio brine pilot, Texas, USA as a case study. Environmental Geology Journal, v. 54, p. 1635-1656.

Doughty, C., and Pruess, K., 2004. Modeling supercritical carbon dioxide injection in heterogeneous porous media. Vadose Zone Journal, v. 3, p. 837-847.

Downey, J. S., 1984. Hydrodynamics of the Williston Basin in the Northern Great Plains. In: D. G. Jorgenson and D. C. Signor, eds., Geohydrology of the Dakota Aquifers, National Water Well Association, Worthington, Ohio, United States, p. 92-98.

Ennis-King, J. P., and Paterson, L., 2003. Role of convective mixing in the long-term storage of carbon dioxide in deep saline formations. SPE paper no. 84344, Presented at Society of Petroleum Engineers.Annual Technical Conference and Exhibition, Denver, CO, 5-8 October 2003, SPE, Richardson, TX.

Estublier, A., and Lackner, A. S., 2009. Long-term simulation of the Snohvit CO_2 storage. Proceedings of the 9th International Conference on Greenhouse Gas Control Technologies (GHGT-9), 16-20 November 2008, Washington DC, USA, v. 1, p. 3221-3228.

Ferguson, G. A. G., Betcher, R. N., and Grasby, S. E., 2007. Hydrogeology of the Winnipeg Formation in Manitoba, Canada. Hydrogeology Journal, v.15, p. 573-587.

Frykman, P., 2012. Review of relevant trapping mechanisms based on site portfolio. CO2CARE Publications. 39 p.

Gale, J., 2004. Geological storage of CO_2: what do we know, where are the gaps, and what more needs to be done? Energy, v. 29, p. 1329-1338.

Gasda, S. E., Bachu, S., and Celia, M. A., 2004. Spatial characterization of the location of potentially leaky wells penetrating a deep saline aquifer in a mature sedimentary basin. Environmental Geology Journal, v. 46, p. 707-720.

Gerhard, L. C., Anderson, S. B., LeFever, J. A. and Carlson, C. G., 1982. Geological development, origin, and energy mineral resources of Williston Basin, North Dakota, American Association of Petroleum Geologists Bulletin, v. 66, p. 989-1020.

Gerhard, L. C., and Anderson, S. B., 1988. Geology of the Williston Basin (United States portion). *in*: L. L. Sloss, ed., Sedimentary Cover-North American Craton, U.S. Geological Society of America, p. 221-241.

Gibson, R. I., 1995. Basement tectonics and hydrocarbon production in the Williston Basin: An interpretive overview *in*: 7th International Williston Basin Symposium, (L. Hunter and R. Schalla, eds.), p. 3-11.

Green, C. P., and Ennis-King, J., 2012. Spatial grid correction for short-term numerical simulation results of carbon dioxide dissolution in saline aquifers. Computational Geosciences, 16, p.1153-1161.

Haidl, F. M., 1987. Stratigraphic and lithologic relationships, Interlake Formation (Silurian), southern Saskatchewan. *in*: Summary of Investigations 1987, Saskatchewan Geological Survey, Misc. Rep. 87-4, p. 187-193.

Halabura, S., 2006. The Mississippian of southern Saskatchewan regional considerations. *in*: C. F. Gilboy and S. G. Whittaker, eds., Saskatchewan and Northern Plains Oil and Gas Symposium 2006. Saskatchewan Geological Society Special Publication, v. 19, p. 146-164.

Hannon, N., 1987. Subsurface water flow patterns in the Canadian sector of the Williston Basin. *in*: M. W. Longman, ed., Williston Basin Anatomy of a Cratonic Oil Province, Rocky Mountain Association of Geologists, p. 229-312.

Hepple, R. P., and Benson, S. M., 2005. Geologic storage of carbon dioxide as a climate change mitigation strategy: performance requirements and the implications of surface seepage. Environmental Geology Journal, v. 47, p. 576-585.

Hermanson, J. L., 2014. Multiphase flow reactive transport modeling of CO_2 storage in heterogeneous reservoirs, Thesis Submitted in Partial Fulfillment of the Requirements for the Degree of Master of Science in the Department of Earth Sciences, Faculty of Science, Simon Fraser University, 278 p.

Hillel, D., 1980. Fundamentals of soil physics. New York: Academic Press, Inc., 413 p.

Hitchon, B., Gunter, W. D., Gentzis, T., and Bailey, R.T., 1999. Sedimentary basins and greenhouse gases: a serendipitous association. Energy Conversation and Management, v. 40, p. 835-843.

Holloway, S., and Savage, D., 1993. The potential for aquifer disposal of carbon dioxide in the UK. *in*: P.W.F. Pierce (ed.), Proceedings of the International Energy Agency carbon dioxide symposium, Oxford March 1993. Energy Conversation and Management, v. 34, p. 925-932.

Holloway, S., 1996. An overview of the Joule II Project: the underground disposal of carbon dioxide. Energy Conversation and Management, v. 37, p. 1149-1154.

Houseworth, J. E., Oldenburg C. M., Mazzoldi, A., Gupta, A. K., Nicot, J. P., and Bryant, S. L., 2011. Leakage risk assessment for a potential CO_2 storage project in Saskatchewan, Canada. Certification framework, LBNL-4915E. Lawrence Berkeley National Laboratory, Berkeley, CA, 53 p.

IPCC (Intergovernmental Panel on Climate Change), 2005. IPCC special report on carbon dioxide capture and storage. Prepared by Working Group III of the Intergovernmental Panel on Climate Change. Cambridge University Press, Cambridge, 442 p.

Kendall, A. C., 1975. The Ashern, Winnipegosis and Lower Prairie Evaporite formations of the commercial potash areas. Summary of Investigations 1975, Saskatchewan Geological Survey, Saskatchewan Department of Mineral Resources, p. 61-65.

Kent, D. M., 1994. Paleogeographic evolution of the cratonic platform – Cambrian to Triassic, Chapter 27. *in*: G. Mossop and I. Shetson (compilers), Geological Atlas of the Western Canada Sedimentary Basin, Canadian Society of Petroleum Geologists and Alberta Research Council, p. 69-86.

Kent, D. M., and Christopher, J. E., 1994. Geological History of the Williston Basin and Sweetgrass Arch, Chapter 27. *in*: G. Mossop and I. Shetson (compilers), Geological Atlas of the Western Canada Sedimentary Basin, Canadian Society of Petroleum Geologists, Alberta Research Council, p. 421-429.

Khan, D. K., and Rostron, B. J., 2004. Regional hydrogeological investigation around the IEA Weyburn CO_2 monitoring and storage project site. *in*: E. S. Rubin, D. W. Keith, and C. F. Gilboy, eds., Proceeding of the Seventh International Conference on Greenhouse Gas Control Technologies, Sept. 5-9, 2004, Vancouver, Canada, Volume 1: Peer-Reviewed Papers and Plenary Sessions, Elsevier, UK, p. 741-750.

Kharaka, Y. K., Thordsen, J. J., Kakouros, E., Ambats, G., Herkelrath, W. N., Beers, S. R., Birkholzer, J. T., Apps, J. A., Spycher, N. F., Zheng, L., Trautz, R. C., Rauch, H. W., and Gullickson, K. S., 2010. Changes in the chemistry of shallow groundwater related to the 2008 injection of CO_2 at the ZERT field site, Bozeman, Montana. Environmental Earth Sciences Journal, v. 60, p. 273-284.

Kihm, J., Kim, J., Wang, S., and Xu, T., 2012. Hydrogeochemical numerical simulation of impacts of mineralogical compositions and convective fluid flow on trapping mechanisms and efficiency of carbon dioxide injected into deep saline sandstone aquifers. Journal of Geophysical Research, v. 117, 23 p.

Kreis, L. K., Thomas, P. L., Burke, R. B., and Whittaker, S. G., 2003. Devonian isopach and structure maps: Initial results of the IEA Weyburn CO_2 Monitoring and storage project area. Summary of Investigations 2003, Volume 1, Saskatchewan Geological Survey, Saskatchewan Industry and Resources, Misc. Rep. 2003-4.1, Paper A-5, 6 p.

Kreis, L. K., Costa, A. L., and Osadetz, K. G., 2006. Hydrocarbon potential of Bakken and Torquay Formations, southern Saskatchewan. *in*: C. F. Gilboy and S. G. Whittaker, eds., Saskatchewan and Northern Plain Oil & Gas Symposium 2006. Saskatchewan Geological Society Special Publication, v. 19, p. 118-137.

Krevor, S. C. M., Pini, R., Zuo, L., and Benson, S. M., 2012. Relative permeability and trapping of CO_2 and water in sandstone rocks at reservoir conditions. Water Resources Research Journal, v. 48, 5 p.

Kumar, A., M. H. Noh, Sepehrnoori, K., Pope, G. A., Bryant, S. L., and Lake, L. W., 2005. Simulating CO_2 storage in deep saline aquifers, Carbon Dioxide Capture for Storage in Deep Geologic Formations - Results from the CO_2 Capture Project, v.2, Geologic Storage of Carbon Dioxide with Monitoring and Verification, S.M. Benson, (ed.), Elsevier, London. p. 977-898.

LeFever, R. D., Thompson, S. C., and Anderson, D. B., 1987. Earliest Paleozoic history of the Williston Basin in North Dakota. *in*: C. G. Carlson and J. E. Christopher, eds., Fifth International Williston Basin Symposium, Saskatchewan Geological Society and North Dakota Geological Society Special Publication, p. 22-36.

Lemieux, J. M., 2011. The potential impact of underground geological storage of carbon dioxide in deep saline aquifers on shallow groundwater resources, Hydrogeology Journal, v. 19, p. 757-778.

Lenhard, R. J., and Parker, J. C., 1987. A model for hysteretic constitutive relations governing multiphase flow, 2. Permeability-saturation relations. Water Resources Research, v. 23, p. 2197-2205.

Leverett, M., 1941. Capillary behavior in porous solids, Transactions of the American Institute of Mining and Metallurgical Engineers, v. 142, p. 152-169.

Li, Y. L., Xu, T. F., Zhang, W., Omambia, A. N., Qui, G. B., and Jiang, L., 2009. Reactive transport modeling and comparison of long-term CO_2 geological storage in geological formations with different mineralogical assemblages. In Calibration and Reliability in Groundwater Modeling: "Managing Groundwater and the Environment: Proceedings of the 7th International Conference on Calibration and Reliability in Groundwater Modeling, ModelCARE 2009, Wuhan, China, p. 459-463.

McCabe, H. R., 1978. Reservoir potential of the Deadwood and Winnipeg Formations, southwestern Manitoba; Manitoba Mines, Natural Resources and Environment, Mineral Resources Division, Geological Paper GP, v. 78-3, 54 p.

McPherson, B. J., and Cole, B. S., 2000. Multiphase CO_2 flow, transport and sequestration in the Powder River Basin, Wyoming, USA. Journal of Geochemical Exploration, p. 65-69.

Morgan, J., and Gordon, D., 1970. Influence of pore geometry on water-oil relative permeability. Journal of Petroleum Technology, v. 22, p. 1199-1208.

Mossop, G. D., and Shetson, I., 1994. Geological atlas of the Western Canada sedimentary basin. Canadian Society of Petroleum Geologists and Alberta Research Council, 510 p.

Nicolas, M., 2006. Petroleum geology of the Devonian Three Forks Formations, Sinclair Field and surrounding area, southwestern Manitoba. Saskatchewan and Northern Plains Oil and Gas Symposium, Proceeding from the Core Workshop, 26 p.

Nicolas, M. P. B., and Barchyn, D., 2008. Williston Basin Project (Targeted Geoscience Initiative II): Summary report on Paleozoic stratigraphy, mapping and hydrocarbon assessment, southwestern Manitoba, Manitoba Geological Survey, Geoscientific paper GP2008-2, 28 p.

Nicot, J. P., 2008. Evaluation of large-scale CO_2 storage on freshwater sections of aquifers: an example from the Texas Gulf Coast Basin. International Journal of Greenhouse Gas Control, v. 2, p. 582-593.

Obdam, A., Van der Meer, L. G. H., May, F., Kervevan, C., Bech, N., and Wildenborg, A., 2003. Effective CO_2 storage capacity in aquifers, gas fields, oil fields, and coal fields. Proceedings of the 6th International, Conference on Greenhouse Gas Control Technologies (GHGT- 6), J. Gale and Y. Kaya eds., 1-4 October 2002, Kyoto, Japan, Pergamon, v. 1, p. 339-344.

Osman, K. T., 2013. Problem soils and their management. *in*: Osman, K. T., (ed) Soils: Principles and management. Springer, Dordrecht, Netherland, p. 161-174.

Palombi, D. D., 2008. Regional hydrogeological characterization of the northeastern margin in the Williston Basin, MSc thesis, Department of Earth and Atmospheric Sciences, University of Alberta, 196 p.

Parker, J. C., and Lenhard, R. J., 1987. A model for hysteretic constitutive relations governing multiphase flow, 1. Saturation-pressure relations. Water Resources Research, v. 23, p. 2187-2196.

Peterson, J. A., and MacCary, L. M., 1987. Regional stratigraphy and general petroleum geology of the U.S. Portion of the Williston Basin and adjacent areas. *in*: Peterson, J. A., Kent, D. M., Anderson, S. B., Pilatzke, R. H., and Longman, M. W. eds., Williston Basin: Anatomy of a cratonic Oil Province. Rocky Mountain Association of Geologists, Denver, CO, p. 9-44.

Paterson, D. F., 1988. Review of regional stratigraphy relationships of the Winnipeg Group (Ordovician), the Deadwood Formation (Cambro-Ordovician) and underlying strata in Saskatchewan. *in*: L. P. Beck, ed., Summary of Investigations 1988, Saskatchewan Geological Survey, p. 224-1343.

Perrin, J., and Benson, S., 2010. An experimental study on the influence of sub-core scale heterogeneities on CO_2 distribution in reservoir rocks. Transport in Porous Media, v. 82, p. 93-109.

Potter, D., 2006. Relationships of Cambro-Ordovician stratigraphy to paleo topography on the Precambrian basement, Williston Basin. *in*: C. F. Gilboy and S. G. Whittaker, eds., Saskatchewan and Northern Plains Oil & Gas Symposium 2006, Saskatchewan Geological Society Special Publication, v. 19, p. 63-73.

Pruess, K., Oldenburg, C. M., and Moridis, G., 1999. TOUGH2 user's guide, version 2.0. Report LBNL-43134, Lawrence Berkeley National Laboratory, Berkeley, CA, 210 p.

Pruess, K., Tsang, C., Law, D., and Oldenburg, C., 2001. Intercomparison of simulation models for CO_2 disposal in underground storage reservoirs. Lawrence Berkeley National Laboratory, Berkeley, CA, 31 p.

Pruess, K., 2005. ECO2N: a TOUGH2 fluid property module for mixtures of water, NaCl, and CO_2. Technical report LBNL-57952, Lawrence Berkeley National Laboratory, Berkeley, CA, 76 p.

Reinson, G. E., and Wardlaw, N. C., 1972. Nomenclature and stratigraphic relationships, Winnipegosis and Prairie Evaporite formations. Bulletin of Canadian Petroleum Geologist, v. 2a, p. 301-320.

Ringrose, P. S., Mathieson, A. S., Wright, I. W., Selama, F., Hansen, O., Bissel, R., Saoula, N., and Midgley, J., 2013. The In Salah CO_2 storage project: Lessons learned and knowledge transfer, Proceedings of the 11th International

Conference on Greenhouse Gas Control Technologies (GHGT-11), 18-22 November 2012, Kyoto, Japan, v. 37, p. 6226-6236.

Rostron, B. J., White, D., Hawkes, C., and Chalaturnyk, R., 2014. Characterization of the Aquistore CO_2 project storage site, Saskatchewan, Canada. Energy Procedia (GHGT-12), v. 63, p. 2977-2984.

Scheidegger, A. E., 1957. The physics of flow through porous media, New York, University of Toronto Press, 353 p.

Schwartz, F. W., and Zhang, H., 2003. Fundamentals of groundwater. New York, Wiley, p. 49-52.

Sorrensen, J. A., Bailey, T. P., Smith, S. A., Gorecki, C. D., Fischer, D. W., Peck, W. D., Steadman, E. N., and Harju, J. A., 2009. CO_2 Storage Capacity Estimates for Stacked Brine- Saturated Formations in the North Dakota Portion of the Williston Basin, Energy Procedia, v. 1. p. 2833-2840.

Spangler, L. H., Dobeck, L. M., Repasky, K. S., Nehrir, A. R., Humphries, S. D., Barr, J. L., Keith, C. J., Shaw, J. A., Rouse, J. H., Cunningham, A. B., Benson, S. M., Oldenburg, C. M., Lewicki, J. L., Wells, A. W., Diehl, J. R., Strazisar, B. R., Fessenden, J. E., Rahn, T. A., Amonette, J. E., Barr, J. L., Pickles, W. L., Jacobson, J. D., Silver, E. A., Male, E. J., Rauch, H. W., Gullickson, K. S., Trautz, R., Kharaka, Y., Birkholzer, J., and Wielopolski, L., 2009. A shallow subsurface controlled release facility in Bozeman, Montana, USA, for testing near surface CO_2 detection techniques and transport models. Environmental Earth Science Journal, v. 60, p. 227-239.

Tesfaye, A., 2009. Steady-state Groundwater Flow and Contaminant transport modeling of Akaki well field and its surrounding catchment, Addis Ababa, Ethiopia, International Institute for Geo-information Science and Earth Observation, Enschede, Netherlands, 153 p.

Vigrass, L. W., 1971. Depositional framework of the Winnipeg Formation in Manitoba and eastern Saskatchewan. Geological Association of Canada, Special Paper no. 9, p. 225-234.

Vigrass, L., Jessop, A., and Brunskill, B., 2007. Regina Geothermal Project, in Summary of Investigations 2007, Volume 1, Saskatchewan Geological Survey, Sask. Industry Resources, Misc. Rep. 2007-4.1, CD-ROM, Paper A-2, 21 p.

van Genuchten, M. T., 1980. A closed-form equation for predicting the hydraulic conductivity of the unsaturated soil. Soil Science Society of America Journal, v. 44, p. 892-898.

Wang, S., and Jaffe, P. R., 2004. Dissolution of a mineral phase in potable aquifers due to CO_2 releases from deep formations: effect of dissolution kinetics. Energy Conversation and Management, v. 45, p. 2833-2848.

Whittaker, S., Rostron, B. J., Khan, D., Hajnal, Z., Qing, H., Penner, L., Maathuis, H., and Goussev, S., 2004. IEA GHG Weyburn CO_2 Monitoring and Storage Project Summary Report 2000-2004, *in*: M. Wilson and M. Monea, eds., Seventh International Conference on Greenhouse Gas Control Technologies, Petroleum Technology Research Centre, v. 1, 273 p.

Xu T., Apps, J. A., and Pruess, K., 2003. Reactive geochemical transport simulation to study mineral trapping for CO_2 disposal in deep arenaceous formations. Journal of Geophysical Research, v. 108(B2), 66 p.

Xu, T., Sonnenthal, E., Spycher, N., and Pruess, K., 2004. TOUGHREACT User's Guide: A simulation program for non-isothermal multiphase reactive geochemical transport in variably saturated geologic media. Lawrence Berkeley National Laboratory Report LBNL-55460, Berkeley, CA, 203 p.

Xu, T., Apps, J. A., and Pruess, K., 2005. Mineral sequestration of carbon dioxide in a sandstone–shale system. Chemical Geology, v. 217, p. 295-318.

Yamamoto, H., and Doughty, C., 2011. Investigation of gridding effects for numerical simulations of CO_2 geologic sequestration. International Journal of Greenhouse Gas Control, v. 5, p. 975-985.

Yamamoto, H., Zhang, K., Karasaki, K., Marui, A., Uehara, H., and Nishikawa, N., 2009. Numerical investigation concerning the impact of CO_2 geologic storage on regional groundwater flow. International Journal of Greenhouse Gas Control, v. 3, p. 586-599.

Zhang, W., Li, Y., Xu, T., Cheng, H., Zheng, Y., and Xiong, P., 2009. Long-term variations of CO_2 trapped in different mechanisms in deep saline formations: A case study of the Songliao Basin, China. International Journal of Greenhouse Gas Control, v. 3, p. 161-180.

Zhang, W., 2013. Effect of modeling factors on the dissolution-diffusion-convection process during CO_2 geological storage in deep saline formations. Frontiers of Earth Science, v. 7, p. 238-256.

Zhou, Q., Birkholzer, J. T., Mehnert, E., Lin, Y. F., and Zhang, K., 2010. Modeling basin- and plume-scale processes of CO_2 storage for full-scale deployment. Ground Water, v. 48, p. 494-514.